Report No. DOT/FAA/NR-91/6



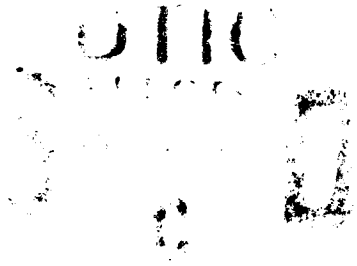



**Project Report**
**ATC-180**

# Terminal Doppler Weather Radar Test Bed Operation – Orlando January – June 1990

D.M. Bernella, Editor

4 November 1991

**Lincoln Laboratory**
MASSACHUSETTS INSTITUTE OF TECHNOLOGY
*LEXINGTON, MASSACHUSETTS*

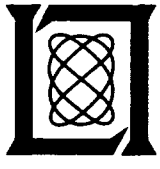

**Prepared for the Federal Aviation Administration.**
**Document is available to the public through the National Technical Information Service, Springfield, Virginia 22161.**

TECHNICAL REPORT STANDARD TITLE PAGE

| 1. Report No. | 2. Government Accession No. | 3. Recipient s Catalog No. |
|---|---|---|
| ATC-180 | DOT/FAA/NR-91/6 | |

| 4. Title and Subtitle | 5. Report Date |
|---|---|
| Terminal Doppler Weather Radar<br>Test Bed Operations – Orlando<br>January – June 1990 | 4 November 1991 |
| | 6. Performing Organization Code |

| 7. Author(s) | 8. Performing Organization Report No. |
|---|---|
| David M. Bernella | ATC-180 |

| 9. Performing Organization Name and Address | 10. Work Unit No. (TRAIS) |
|---|---|
| Lincoln Laboratory, MIT<br>P.O. Box 73<br>Lexington, MA 02173-9108 | 11. Contract or Grant No.<br>DTFA-01-L-83-4-10579 |

| 12. Sponsoring Agency Name and Address | 13. Type of Report and Period Covered |
|---|---|
| Department of Transportation<br>Federal Aviation Administration<br>Systems Research and Development Service<br>Washington, DC 20591 | Semiannual Technical Summary<br>1 January through 30 June 1990 |
| | 14. Sponsoring Agency Code |

15. Supplementary Notes

This report is based on studies performed at Lincoln Laboratory, a center for research operated by Massachusetts Institute of Technology. The work was sponsored by the Department of the Air Force under Contract F19628-90-C-0002.

16. Abstract

This semiannual report for the Terminal Doppler Weather Radar program, sponsored by the Federal Aviation Administration (FAA), covers the period from 1 January 1990 through 30 June 1990. The principal activity of this period was the transport and reassembly of the FL-2 weather radar test site from Kansas City, MO to Orlando, FL and the change of radar frequency from S-band used in Kansas City to C-band for Orlando operations. Site operations to prepare the FL-2C radar site for summer testing began in January and continued through May, when testing began.

This report describes the RF hardware, the data collection, the computer systems at site, and the networks between Orlando, FL and Lexington, MA. Also included are discussions of the microburst and gust front algorithm development, data collection, display terminals, and training for Air Traffic Control (ATC) supervisors and controllers.

| 17. Key Words | | 18. Distribution Statement |
|---|---|---|
| weather radar | Doppler radar | This document is available to the public through the National Technical Information Service, Springfield, VA 22161. |
| low-altitude wind shear | TDWR | |
| operational demonstration | Orlando | |

| 19. Security Classif. (of this report) | 20. Security Classif. (of this page) | 21. No. of Pages | 22. Price |
|---|---|---|---|
| Unclassified | Unclassified | 99 | |

FORM DOT F 1700.7 (8-72) Reproduction of completed page authorized

## ABSTRACT

This semiannual report for the Terminal Doppler Weather Radar program, sponsored by the Federal Aviation Administration (FAA), covers the period from 1 January 1990 through 30 June 1990. The principal activity of this period was the transport and reassembly of the FL-2 weather radar test site from Kansas City, MO to Orlando, FL and the change of radar frequency from S-band used in Kansas City to C-band for Orlando operations. Site operations to prepare the FL-2C radar site for summer testing began in January and continued through May, when testing began.

This report describes the RF hardware, data collection, the computer systems at site and the networks between Orlando, FL and Lexington, MA. Also included are discussions of the microburst and gust front algorithm development, data collection, display terminals, and training for Air Traffic Control (ATC) supervisors and controllers.


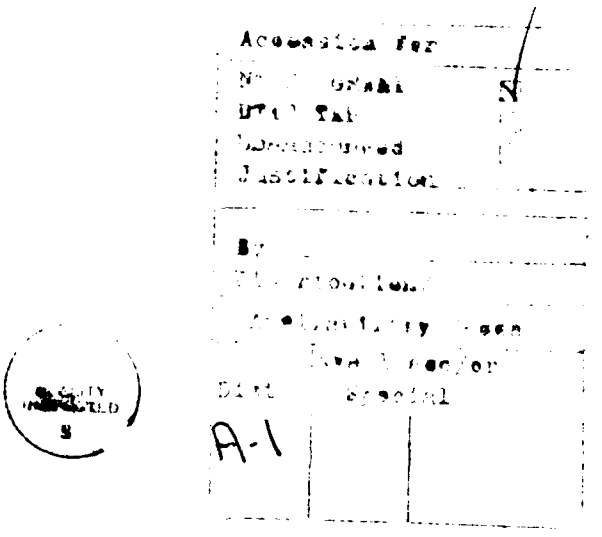

## ACKNOWLEDGMENTS

All the members of the Group 43 TDWR Testbed team made substantial contributions to this report, either through direct work on the project or through writing or contributing to portions of the body of the report. Many team members contributed to one or more sections of the report.

Much credit must be given to the section editors for their diligent efforts and patience in collecting and editing contributions and for much of the actual section writing. Particular thanks goes to Leslie Mahn for her excellent job of tracking contributions, compiling, editing and rewriting, and producing the final copy of a report this comprehensive.

### Section Editors

| | |
|---|---|
| D. Bernella | Introduction and Background |
| W. Drury | TDWR Testbed |
| G. Rappa | Real-Time Computer Systems |
| M. Isaminger | Orlando Site Operations |
| E. Ducot | Data Analysis and Processing |
| B. Stevens | Data Quality |
| D. Klingle-Wilson | Algorithm Development |
| D. Klingle-Wilson | Orientation and Training |
| M. Wolfson | Meteorological Analysis |

### Group 43 Contributors

A. Abrevaya
P. Biron
J. Boisseau
S. Campbell
E. Chornoboy
D. Clark
V. Coel
J. Cullen
S. Dajnak
R. DeLaura
R. DeMillo
D. Diskin
J. DiStefano
A. Dockrey
M. Donovan
E. Eastburn
M. Eby
N. Fischer
K. Flemming
B. Forman
R. Hallowell
N. Hartmann
L. Henshaw
D. Hynek
A. Jackl
M. Liepins
J. Maccini
M. Maciolek
N. Mager
D. McLaughlin
P. Mitchell
O. Newell
S. Olson
P. Pawlak
D. Piercey
J. Pieronek
D. Rhoda
T. Sen Lee
S. Stanfill
B. Stevens
J. Stillson
T. Sykes

J. Anderson (University of Wisconsin)
J. Hansman (M.I.T.)
P. Ray (Florida State University)
R. Srivastava (University of Chicago)
J. Straka (University of Wisconsin)
C. Wanke (M.I.T.)

Special thanks goes to James Evans for his helpful comments and thorough review of this report.

## TABLE OF CONTENTS

TABLE OF CONTENTS
(Continued)

TABLE OF CONTENTS
(Continued)

TABLE OF CONTENTS
(Continued)

## LIST OF ILLUSTRATIONS

## LIST OF ILLUSTRATIONS
## (Continued)

## LIST OF TABLES

# 1. INTRODUCTION

## A. BACKGROUND

For the past several years, the Federal Aviation Administration (FAA) has supported Lincoln Laboratory research in the use of Doppler radar for the detection of weather that is hazardous to aviation . The focus of the research during this reporting period has been in direct support of the Terminal Doppler Weather Radar (TDWR) program which seeks to develop and field a reliable, automated system for detecting hazardous weather (especially low-altitude wind shear due to microbursts and gust fronts) in an aircraft terminal area. Wind shear due to microbursts has caused more US air carrier fatalities in the past 20 years than any other weather hazard.

A key element of the Lincoln program is the TDWR testbed radar (FL-2) which has furnished the weather data used to develop and refine the wind shear detection algorithms being provided to the production TDWR contractor. Additionally, the FL-2 system has been used to develop and test important radar signal processing features (e.g., for suppression of ground clutter, velocity dealiasing, and avoidance of wind shear data obscuration by range aliased returns from distant storms) and candidate TDWR scan strategies.

The first use of the FL-2 testbed was in 1985 at a site near Olive Branch, MS. This site was located approximately 10 miles southeast of the Memphis International Airport in Memphis, TN. Figure 1-1 shows the exact location of the site relative to the airport, along with the locations of 30 ground-based Mesonet weather stations and a C-band Doppler radar operated by the University of North Dakota (UND) as part of the TDWR program. At the Memphis site and all subsequent sites, both the UND C-band radar and the Mesonet stations were used for off-line analysis to verify detections and to help identify missed detections or false alarms.

The testbed commenced gathering data early in the summer of 1985 and continued through various weather conditions into November 1985. During the period, 102 microbursts and 79 gust fronts were identified, either in real time or during off-line playback analysis activities.

The testbed and all other components of the program were dismantled in December 1985 and shipped to Huntsville, AL to gather data in another geographical environment and also to participate in the NWS/FAA/NASA-sponsored Microburst and Severe Thunderstorm (MIST) program as part of the Cooperative Huntsville Experiment (COHMEX). Although the individual goals of the various MIST experiments were different from the goals of TDWR operations, much of the data gathered from the individual sensors were useful for reference and verification of data.

General operations in Huntsville began in April 1986 and lasted until January 1987. During this period, data recording was much more reliable than the previous year because of several enhancements both to hardware and software. Figure 1-2 shows a comparison between the number and strength of microbursts that were detected in 1986 versus those detected in 1985. The figure shows that the number of strong events (i.e., >25 m/s) was about equal in both years. However, a higher number of weaker events were detected in 1986. This fact is explained by the enhanced radar performance and increased operator experience in 1986.

Microburst data from Memphis were used to develop an initial microburst detection algorithm based on analysis of the surface outflow velocity field. Promising results with this algorithm provided the basis for the FAA to commence with a formal TDWR development program. Subsequent data sets from Huntsville were used to refine the microburst detection algorithm to include the use of storm features aloft. In addition, the radar operational experience gained with FL-2 was used as the basis for specification of many key features in the TDWR Technical Requirements document.

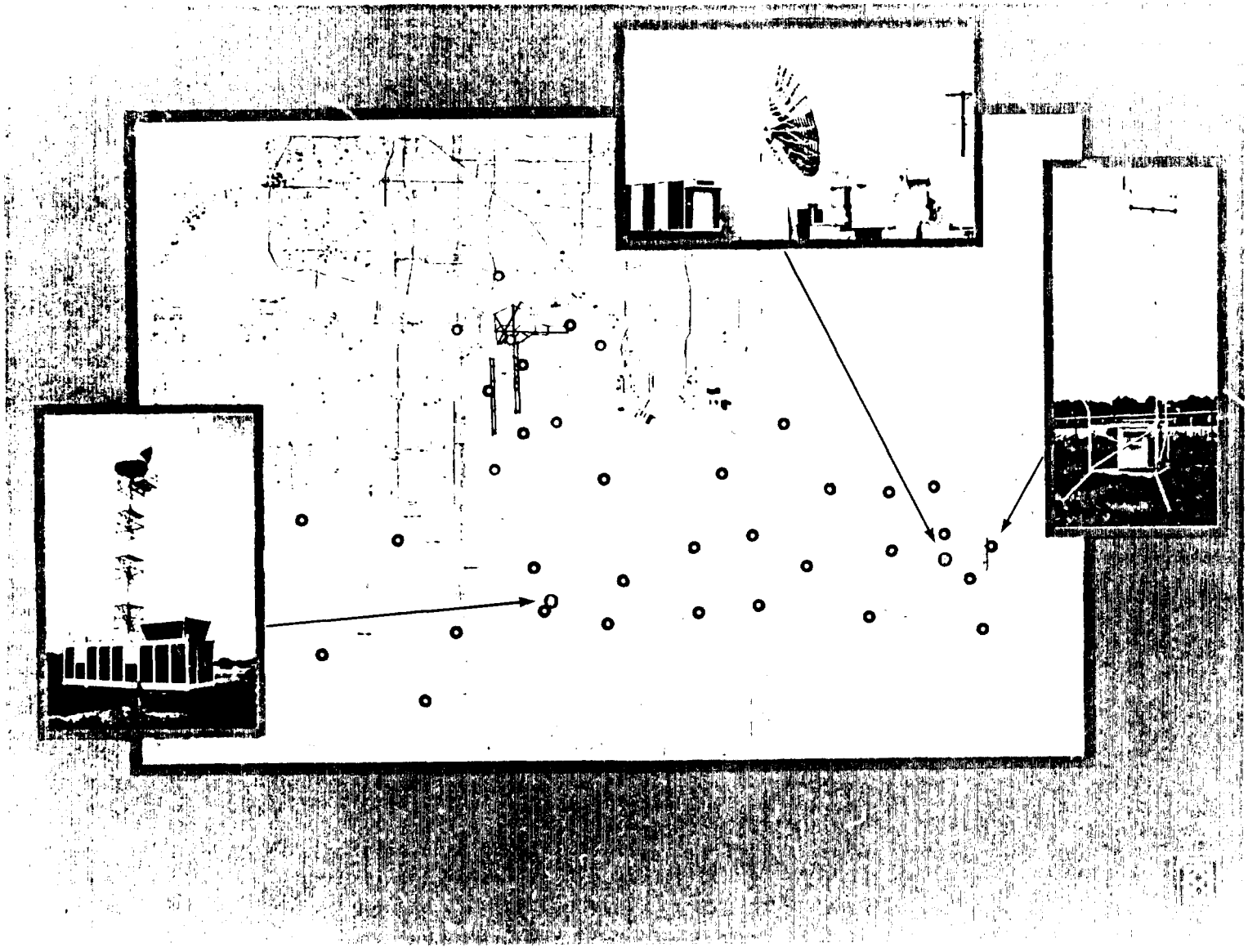

*Figure 1-1. Locations of site near Olive Branch, MS, 30 ground-based Mesonet weather stations, and C-band Doppler radar operated by UND.*

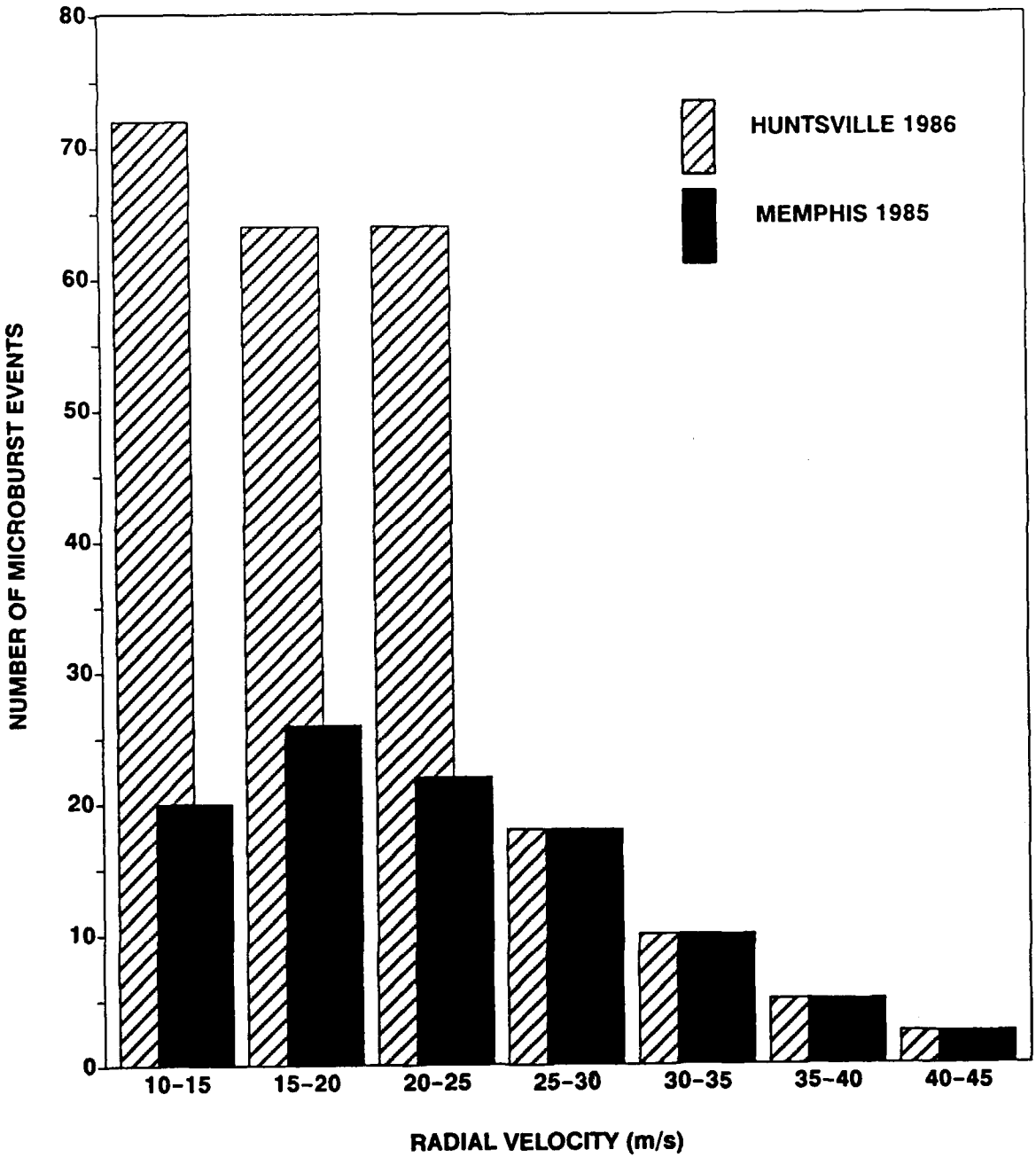


*Figure 1-2. Comparison of the number and strength of microbursts detected in 1986 versus those detected in 1985. Subsequent testing in 1987-1990 generally found many more microbursts than were detected in 1985-1986.*

Following the Huntsville operation, the system was moved to Denver, CO where studies from earlier years (e.g., JAWS [1] and CLAWS [2]) showed a high incidence of "dry" microbursts. The "dry" microburst, with little water content to provide radar backscatter, is a particularly stressing situation for the radar and the wind shear detection algorithms. Another reason for working in the Denver area was to prepare for an Operational Demonstration of the TDWR concept in conjunction with the Stapleton International Airport in 1988. If successful, the demonstration would lead to a TDWR production contract being implemented in a faster-than-usual time frame.

The radar and associated program components were disassembled and shipped to Denver, CO in March 1987. During the 1987 summer storm season, data was gathered on many different hazard-producing weather systems. Algorithm development continued and performance was evaluated and compared with the Huntsville and Memphis results. Radar system upgrades were implemented in anticipation of the 1988 Operational Demonstration, as were scan strategies and operational procedures.

A gust front algorithm developed by the National Severe Storms Laboratory (NSSL) was tested extensively for the first time during 1987. A team from Lincoln Laboratory and NSSL worked closely to develop an improved version of the algorithm for the 1988 demonstration. Algorithms developed by Lincoln Laboratory to minimize contamination of data by range aliased weather echoes (through adaptive selection of pulse repetition frequency) were refined and tested.

The 1988 Operational Demonstration during June, July and August was very successful. [3] Figure 1-3 shows that the distributions of radial shear velocities were essentially the same in Denver as in Huntsville, but with a much higher incidence in the Denver area. On the basis the successful operation, the FAA initiated a contract through a competitive bid to produce 47 production TDWR systems. The Raytheon Company, Sudbury, MA, was the successful bidder for this contract.

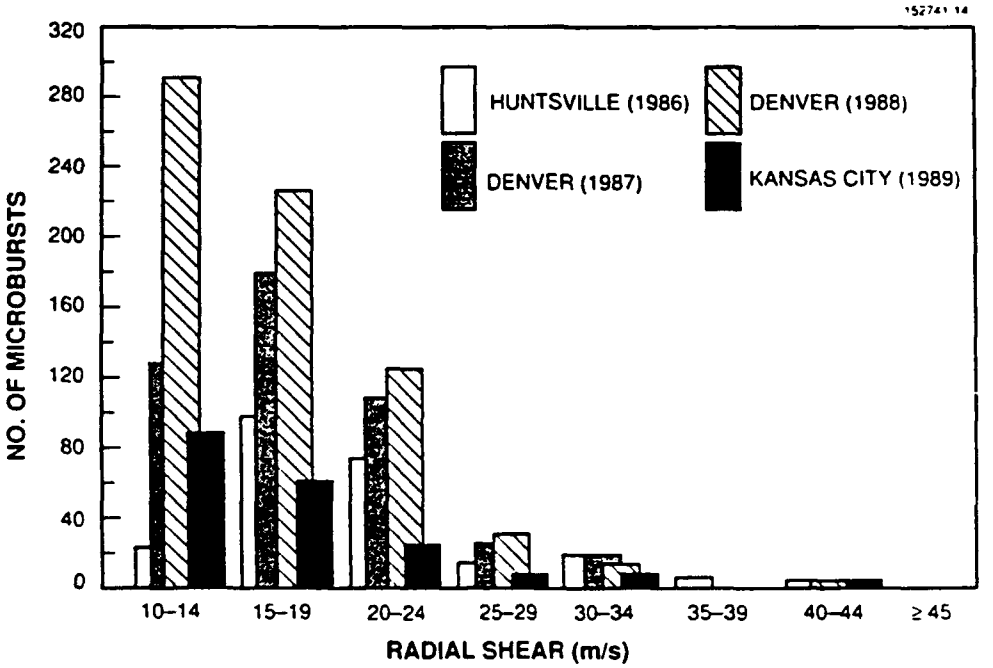


*Figure 1-3. Distribution of the radial shear across microbursts for 1986-1989 measurements.*

To continue refinement of the wind shear detection algorithms in concert with early development work by Raytheon, the FL-2 testbed was moved to Kansas City for the 1989 summer storm season. This move was to facilitate evaluation of fast moving storms traveling across the midwest plains. Further tuning of the detection algorithms was required to cope with a high false-alarm rate noted in Kansas City area.[4] The results of the Kansas City experiments were analyzed and some modifications incorporated in the FL-2 testbed software.

Finally, the testbed was dismantled in October 1989 and shipped to Orlando, FL to operate in the unique environment of central Florida. The area around Orlando and Tampa has the highest incidence of thunderstorms in the US. During the move to Orlando, Westinghouse Corporation was modifying the testbed transmitter to operate at C-band, the RF frequency band designated for the production TDWRs. Also, the testbed signal waveforms, signal processing, and product display system were modified to reflect the features of the Raytheon production TDWR design. The Orlando operations will be the last major weather environment for testbed operations before the production TDWRs become deployed.

## B. SUMMARY OF THIS REPORT

The following sections of this report cover the testbed operation for the period from 1 January 1990 through 30 June 1990. During this period, the majority of emphasis was on preparation for and participation in an Operational Demonstration scheduled to begin on 18 June 1990 and to extend until 28 August 1990. The specific objectives of this demonstration were to evaluate the following items, both from technical and air traffic control (ATC) user viewpoints:

a. Microburst detection,

b. Gust front detection and wind shift prediction,

c. TDWR warning functions,

d. TDWR as a planning tool,

e. System operation at C-band with 0.5 degree antenna beamwidth,

f. TDWR/Geographic Situation Display (GSD) product display formats and user interfaces,

g. New products, such as storm motion, and

h. Raytheon-developed TDWR data quality algorithms.

Section 2 of this report describes the site construction and system reassembly in Orlando, FL, as well as the modifications made to the testbed hardware and digital signal processors. Section 3 discusses the real-time computer systems, their operations, and interactions with the overall system. Hardware failures caused by the move from Kansas City, along with the system's substantial modifications, created many challenges for the testbed personnel, and maintaining reliable operation became a critical issue.

Section 4 covers the measurements and operation employed in getting the system ready for the Operational Demonstration. These operations included the TDWR, Low-Level Wind Shear Alert System (LLWAS) and Mesonets, the UND radar and aircraft, and weather balloon soundings. Data processing and analysis procedures and tools available during this period are discussed in Section 5, whereas Section 6 provides details on the data quality issues and how they interact with the wind shear algorithms.

The work and results of the algorithm development and evaluation are described in detail in Section 7. Section 8 presents a discussion on ATC personnel training, the results of past training in Denver and Kansas City, and changes implemented for the Orlando operation. And finally, Section 9 presents several meteorological issues resulting from work over the past several years.

# 2. TERMINAL DOPPLER WEATHER RADAR TESTBED REFINEMENTS AND OPERATIONS

## A. RF HARDWARE

### 1. Radome

The antenna radome is an inflatable, Teflon-coated fiberglass bag, 55 ft in diameter, manufactured by Chemfab Corporation of Buffalo, NY. Inflation of the bag is maintained by a dual-blower pressure system controlled by an external anemometer. Pressure is kept at three inches of water, unless the wind velocity exceeds 55 mph, when the pressure is raised to seven inches of water. The radome has protected the antenna and pedestal for the past six years at four different sites. It has exhibited no problems and has required no maintenance.

The radome was folded, loaded into a covered trailer, and transported from Kansas City to Orlando. It was erected in May without incident and it has not exhibited any problems.

### 2. Antenna

The antenna consists of a 33-ft diameter parabolic reflector and a horizontally-polarized, focus-mounted feed system. The reflector and feed support structure was designed, built, tested and installed by H&W Industries of Cohasset, MA. The RF feedhorn was designed and fabricated at Lincoln Laboratory. The antenna has been in use since 1984 at sites in Memphis, Huntsville, Denver, Kansas City, and Orlando. It has exhibited no problems, and maintenance has consisted of periodic tightening of the bolts in the back-up structure.

The antenna was disassembled after the 1989 summer operations in Kansas City, MO. The antenna sections were returned to the manufacturer to be reassembled and fitted with a new feedhorn and waveguide, reflecting the change of radar frequency from S-band to C-band. Pattern measurements were taken on the test range at H&W, with the following results:

| | |
|---|---|
| Gain: | 52 dB |
| Beamwidth: | 0.42° |
| Level of first sidelobe (azimuth): | -24 dB |
| Level of first sidelobe (elevation): | -22 dB |
| Efficiency (approximate): | 63 percent |

Since the reflector had been in constant use as well as disassembled, moved and re-assembled five times since manufacture, it was decided to survey the surface tolerance while the unit was at H&W. The original specified tolerance was .035 in, and the measured tolerance when delivered six years ago was .026 in. The tolerance as measured at H&W was .028 in. In view of the service that the reflector has provided, it is indicative of the excellent H&W design and workmanship that the surface exhibited such a small degree of degradation.

The antenna was shipped to Orlando in April and erected at the new site without incident. It has been operating since that time with no maintenance, except for the aforementioned periodic bolt tightening.

### 3. Pedestal

The Scientific Atlanta model 3315 pedestal was obtained from the FAA Technical Center in 1984. It was modified by the Lincoln Laboratory Control Systems Group to meet the Next Generation Weather Radar (NEXRAD) and TDWR Technical Requirement of 30°/sec peak azimuth velocity. The new azimuth gearbox was equipped with a forced-flow lubrication system. The synchro-to-digital converter (SDC) that encodes the antenna position was replaced with a unit that performs conversions at a rate which supports the maximum velocity of the pedestal.

Upon removal from the Kansas City installation, the pedestal was shipped to Lincoln Laboratory for evaluation and rework. Measurements for wear, hardness and backlash were made on the azimuth gear systems. One pinion gear showed excessive wear, and that gearbox was returned to the manufacturer for rebuilding. Since the bull gear also showed considerable wear, the spare azimuth platform was used when re-assembling the pedestal. The platform contains the bull gear and azimuth bearing. The new, spare gearbox also was installed during re-assembly in place of the worn gearbox.

While at Lincoln Laboratory, the S-band rotary joints were replaced with C-band units. The azimuth joint had to be relocated because it was formerly housed in the pedestal extension tube which was not used at Orlando.

The pedestal was installed in April and has since performed without incident. The C-band rotary joints were manufactured with extremely close internal tolerances, and the elevation unit seized after about one month of use because of misalignment of the waveguide during installation. The spare joint was installed and the damaged unit returned to the vendor for rework with larger tolerances.

### 4. Transmitters

The S-band transmitter is one channel (modified) of a regular production ASR-8 radar on loan from the U.S. Navy. This transmitter was used for the experiment in Kansas City and was moved to Orlando intact since, at the time of the move, it was not clear that we would be shifting operations to C-band for the 1990 season.

A C-band transmitter was custom built for Lincoln Laboratory by Westinghouse Electric Corporation of Baltimore, MD. This transmitter uses technology employed in the Airport Surveillance Radar (ASR-9) and NEXRAD S-band transmitters, both of which were built by Westinghouse. The only C-band klystron amplifier available in 1990 was the VKC-7762B manufactured by Varian for the U.S. Navy Terrier Missile System. Two such tubes were procured for use in this transmitter. In order to emulate the TDWR transmitter currently being manufactured by Raytheon, the VKC 7762B was operated at about one-fourth its normal output power. In this mode, the tube is very inefficient, requiring both excessive RF drive power and beam current. Westinghouse has used a traveling wave tube (TWT) amplifier as a driver and a specially designed, highly regulated high-voltage power supply. In addition, the focus magnet for this tube requires much more power than that of either NEXRAD or ASR-9, so a free-standing, high-current DC power supply was installed adjacent to the transmitter cabinet.

A second complication of using the VKC-7762B was the requirement that it be liquid cooled. A heat exchanger unit was mounted outside the radar shelter, with large-capacity hoses connected to a manifold on the rear of the transmitter cabinet. Water is circulated at a rate of 23 gallons per minute, and the radiator is capable of transferring 22 kW of heat from liquid to air.

Protection is afforded by closely monitoring both temperature and flow-rate in the transmitter cabinet. Specifications for the transmitter are:

| | |
|---|---|
| Radiated frequency: | 5500-5650MHz |
| Peak power: | >250 kW |
| Pulse width: | 1 μ sec |
| Pulse repetition rate: | 325-2400 pps |
| Integrated instability ratio: | at least -55 dB (design goal) |

In final testing, stability of about -52 dB was demonstrated at pulse repetition frequencies (PRFs) below 2000, with about 3 dB degradation at 2400 pps. It was determined that performance is impaired by a 60-Hz component in the TWT output spectrum. When the stability of the transmitter alone was measured, it was found to be about -57 dB at PRFs below 2000.

It was noted that the output spectrum of transmitter energy was wider than one would expect from the phase-pushing characteristics of the klystron tube. Investigation revealed the cause to be excessive rounding of the top of the modulator pulse waveform. This proved to be a heretofore unknown characteristic of the ASR-9 modulator as well, resulting in wasted power since the transmitted spectrum exceeds the receiver bandwidth.

To install the transmitter in time for the 1990 storm season in Orlando, it was decided to accept it with the proviso that Westinghouse would continue to work on stabilizing the TWT driver amplifier using the spare unit and that further investigation would be done on the ASR-9 modulators to reduce the spectral widening. Final testing took place in Baltimore in April, and the transmitter was installed on site near the end of that month. The S-band ASR-8 transmitter was removed and shipped to Lincoln Laboratory for storage.

The C-band transmitter continued to perform well throughout the reporting period. A water leak developed in the cooling manifold at the rear of the cabinet, and Westinghouse is having a replacement manifold manufactured.

Slight modifications to the internal control circuits were performed to give positive local control of high-voltage activation and waveguide switch position. These features were not implemented in the ASR-9 system.

### 5. Receiver/Exciter

The receiver and exciter chassis were designed and built by Lincoln Laboratory. Both units contain many built-in-test features which emulate the TDWR radar design. These test features can be controlled from the Concurrent computer or locally from front panel switches. The exciter system provides a one-microsecond pulse of RF at 10 mW power to drive the TWT amplifier. It also provides the five timing pulses necessary to operate and trigger the transmitter and its various regulation circuits. Provision is made to shift the phase of the transmitted pulse and receiver coherent local oscillator (COHO) from pulse to pulse to reduce the effects of second-trip echos.

Some of the exciter functions are contained in the radar controller module. When it was not clear that the new transmitter would be delivered in time for the 1990 season, it became necessary to maintain a radar controller that could accommodate both the S-band and C-band radar systems–two vastly different tasks. Consequently, an add-on package was designed to operate with the existing S-band radar control module. The entire assembly was to be known as the "interim controller." This module permits computer control of the pulse repetition rate, the

COHO phase shifter, high-voltage inhibition and waveguide switch position. Remote control of all the built-in-test features is not implemented, and these features must be initiated from the front panel switches. However, all status signals are passed through the interim radar controller to the Concurrent computer for system monitoring.

A new radar controller is being designed for the C-band system only, and all features will be available from it. The design will not be accomplished in time to install the new module for the 1990 season, but little is sacrificed by using the interim unit.

A key feature of the receiver is the instantaneous automatic gain control (AGC). The received signal is delayed by one range sample interval while the AGC system measures the signal magnitude. The output from a 20-dB coupler is fed through a logarithmic amplifier and then digitized in a six-bit "flash" analog-to-digital (A/D) converter at a rate of 15 Mega-samples per second. A digital peak detector selects the largest A/D output in the range interval, and this number is fed forward to control a digital attenuator in 3-dB steps. This control value is also passed to the signal processor. The amount of inserted attenuation serves to keep the in-phase and quadrature (I and Q) video signals within the 60 dB range of the following 12-bit A/D converters on a sample-to-sample basis.

The receiver has about 109 dB gain, with nearly 100 dB instantaneous dynamic range. Not all of the dynamic range is useful, however, due to limitations in the signal processor subsystem. Receiver noise is about -105 dBm.

Sensitivity time control (STC) is accomplished by a digitally controlled attenuator constructed as an integral part of the transmitter/receiver (T/R) limiter switch. Normal operation utilizes an STC curve that inserts attenuation inversely to the second power of radar range at all ranges less than 10 km.

The receiver/exciter equipment was tested in Kansas City to the degree possible without a transmitter. It was moved to Orlando and installed in place of the S-band equipment where it has continued to perform in the manner intended.

### 6. Plans for Next Reporting Period

The radar will be operated much of the time during the summer and fall in support of the TDWR emulation program which is exporting weather products to the Orlando Airport control tower. There are no plans to make any changes to the radome, pedestal, antenna or receiver/exciter. After the storm season has passed, the transmitter will be moved to Westinghouse in Baltimore where the newly-developed VKC-8387 air-cooled klystron will be retrofitted to it. The new radar controller and a new signal processor that is associated with it will be built, tested and moved to the Orlando site to replace the current signal processor and data acquisition and analysis (DAA) equipment (see section B).

## B. DIGITAL PROCESSORS

The front end digital processors in the FL-2 system perform the initial processing and reduction of the raw data received from the RF Receiver. These processors currently consist of the Signal Processor (SP), a dual set of Data Acquisition and Analysis computers (DDAA), as well as a new generation Data Acquisition and Analysis computer (NDAA). A Radar Controller (RC) also provides the hardware and software interfaces for computer control of the RF hardware.

All of these front end components were designed to meet prior year's requirements for operation of FL-2 at S band, and have been adapted to meet this year's requirements at C band. A completely new Radar Controller (NRC) and Programmable Signal Processor (PSP) are currently being designed and built. This new package will enable FL-2 to meet all operational requirements at C band.

### 1. Signal Processor

The Signal Processor collects the raw digitized I and Q data samples from the A/D converters in the radar receiver. The processed returns are fed to the DAA. This special purpose digital processor was designed and built at Lincoln Laboratory.

Two SPs have been built: one for use in the FL-2 testbed and the other for use at Lincoln Laboratory for hardware and software development. The initial installation was at the Memphis FL-2 site in 1985, after which it was moved to Huntsville, Denver, and Kansas City. This SP is now installed in the Orlando FL-2C testbed.

The functionality of the SP has been increased each year to meet the added requirements for FL-2C operations. These functions currently include the following capabilities:

a. AGC normalization. The data received from the radar receiver is brought into the range of the A/D converters by an AGC circuit. The AGC gain value is used by the SP to convert the A/D data into a 16-bit digital word which compensates for the AGC process.

b. Pulse interference detection and elimination. Successive pulse data returns in the same range gate are checked for anomalous values, and a smoothing algorithm is applied.

c. Zero-Doppler clutter suppression by 39 point FIR filters with notch widths of 1-3 m/s. Several sets of filter coefficients are available at one time, and up to 50 dB of clutter suppression can be obtained. This is the major computational task in the SP, using eight banks of filter hardware working in parallel to obtain the needed computational throughput. Special control logic was recently installed so that the output data compensates for the filter time delay.

d. Integration of the filtered pulse returns in each range gate over the antenna beam width to form the three (0, 1, 2) lag product estimators that are sent to the DDAA computers. Three complex autocorrelators circuits operate in parallel to generate these results.

The Concurrent host computer downloads control parameters to the SP at the start of each antenna tilt. These parameters select the filter coefficients and the operational modes of the SP during each tilt. The integration period for the autocorrelators can be set either to a specific number of pulses or to the times when the antenna slews through an integer degree of azimuth position. The antenna position and other radar information are sent as headers, along with the radar data, to the downstream processors so that validity of the data can be determined.

A time series buffer (TSB) port was recently added to the SP so that radar pulse data, filtered or unfiltered, from selected parts of the radar volume scan can be sent directly to the host Concurrent computer for specialized processing.

A fundamental change was made in the clock signals in the SP for this year's operations in C band. The range sampling interval in previous years for S-band operation was 120 meters, which required an 800 nanosecond clock. The C-band mode uses a 150 meter range gate and a one-microsecond clock. The maximum radar PRF and the range data collection modes also have been changed for C-band operation. All of the modifications necessary have been installed and the SP is working satisfactorily after the move to Orlando.

### 2. Dual DAA

Two parallel Data Acquisition and Analysis processors (DDAA) transform the autocorrelator lags data from the SP into the compressed factors data format used by the Real Time System in the Concurrent host computer. The DDAA also acquires antenna and control status information and aircraft beacon messages. These are merged in the proper sequence with the factors data for the host computer.

The DAAs are Lincoln Laboratory-built processors that were designed to be used in conjunction with the Signal Processor. Two are installed in the FL-2C testbed in order to meet performance and throughput requirements. One additional processor is used at Lincoln Laboratory for hardware and software support and development.

Each DAA contains three identical programmable Processor Elements (PE) which communicate through a multi-ported memory. All of the computational processing and the data collection from the SP is performed by these PE's. An additional monitor processor element performs all the communications with the Concurrent host computer. One of the two DAAs in the testbed had a multiplexer input which is used to collect the aircraft beacon and real-time clock data. The application software in both DAAs is identical.

The SP divides the data it sends to the two DAAs at the half-range point so that each DAA has approximately the same workload. The two DAAs process each radial of lag data in parallel and send the results to the host computer. There the half-radials of factors data are merged into full radials before further processing is performed.

Only minor changes were required in the DAA software for C-band operations at Orlando. One change was to adapt to the new range data collection modes, and the other for a change in aircraft beacon messages. The DDAA is currently operating satisfactorily at the Orlando site.

### 3. New DAA

A new DAA (NDAA) processor was installed in the FL-2 testbed at Kansas City shortly before the end of the 1989 summer operations. This consists of a set of three programmable high-speed vector processors, and a Sun-4 workstation. The vector processors obtain filtered pulse data from the Signal Processor and perform the computation-intensive tasks of autocorrelation and factors generation. The Sun-4 reformats the factors data for the Concurrent host computer and also performs the other data management and control functions of the DDAA.

Operation of the NDAA at Kansas City was satisfactory, with some improvement in data quality from the increased word length and dynamic range in the computational elements of the new processors. Modifications to the NDAA for operation with the C-band system after the move to Orlando were less successful than with the other processors. The NDAA consistently lost synchronization with the SP after less than an hour's operation.

### 4. Programmable Signal Processor

A completely new set of front-end processors is currently being developed for the testbed to permit full use of the C-band capability for FL-2 and to provide comparable functionality to the FAA production TDWR radar system. This new package will contain a new RC to control the radar and a new PSP that performs all the functions of the SP and the DAAs.

### a. Radar Controller

A new RC that will support the C-band radar and the new PSP was designed and built during this reporting period. The RC receives commands from the Concurrent Control Computer (CCC). It interprets these commands to provide the appropriate control signals for the radar transmitter and receiver and for the antenna positioning hardware. The RC also provides the CCC with complete radar status and National Bureau of Standards (NBS) time of year received via satellite.

Additionally, the RC collects digitized video and AGC values from the receiver. It provides this data to the PSP on a pulse-by-pulse basis at real-time rates, along with pertinent radar status and time information. The control computer's start-of-tilt and scan parameters and PSP control information are also merged with the data stream. The merging of control, data and status in the RC obviates the need to synchronize data and control information downstream in post-processing programs, a requirement that has proven difficult to satisfy in the past. A subset of the data stream is stored in a buffer for access by the control computer and used for pre-mission system calibration and diagnostic testing.

The RC contains fully redundant logic with built in test features that permit fault detection and hardware substitution by the CCC. Also included are a radar antenna simulator and a digitized video simulator that are used for off-line control software and algorithm testing, and for system diagnostics and fault isolation.

Construction of the RC is now complete. Additional redundant hardware will be built and installed after testing and integration with the radar system at the testbed site is complete.

### b. Programmable Signal Processor

A new signal processing system has been designed which will replace the existing signal processor and DAA used in the FL-2 field system. A similar signal processing system is currently operating in the FL-3 system. The new system is based on commercially-available, single-board computers and single-board math accelerators. The system consists of three modules: Signal Processor, Time Series Buffer, and Control Processor.

#### *Signal Processor*

The signal processor design consists of 20 Mercury Computer Systems MC3200 Math Accelerator boards housed in two VME-bus card cages. Each of the MC3200 boards operates at a peak processing speed of 25 MFLOPS (Million Floating Point Operations per Second), yielding a total peak processing capability of 500 MFLOPS for the entire system. All calculations are performed using IEEE standard 32-bit floating point numbers. The signal processor boards will perform the following functions:

1. AGC normalization,

2. Pulse Interference Detection/Discrimination,

3. Clutter Filtering–39 tap finite impulse response filter or six-pole infinite impulse response filter,

4. Autocorrelation, lags (moments 0, 1, 2)

5. Reflectivity,

6. Velocity, and

7. Velocity spectral width.

Each of the two signal processor card cages will have an input processor consisting of a MC68030-based single board computer and a custom interface board. The input processor supplies raw in-phase, quadrature, and AGC data from the radar to the math accelerators. Ancillary data such as transmitter timing, antenna position, and control information is disseminated to the math accelerators via the input processors. All data passed to the math accelerators is transferred via VME bus block mode transfers at burst rates of 25 Megabytes per second. The signal processor card cages are connected to the control processor via VME bus couplers.

*Time Series Buffer*

The time series buffer consists of an input board similar to the one described above for the signal processor, a 32-Megabyte memory board, and a tape drive controller with two nine-track tape drives. Data is generated by the radar at a constant rate of four Megabytes per second. The time series buffer will be able to capture data at an average data rate of 0.5 Megabytes per second–a speed limit imposed by the nine-track tape drives. The system can capture up to eight seconds of the full data stream in the 32-Megabyte memory board which can then be recorded on tape at the 0.5 Megabyte per second rate. It is also possible to select a small portion (12 percent) of the data stream and record it continuously on tape. Should there be a requirement for higher data rate recordings, faster recording devices can be connected to the time series buffer.

The time series buffer can also provide a limited range of test signals to the signal processor to provide a stand-alone digital test capability.

*Control Processor*

The control processor consists of a Sun model 3/120 computer system in a VME card cage, a video controller, a color monitor, a tape drive controller, two nine-track tape drives, and a MC68030-based single-board computer. The control processor is connected to the signal processor and time series buffer via VME bus couplers. The control processor is connected to the Concurrent computer system via a DR11-W interface board.

The Sun computer in the control processor initializes and loads the real-time software into the math accelerators and all of the single-board computers used elsewhere in the system. It also can be used as a development tool to write and debug software used in the math accelerators and the single-board computers.

The single board computer in the control processor performs the following functions:

1. Interrogation of all of the math accelerators and readout of results from them as they become available,

2. Concatenates the output from the signal processors into logical radial structures,

3. Sends the radial data to the Concurrent computer system for further processing,

4. Sends the radial output to the video controller which provides a real-time diagnostic display, and

5. Records the output data on nine-track tape.

*Software*

Approximately 95 percent of the software for the signal processing system is written in the C programming language. A few routines which are computationally intensive are microcoded in the math accelerators or written in assembly language for the single-board computers. Heavy use of a scientific algorithm library for the math accelerators keeps the system performance at an acceptable level.

The data coming into the system is divided on range boundaries by the input processors for signal processing by the math accelerators. For example, if the system is processing 800 range gates per transmitted pulse, the input processor will supply data for 40 range gates to each math accelerator board from each pulse. The input processor formats and transfers only the data required by each math accelerator in the card cage in which the input processor resides. By using two card cages and isolating bus couplers, each bus receives half of the load that a single bus system would receive.

The math accelerator boards operate autonomously. Each board operates on the data which it receives, without interaction with the other accelerator boards. Output data is stored in circular buffers capable of storing several seconds of data, giving the single-board computer in the control processor ample time to retrieve the output.

The single-board computer in the control processor queries the math accelerator boards several times per second and removes the data stored in their output buffers. Synchronization data stored with each set of output data is used to re-assemble the pieces of data for each radial. The single-board computer has access to the output data from the autocorrelators, output from factors processing (an intermediate product), and output from moments processing (reflectivity and velocity estimates). The single-board computer will send the moments data to the Concurrent computer and to the video controller.

The control processor has access to the tape drives in the time series buffer card cage when time series data is not being recorded. Therefore, the system can record any two of the following products simultaneously:

1. Time Series Buffer Data (raw I and Q),
2. Autocorrelator output,
3. Factors, or
4. Moments.

Under normal operating conditions, factors output will be recorded on nine-track tape. At this time there is no plan to record either the autocorrelator output or the moments output, except for diagnostic use.

Diagnostic software for the system will consist of at least the following tools:

1. Single Gate Processor (SGP),
2. A-Scope,
3. Autocorrelator and I/Q data display,
4. Ramp test,

5. Buffer test, and

6. Synchronization test.

Error logging will be supported using the Sun computer in the control system. Errors detected during operation will be recorded on disk and will be displayed on the console.

***Plans for Next Period***

All of the major components of this processing system have been ordered. During the next reporting period, efforts will focus on the design and development of real-time software and diagnostics. The input interface that transfers data from the radar controller to the input processor will also be designed in the next period.

# 3. REAL-TIME COMPUTER SYSTEMS

A network of minicomputers and workstations provides the link between the front-end radar data acquisition hardware at the Orlando, FL field site (FL-2C) and the displays in the ATC Tower. This network connects a 3280MPS multi-processor super-minicomputer manufactured by Concurrent Computer Corporation, nine Sun servers, four Sun workstations, and two Symbolics LISP machines. A simplified view of the network is depicted in Figure 3-1. This figure illustrates the three independent ethernets that provide interprocess communication:

a. The base data ethernet, a raw ethernet (no handshaking) for base data broadcast at real-time rates.

b. The products ethernet, which doubles as the channel for algorithm product data communication between processors and the system backbone for file access.

c. The tower ethernet, which serves the same function in the tower as the products ethernet does at FL-2C.

The 3280MPS (RTS) is the main computer at FL-2C. It is used for real-time control of the radar system, radar antenna movement, signal processor, and DAAs (and is also the host for DAA software). Additionally, it performs high-speed data recording, display computation and management, system control, and data communication.

Some detection algorithms, such as the storm motion algorithm and the National Severe Storms Laboratory (NSSL) version of the gust front algorithm that was used operationally, execute on RTS, but the bulk of the post-base-data-generation functions (detection algorithm execution, analysis and tower display creation, data and product service) are distributed across the Sun and Symbolics systems at both FL-2C and the Control Tower. The assignment of functions to systems is summarized briefly in Table 3-1.

The data flow throughout the network begins with conditioned base data generated by RTS and broadcast on the base data ethernet to selected algorithms on the Sun processors. From the base data, the algorithms (whether executing on the Suns or the Concurrent) generate either intermediate or final products. These products are written in a Lincoln-specified archive format. Each machine relies on a combination of vendor-supplied transmission control protocol (TCP) networking software and Lincoln-developed communications management software to transmit and interpret these product records. Product traffic is carried on the product ethernet at FL-2C. Selected products, required to produce the displays in the tower, are transmitted over a 56 kilobaud synchronous communication link to the Tower ethernet where the products are available to the remote display systems. (The link between Ted at FL-2C and Tracon located in the Terminal Radar Approach Control facility (TRACON) at the Control Tower supports the flow of products.)

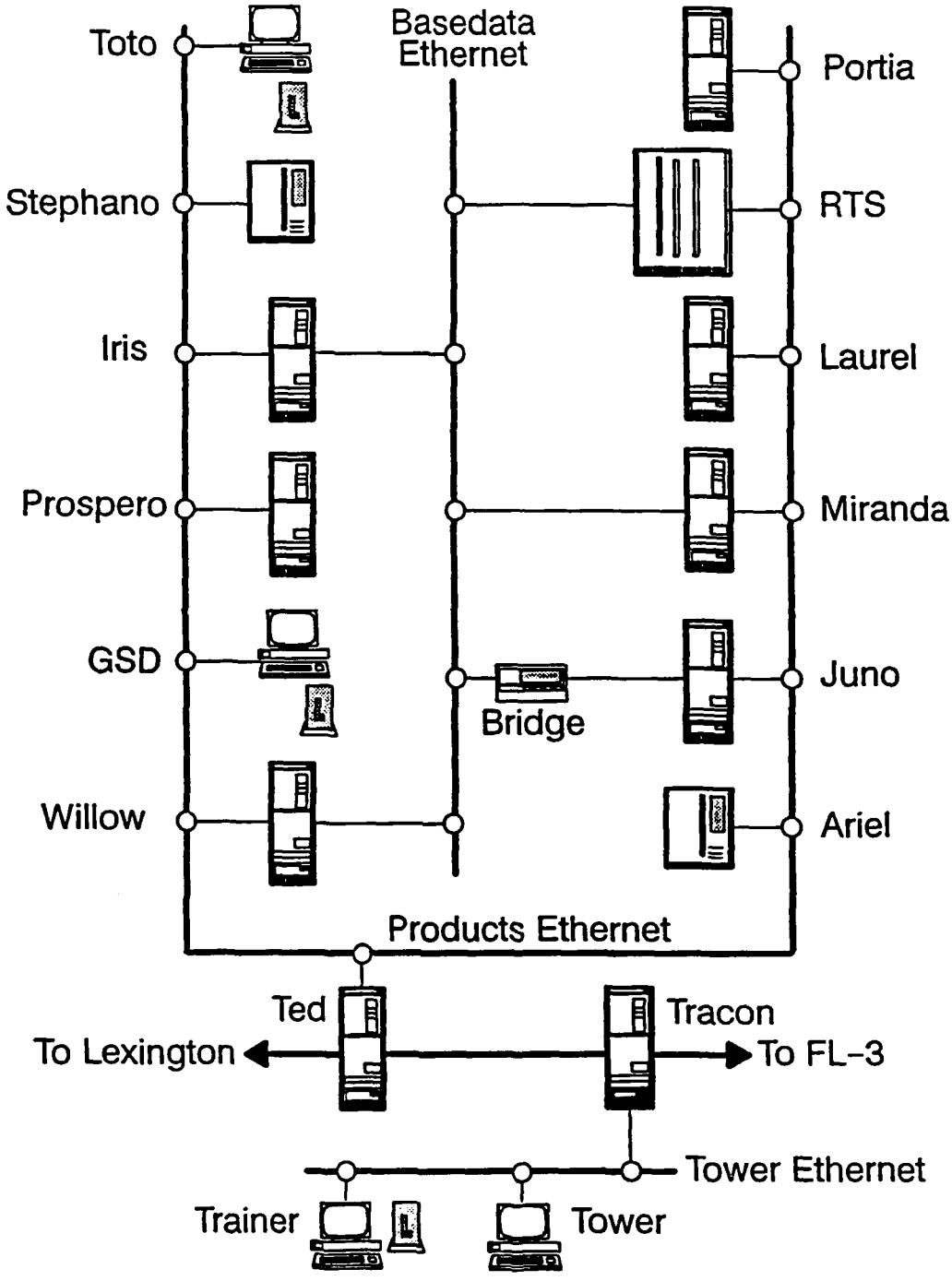


*Figure 3-1. Testbed computer network.*

## Table 3-1.
## Processor/Function Assignment.

| Name | Type | Function |
|---|---|---|
| RTS | Concurrent 3280MPS | Real-time control (radar system, antenna, signal processor, DAA<br>Data recording<br>Data quality editing<br>Data distribution<br>Gust front, PRF Selection, Storm Motion, Precipitation, and Tornado Vortex (TVS) algorithm execution |
| Juno | Sun 4/260 | Microburst feature extraction<br>Microburst shape generation |
| Ariel | Symbolics 3650 | 3D microburst structure recognition<br>Microburst alarm generation |
| Iris | Sun 4/330 | Advanced gust front feature extraction |
| Stephano | Symbolics 3650 | "Hot" spare for Ariel<br>Gust front feature association and discrimination (AGFA)<br>Gust front detection and hazard generation (AGFA) |
| Prospero | Sun 3/280 | Gust front update processing<br>Cockpit display generation and management<br>System heartbeat generation |
| Willow | Sun 3/480 | Real-time resampling<br>Gust front display and truthing system support |
| Laurel | Sun 3/260 | Microburst display and truthing system support |
| Miranda | Sun 4/260 | Significant weather identification<br>Scan mode processing<br>Product data recording |
| Portia | Sun 4/280 | New DAA control (not used operationally) |
| Ted | Sun 3/160 | Communications gateway management |
| GSD | Sun 3/60C | GSD server execution<br>GSD processing and display |
| Tracon | Sun 3/260 | GSD processing and display (runway configurations slave to Tower)<br>Communications Gateway Management |
| Tower | Sun3/60C | GSD processing and display |
| Trainer | Sun 3/60C | GSD processing and display (demonstration system) |
| Toto | Sun 3/60C | Spare |

## A. CONCURRENT REAL-TIME SYSTEM

### 1. Concurrent 3280 MPS Hardware

During the second half of the reporting period (once the site had been reassembled in Orlando), there were chronic (though infrequent) system crashes which were traced to failing circuit boards and out-of-revision boards which contained engineering errors. Concurrent maintenance personnel determined that many of the boards in the system were several revisions old; they ordered new boards and made plans to upgrade the system. Meanwhile, the occasional system crashes had to be tolerated since compatible replacement boards were unavailable.

### 2. Real-Time System Software

The FL-2 Real-Time System (RTS) operates in the Concurrent Computer Corporation (formerly Perkin-Elmer) Model 3280MPS minicomputer. Its functions are:

a. Acquisition of preprocessed radar sample data (factors) from the DAA.

b. Recording of DAA data on magnetic tape.

c. Converting the DAA factors data to base data (signal-to-noise ratio (SNR), reflectivity, velocity, and spectrum width) for each radar sample gate.

d. Conditioning the base data by applying data quality editing procedures.

e. Resampling the base data from polar to rectangular coordinates for output to color displays.

f. Transmitting resampled base data images and other weather products to remote computer systems and workstations.

g. Providing a real-time database and hosting environment for algorithms for automated detection of hazardous weather phenomena.

h. Providing manual and semi-automated operator control over recording, processing, and display of weather data.

#### a. Data Acquisition and Recording

This portion of the RTS is responsible for reading radar data and other information (such as aircraft beacon reports) from the DAA (or dual DAAs) via a direct memory access (DMA) link and for recording the data and information on 6250 bpi/125 ips magnetic tape drives. The DMA link is either custom-built at Lincoln Laboratory or it is a Digital Equipment Corporation DR11-W, depending on the version of DAA being used. This capability was not changed during the reporting period.

#### b. Base Data Generation and Conditioning

In this intermediate processing step, base data (signal-to-noise ratio, reflectivity, velocity, and spectrum width) are produced from the DAA factors. This process is computationally demanding and so is performed largely by table look-up. This is an optional stage in the data path since current plans are for front-end computers to perform this operation.

Once the base data have been generated, they may be conditioned by application of various data quality editing procedures. Currently available editors are (in order of their application):

a. Raytheon point target removal (new for 1990).

b. Clutter residue map-based editing.

c. Range obscuration editing.

d. Raytheon velocity dealiasing (new for 1990)

Only minor changes were required for the testbed conversion to C-band. A more substantial enhancement was the implementation of a new base data format to improve the performance of the point target removal and velocity dealiasing software. New format base data are converted to the more compact standard format before distribution to the rest of the system.

The base data distribution procedure was modified to take advantage of the "tilt reason code" established with the scan editor. Using the information in this code, each tilt (scan of the radar at a given degree of elevation) can be individually targeted for the appropriate tasks (editors and algorithms); non-targeted tasks do not receive base data, thus reducing intertask communication, contention for shared memory access, and to a lesser extent, central processing unit (CPU) time. However, the primary motivation for this enhancement was the need to differentiate between the "first" and "second" dual scans used as part of the Raytheon velocity dealiasing algorithm. This differentiation is scan strategy-dependent and must be specified with the scan editor.

**c. Data Distribution**

Data distribution is a two-stage process, beginning with the data as recorded on tape and ending with whatever task (e.g., resampler, or weather detection algorithm) might request the data:

a. Physical records received from the DAA are placed in "tape buffers" for recording. The tape buffers are accessed by a series of intermediate processing tasks which extract and derive particular pieces of information (e.g., radar sample data, aircraft beacon reports) to be distributed to the rest of the system.

b. After intermediate processing, the data are distributed to the rest of the system via a "data stream" mechanism. Each stream represents a particular type of data and may be accessed by any task in the system.

Data are not dropped from the system until every task accessing that type of data has had a chance to acquire the data or until data shedding occurs due to exhaustion of buffer space. Data distribution was enhanced during the reporting period by increasing the amount of buffer space available and by increasing the number of tasks which could simultaneously access the data streams.

**d. Resampling and Display**

The resampling and display tasks enable the operators to observe the data collection process and to evaluate appropriate scan strategies for collecting meaningful and useful data.

The resampling procedure converts the polar base data (reflectivity, velocity, and spectrum width) into three 256-by-256 bin Cartesian images using a "nearest gate" approach. The value placed into a bin is selected from the polar gate which is spatially closest to the center of that bin. This capability was not changed during the reporting period.

The display task, utilizing the Genisco color computer and three monitors (one each for reflectivity, velocity, and spectrum width), turns the resampled data into color pictures. It displays aircraft beacon information, map overlays, and algorithm product overlays on top of the base data, all under operator control.

### e. Operator Interface

The operator interface to RTS is made up of an operator command entry terminal and a system status monitor terminal. The command entry terminal is serviced by a task which interprets and distributes operator commands and displays command responses (including entry errors). The status monitor terminal displays system status reports as well as warning and error messages.

### f. Communication

This portion of RTS is responsible for exporting base and algorithm product data to external computer systems and workstations. Two ethernet connections are used for all external data communication: a) a raw ethernet (no handshaking) for base data broadcast at real-time rates and b) a TCP ethernet protocol for algorithm product data.

There was a new requirement to import automatic scan mode selection information to be used by the scan control software. In response, a general purpose "client" software task was written. This task interfaces between the TCP ethernet protocol, used by workstation-based algorithms for data communication, and the Concurrent-based data streams, allowing algorithm products generated outside the Concurrent to be distributed within the Concurrent. It can be configured at run-time to control which algorithm product will be accessed and which data stream will be produced.

## 3. Radar Control System

Figure 3-2 illustrates the FL-2C testbed front-end control hardware and software configuration used during the reporting period. The three primary components of the radar control system are the scan control interface program, the antenna control program, and the radar control program. The time series program is started only when time series data collection is necessary.

### a. Antenna Control

The antenna control program converts operator-specified scan strategies (see Scan Control) into appropriate antenna pedestal azimuth and elevation motion. The program polls the antenna for current status and generates motion commands based on the current status and the desired motion. The program runs in the 3280 and communicates with the radar controller by means of a Universal Logic Interface (ULI). The radar controller functions as an interface to the Scientific Atlanta pedestal servo electronics.

One modification was made to the antenna control software during the reporting period. The antenna control program was changed to reduce the amount of preprocessing performed on scan definitions passed by the radar control program. This was done to isolate all scan parameter manipulation to within the radar control program, thereby simplifying the antenna control program.

b. Scan Control

The scan control software accomplishes the following:

a. Provides users with scan control, via the scan editor, by which a number of scans–plan position indicator (PPI), range height indicator (RHI) and fixed azimuthal elevation (POINT)–can be defined, executed, and monitored. The scan editor is an interactive program that permits the radar operator to easily define and modify a scan, store the scan on disk, retrieve the scan from disk, submit up to 15 scans for execution, and maintain up to 32 scan definitions simultaneously.

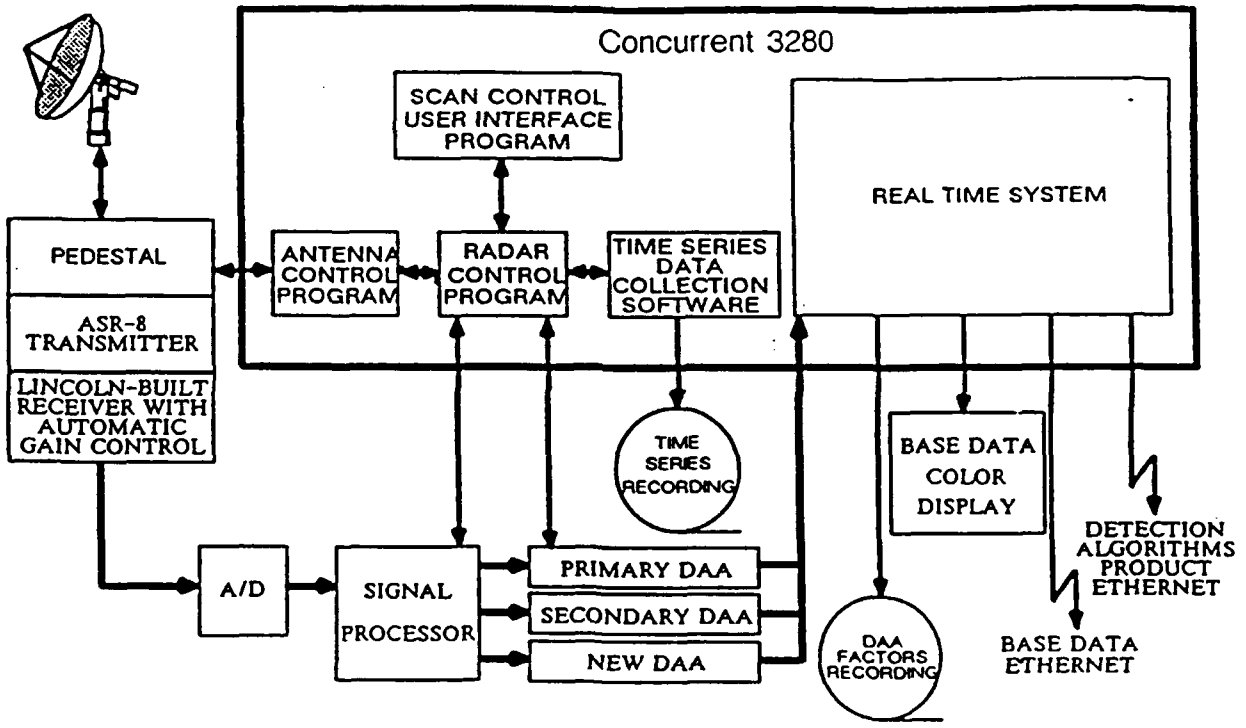


*Figure 3-2. FL-2C radar control hardware/software configuration.*

b. Translates scan definitions into sequences of commands to be distributed as required to the antenna control software, the signal processor, the DAAs, the time series data collection hardware and assorted application software packages (e.g., the beacon tracking program, the automatic scan mode selection program).

c. Provides operator access to useful scan control functions, including:

1. Real-time aircraft beacon tracking in which scans are dynamically defined to include selected aircraft positions.

2. Time series recording of either filtered or unfiltered I and Q radar measurements.

3. Antenna control program simulation for software development and testing in the lab.

d. Provides a scan monitoring capability which reports scan, radar, and antenna information.

The scan control software is comprised of a number of tasks, each providing a subset of the total capability, and each of which is closely coupled to the other tasks. Communication among the tasks is achieved through shared data areas in memory, disk files, and/or intertask messages.

The following changes were made to the scan control software during the reporting period:

a. The scan control software was modified to support automatic scan mode selection. Scan schedules containing a collection of PPI, RHI, and POINT scans were tagged with a mode name. Scan modes were requested either manually or automatically. Automatic scan mode selection involved receiving and processing mode request messages from the scan mode selection algorithm that was developed to run on a Sun system. Scan control mode selections were based upon existing weather conditions and a user-defined scan "scenario" that described the radar situation with respect to the airport, either on-airport or off-airport. It is expected that other experimental scan scenarios will be developed for test purposes.

b. Two new range sampling modes were developed to accommodate the new range gate spacing of the C-band radar system. One mode was designed to extend out to 90 km, with 150-meter resolution. The second mode, intended for long-range scanning, skipped 33 km and extended out to 392 km, with a resolution of 450 meters.

c. A new software package was added to the radar control software library to maintain system parameters and/or system value lists that were tagged with specific dates and times. This package was designed to maintain real-time control and calibration parameters that were in use at any date and time for real-time or playback operations.

d. A new scan parameter was added to define an elevation angle associated with auto-zero circuit control. When the elevation associated with a tilt is above a user-specified angle, the auto-zero circuit in the radar receiver is enabled. When the auto-zero circuit is enabled, it attempts to remove DC bias from the receiver I and Q channels. Auto-zeroing must be enabled occasionally to compensate for a time-varying bias. During TDWR scanning, the highest elevation tilt of each scan was run with the auto-zero circuit enabled.

e. A new range gate clipping algorithm was developed to reduce the number of range gates processed by the signal processor. Without range gate clipping, the data rate associated with higher pulse frequencies exceeded the signal processor timing capability. For each tilt, the radar controller program computed and implemented the maximum number of range gates that could be processed as a function of the requested pulse frequency and range sampling mode.

f. A new set of user control commands were added to the real-time (and off-line) radar control software to properly activate and deactivate the FL-2 software-controlled front-end hardware. Precautionary steps were required to safely trigger the activation of the waveguide switches (primary and secondary) and the transmitter high voltage.

g. After the FL-2 radar hardware was correctly processing C-band data, measurements of the system calibration constants were made. The following system parameters were checked for correctness:

1. Radar range (distance) to first gate.

2. AGC coefficients.

3. Receiver noise level.

4. Receiver gain.

5. Transmitter power.

6. STC response curve out to 10 km.

7. Actual PRFs were measured to verify the requested PRF values.

## B. SUN REAL-TIME SYSTEM

### 1. Sun Network

The structure of the network has remained unchanged since 1988. Network enhancements have taken the form of new machines and hardware upgrades.

As depicted in Figure 3-1, there are four machines connected to the base data ethernet. Only these machines can host algorithms requiring direct access to conditioned base data. These algorithms are:

a. Microburst feature extractor executing on Juno. The bridge between Juno and the base data ethernet prevents the process from receiving data for range gates beyond 45 km.

b. Advanced gust front algorithm (AGFA) feature extractor, executing on Iris.

c. Real-time resampler, used for real-time analysis and weather image export, executing on Willow.

d. Significant weather determination, a portion of the scan mode selection algorithm, executing on Miranda.

Because these algorithms are extremely input/output (I/O) intensive, most of the hardware upgrades made during this reporting period were made to these machines. Memory was added to the systems to eliminate paging. Willow, the only Sun-3 on the base data ethernet, was upgraded from a Sun 3/260 to a Sun 3/480, with a substantial increase in performance. A new Sun 4/200 system, Miranda, was added to the network to handle processes new in 1990. A faster Sun 4/300 CPU board was installed in Iris, the Sun-4 used to support the advanced gust front algorithm, so that it could be run in real time in parallel with the NSSL gust front algorithm running on the Concurrent.

Traffic on the products ethernet at FL-2C continues to be modest, despite a substantial increase in the interprocess communication requirements for 1990. In part, this load is modest because network file system (NFS) traffic is extremely light during operations; machines with heavy disk I/O requirements also have large local disks. Files generated in real time are rarely accessed remotely. The connection between the analysis display stations (Willow and Laurel), each using resampled images stored on Willow's disk, is the primary exception.

Network traffic is more of an issue on the Tower network. Product flow is nearly that of the products ethernet at FL-2C, but Tower, the machine in the Tower cab, is a diskless client of Tracon and generates substantial NFS traffic. Although a new stand alone machine, Trainer, was added to the Tower network for air traffic control (ATC) training and advanced product demonstrations during this reporting period, its use was not expected to appreciably affect the Tower ethernet.

Late in 1989, the operating system for the Sun network was upgraded to match that used in Lexington (Sun/OS 4.0.3). Two NFS patches, intended to eliminate disk access problems for systems supporting diskless nodes, were installed just prior to operations. These patches were particularly critical to the stability of the Tower ethernet.

### 2. Real-Time Displays

The workstation display software on the Suns was designed to display radar and algorithm data for analysis purposes. It does so by taking advantage of the workstation's unique environment to provide a much faster, more flexible, and more interactive capability than earlier generation displays were able to provide. Zooming, panning, user-programming, multi-window interaction, larger images, real-time operation, and a greater variety of colors are all available through a combination of the workstation's native capabilities and software designed to exploit them.

The workstation development, begun in March 1986, led to a collection of programs commonly referred to as "Weather Shell" (WxShell). WxShell refers specifically to two related processes responsible for the graphical and textual presentation of data to the user. The true WxShell processes run an interpreter which accepts commands and/or scripts at the user's (interactive) request to perform the desired action. Since it is programmable at run time, the same software is suitable for use in both the real-time and off-line analysis contexts. The other processes (database, data gathering, etc.) are independent, but all have a common and flexible network/server/client orientation.

By the end of 1989, the development of WxShell, now considered a mature product, was mostly complete. During this reporting period, the real-time functionality was largely unchanged; additional capabilities were added for analysis support, including enhanced beacon, dual-Doppler, and new algorithm products displays and augmented display options.

WxShell will continue to evolve in the coming months. Planned enhancements include the expansion of WxShell's capabilities to work with data which does not include complete specification of its world coordinates; the improvement in WxShell's ability to access data by time and/or sequence increment; improvements in speed and ease of use; the development of on-line contouring and more flexible display attributes; and the creation of more sophisticated animation, dual-Doppler, and beacon analysis and display.

### 3. GSD

In late 1989, the FAA requested that Lincoln Laboratory develop a Geographic Situation Display (GSD) which would emulate, as closely as possible, the GSD to be fielded by Raytheon. WxShell was used to provide the basic graphics display capability and was supplemented with additional functions and programs as appropriate to complete the system. Work on the GSD continued throughout the winter and early spring, resulting in a system that could support Raytheon-style DFU displays in the Tower cab, the TRACON, and at both the FL-2C and ASR-9 testbed field sites.

The full GSD software suite included:

a. A menu input program based on a simple prototype obtained from Raytheon,

b. Processes which transformed LLWAS wind data, runway configuration information (obtained from the menu process), and microburst and gust front alarms into textual and graphic runway alarms,

c. WxShell processes to display text, graphics, and status,

d. A non-WxShell process to produce the ribbon display, and

e. Support processes to collect various files and information for monitoring and controlling the GSD display.

Among the support processes borrowed from the rest of the real-time system was *Gather2*, used by the real-time analysis displays to acquire data to be displayed and by the real-time archivers to capture data to be stored.

A number of changes are planned for the GSD for the 1991 operational season in Orlando. Among these are:

a. Provide support for the plasma ribbon displays manufactured to Raytheon's specifications,

b. Incorporate a facility for testing alternative user interfaces,

c. Expand display options to support proposed weather products, including microburst prediction and tornado vortex signature, and

d. Modify specific GSD operation and display to match the evolving Raytheon system.

## 4. New Algorithms and Processes

The Lincoln Laboratory GSD was a replacement for the National Center for Atmospheric Research (NCAR) GSD. It did not affect the network configuration or allocation of resources since it ran on the same hardware, both at FL-2C and in the Tower, as during the 1989 season. However, there were a number of algorithms and ancillary processes added elsewhere in the system. These additions are described below.

### a. Scan Mode

The TDWR is specified to switch automatically from Monitor to Hazardous scan modes when hazardous weather is close to the airport. An algorithm was developed to integrate information derived from the base radar data with the output of the microburst and gust front algorithms to identify the hazard mode. The software to support automated scan mode selection was implemented and installed at FL-2C. Because additional work was required for the GSD to support mode-sensitive time outs, the outputs of the algorithm, particularly the switch to monitor mode, were not used to control the radar operationally. The scan mode algorithm will be used in 1991.

### b. Cockpit Server

The cockpit display server is a process that delivers output from various feature extractors to a small (1.5" x 2") display installed in the cockpit of an aircraft. Communications to the cockpit display is achieved with packet modem radios. The end result is a miniature, "stripped down" version of the GSD.

### c. Gust Front Update

The basic gust front algorithm produces detections and forecasts every five minutes. A simple program, called the gf_update process, filters the output stream of the gust front algorithm and reports the output at one-minute intervals for the scan select algorithm, the cockpit display server, and the GSD.

### d. System Control Processes

A number of processes were added to the system to control and validate the flow of data to the tower without requiring operator intervention to modify hardware connections. These processes were put in place to avoid any confusion on the part of ATC observers in the Control Tower between playback and live data. This had been a problem in the past when observers started the Tower and Tracon computers during periods that were outside of designated operational times.

### e. Training System

A new system was added to the network at the tower to support the training of ATC personnel. A stand-alone GSD was created to allow controllers and supervisors to exercise the system under all anticipated weather conditions. The system contains a set of "canned" data cases (initially captured during operations in Kansas City), a simulator to distribute the data at real-time rates, and an interface to permit case selection. The software also is configured to allow live operation on special occasions. Both the case selection and data distribution mechanisms are flexible, allowing cases to be added easily to the system.

## C. SYMBOLICS REAL-TIME SYSTEM

There are two Symbolics 3650 LISP machines at FL-2C, each with 376 MB of disk storage. Depending on the mode of operation of FL-2C (e.g., delivering data to the tower or not), these systems perform different functions in the system. Ariel, with two megawords of memory and a floating point accelerator, is dedicated to the microburst system. It accepts feature information from the feature extractor running on Juno, performs all 3D processing, and generates microburst alarms which it passes to the microburst shape generator executing on Juno. Stephano, with three megawords of memory, is kept running in standby mode during operations, ready to provide a nearly instantaneous replacement for Ariel in the event of a system failure. When data are not being delivered to the tower, Stephano is used as part of the advanced gust front algorithm. In this mode, Stephano accepts feature information from the advanced gust front feature extractor running on Iris, performs feature association and discrimination, and produces the gust front detection and hazard information.

There were no hardware or operating system changes to the Symbolics machines during this reporting period. The latest version of the microburst algorithm Symbolics software, version 32, was installed at the site in May. This version of the software included a capability for setting the site-adaptable parameters in the Symbolics portion of the algorithm at run time (this capability already existed for the Sun-4 microburst algorithm feature extraction software). Other new features included the microburst prediction product and storm mass/volume/center of gravity computations. Changes to the gust front Symbolics software were primarily structural, reflecting the transition of LISP portions of the feature extractor to the Sun-4.

# 4. ORLANDO SITE OPERATIONS

## A. FL-2C MEASUREMENTS

### 1. Data Collection

During the last two weeks in May 1990, the FL-2C radar in Orlando, FL was operational for calibration on final checkout. The radar operated in a data-collection mode for 102 hours in May and June, collecting 97 tapes. The initial measurements on 22 May were used to verify the position of the antenna and the range to first gate offset. The radar calibrations were completed by 1 June; however, there were still minor modifications after this date. Beginning in early June, the entire system was checked daily to verify the stability of the calibration constants. There were no anomalies reported with the radar calibrations in June.

Over a five-week period from 27 May through 30 June, 150 microbursts and 32 gust fronts were observed in the Orlando area. A number of these (19 microbursts and seven gust fronts) were detected within 3 nmi of Orlando International Airport (MCO). There were two major microburst periods, from 2 through 9 June and from 20 through 26 June. The most active day was 5 June, with 18 microbursts. The number of events observed in Orlando thus far is comparable to Denver in terms of microburst frequency.

The majority of the microbursts were detected in the late afternoon hours between 1400 and 1800 hours local time (Figure 4-1). There was a slight peak in microburst activity between 1600 and 1700 hours. The hazard from microbursts in Orlando is confined mainly to the afternoon hours. The frequency of gust fronts was fairly evenly distributed between 1300 and 1800 hours.

The distribution of microburst and gust front intensities in Orlando is similar to other TDWR testbed locations. More than one-third of the microbursts were weak, with velocity differentials less than 15 m/s, while one out of six reached 25 m/s or greater (Figure 4-2). The strongest wind shear was 36 m/s on 5 June, while the strongest airport event reached 30 m/s on 6 June. The maximum velocity for the airport microburst occurred within a distance of 2 km, which would have presented a significant hazard to a departing or approaching aircraft.

All of the gust fronts this period were weak or moderate, with velocity differentials less than 15 m/s. This is somewhat different from the distribution of gust front intensities in the mid-west (Kansas City) where squall lines produce much stronger gust fronts. Orlando gust fronts are primarily more eastward and westward, and they are oriented azimuthally with respect to FL-2C while crossing the airport. This combination of weak velocities and azimuthal orientation will present quite a challenge to the detection of airport gust fronts in Orlando from the current TDWR testbed location.

Figure 4-3 is a plot of the reflectivity distribution of Orlando wind shear events. Essentially all of the microbursts were associated with maximum surface reflectivities of 40 dBZ or greater. The small number of microburst events with reflectivity less than 40 dBZ are under investigation. It appears that clutter contamination due to birds gave rise to a microburst-like divergent signature in the data. Approximately three quarters of the gust fronts had reflectivity thin lines which might enhance the detection of Orlando gust fronts. The maximum surface reflectivity was typically between 10 and 19 dBZ.

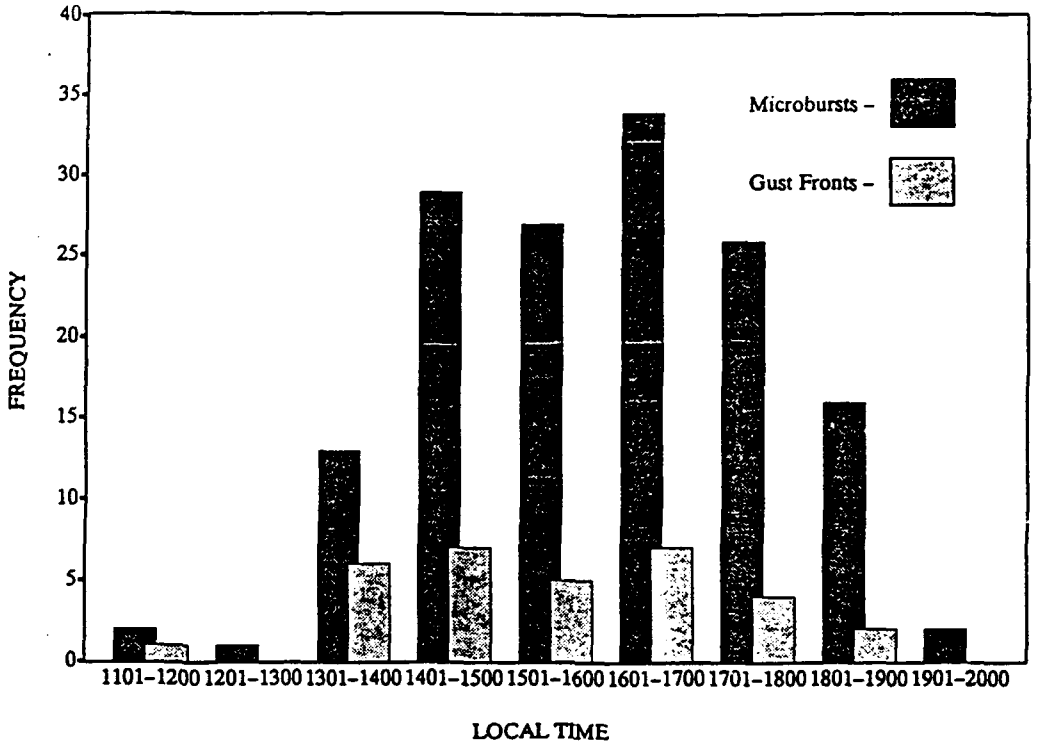


*Figure 4-1. Hourly distribution of Orlando wind shear events in May and June 1990.*

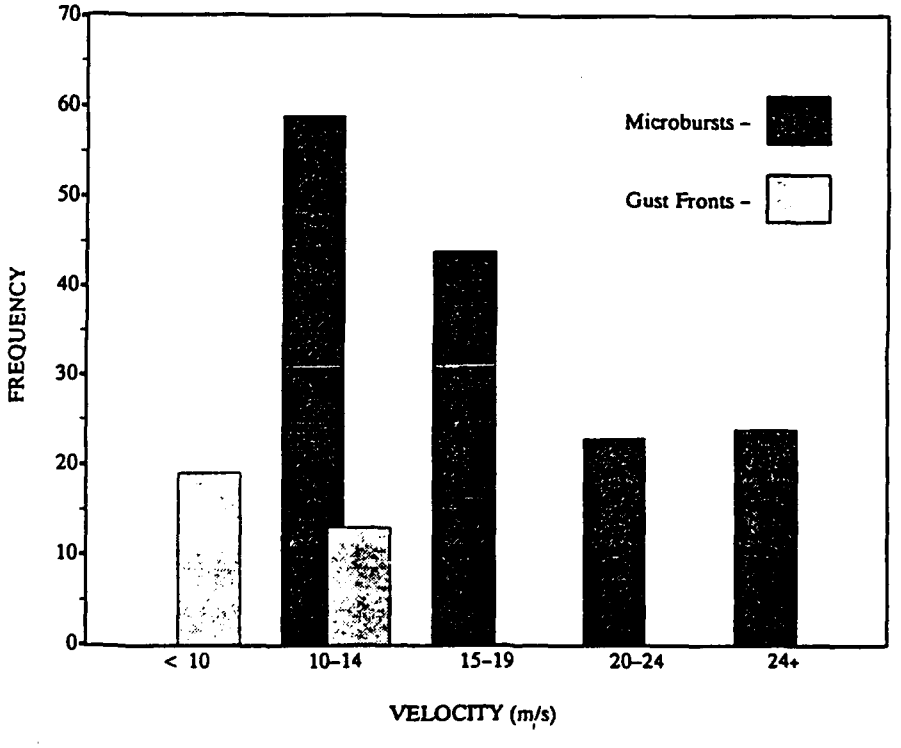


*Figure 4-2. Maximum velocity of Orlando wind shear events in May and June 1990.*

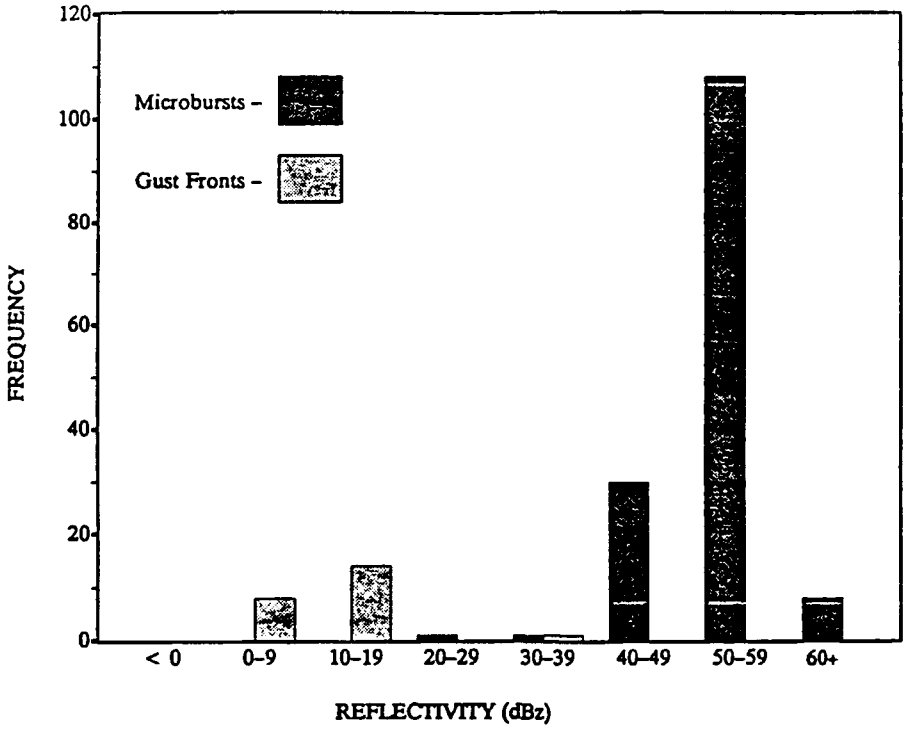


*Figure 4-3. Maximum surface reflectivity of Orlando wind shear events in May and June 1990.*

Once the system was operational, a high priority was to determine if the change to C-band affected the performance of the algorithms. This had to be accomplished prior to the TDWR testing at MCO. Thus far, the microburst algorithm has had no problem detecting events.

### 2. Data Anomalies

During the first two weeks, the radar did not appear to detect clear air reflectivities beyond 30 km. This problem was alleviated once the radar was fully calibrated and the radar constants were verified. Clear air returns in June were typically detected to a range of 40 or 60 km.

Another data quality concern is the noisy velocities detected with high-reflectivity clutter regions. The noise is related to filter width and PRF, with the worst-case scenario being the widest filter at the lowest PRF. This increase in noise is somewhat expected since there is less integration at the lower PRF. While a clutter map might help suppress this problem, there is still the possibility of additional clutter breakthrough due to ducting of the radar beam. In these instances, the noisy data might impair performance of the velocity dealiasing technique. The problem is still being analyzed.

After FL-2C was fully calibrated, there was some concern that the reflectivities were high. This will be further investigated once UND and Massachusetts Institute of Technology (MIT) radar data are available. The occurrence of several storms over the airport will be examined to determine if reflectivities from FL-2C are consistently higher.

Other data anomalies noticed in real time were as follows:

a. Missing data from the secondary DAA,

b. Velocity unfolding problems, and

c. Increased clutter breakthrough after the passage of gust fronts.

It should be pointed out that this is the first time unfolded velocities were displayed in real time, and there is an increased awareness of unfolding errors. All of these issues have been reported to Lincoln and Raytheon analysts and are under investigation.

## B. LLWAS AND MESONET OPERATIONS

The LLWAS system at Orlando is composed of a network of six sensors located around the airport. Wind speed and direction data are archived on magnetic tape at FL-2C and shipped to the Laboratory every two weeks for translation and analysis. The first data from Orlando was collected on 12 June. There were no periods of lost data during this time.

The Orlando Mesonet will consist of 40 FAA-Lincoln Laboratory Operational Weather Studies (FLOWS) weather stations and a six-station LLWAS. Site selection for the 40 FLOWS stations began in early January 1990. The preliminary configuration for this network sets nine stations on and 31 stations off airport property. Area coverage for the network is expected to be approximately 400 square kilometers (average station spacing slightly greater than 2 km) and will be centered on MCO. The planned configuration of the Orlando Mesonet is depicted in Figure 4-4.

As in previous years, the LLWAS stations will collect only wind information (speed and direction at approximately seven- to ten-second intervals), whereas the FLOWS surface weather stations will collect various meteorological data such as barometric pressure, temperature, relative humidity, precipitation rates, and wind speed and direction. The sampling rates for the FLOWS stations will be similar to those rates that were in effect at Kansas City during 1989. That is, the data will be represented by one-minute averages for all sensors except wind speed and direction. These sensors will, for 25 of the stations, collect average and peak wind data, along with average direction for each minute. The remaining 15 stations will act to emulate the enhanced LLWAS (see Figure 4-4) by collecting wind data, both speed and direction, every 15 seconds. Also, to emulate the enhanced LLWAS properly, the wind sensors will be mounted atop 100-ft towers to avoid local obstruction effects.

By the end of June, 30 out of a possible 40 contracts had been agreed upon by local land owners. This action enabled Lincoln Laboratory to begin erecting weather stations on agreed-upon sites. As of 30 June, 20 FLOWS stations, along with the six-station LLWAS, were operational.

## C. UND RADAR MEASUREMENTS

During the spring, the UND radar and support equipment were moved from Kansas City, MO to Orlando, FL. Site construction was delayed throughout May and June because of various problems with permits and zoning. These problems were documented for the FAA by Alan Borho (UND). Thus, there were no UND radar measurements in support of the TDWR project this reporting period.

## D. AIRCRAFT MEASUREMENTS

The UND Cessna Citation, an instrument-equipped jet aircraft, was available to collect data in Orlando on 18 June. The focus of aircraft operations in Orlando shifted from turbulence measurements to low-level wind shear penetrations. Whenever cells were detected near the airport, the Citation would sequence into the approach pattern to the impacted runway. The altitude of these penetrations was typically 200 ft above ground level (AGL), depending upon cell dynamics and outflow strength. The success of each mission was dependent on the traffic volume in the vicinity of the airport. There were numerous examples where the Citation's approach was delayed while they were sequenced behind other aircraft. Nonetheless, aircraft measurements through primarily weak microbursts were collected on four days. The strongest downdrafts reported by the aircraft were 10 m/s on 22 and 24 June.

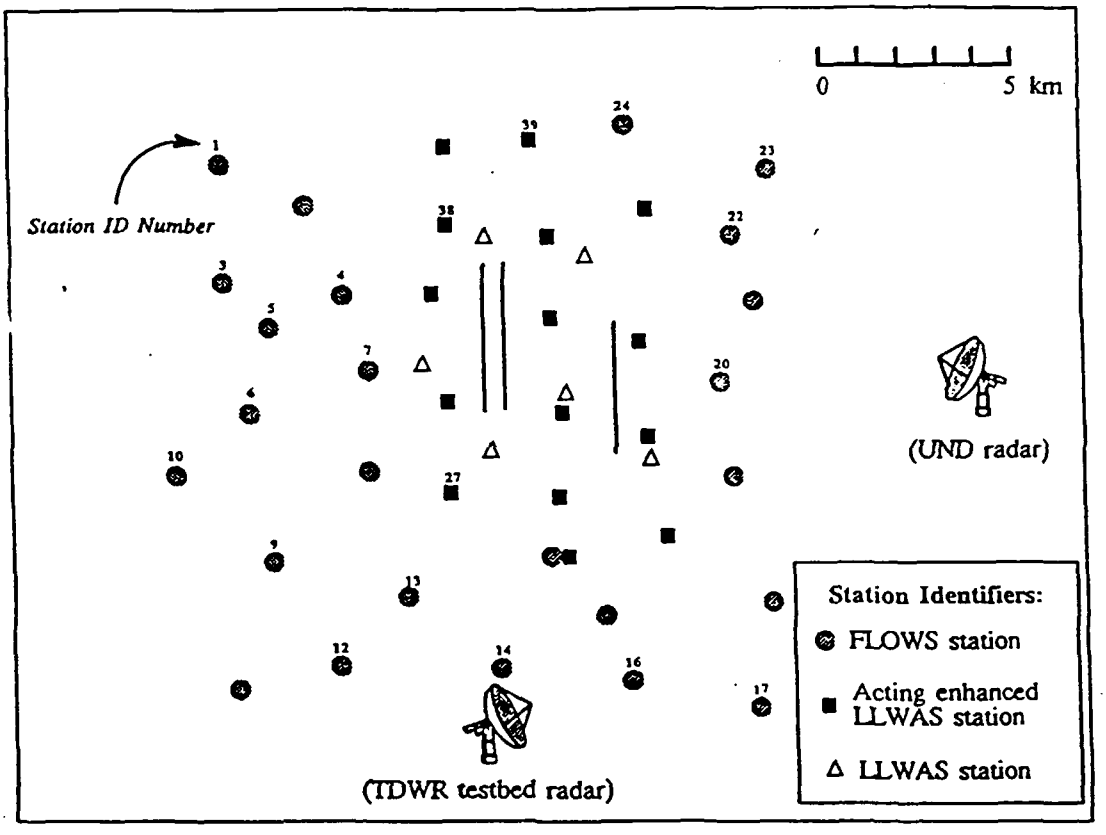


*Figure 4-4. Mesonet configuration for Orlando, FL. The FLOWS stations, including those acting as enhanced LLWAS, along with the actual LLWAS stations, are indicated. FLOWS stations identified with an ID number are operational as of 30 June 1990. Radar sites and runways from MCO are also shown.*

## E. SUPPLEMENTAL MEASUREMENTS

There were no data collected in support of upper-air soundings, lightning, or clutter during this period.

### 1. Soundings

Upper-air measurements will be collected in Orlando with the NSSL Cross-Loran Atmospheric Sounding System (CLASS) sounding system to assist in numerical modeling studies of microbursts. The balloons and radiosondes were received on site in June. Air traffic control personnel at MCO were contacted concerning a site for the launches. The FL-2C radar site is in the flight pattern, while UND is not available because of construction delays. An alternative location 9 km east of the airport was selected prior to the completion of the UND site. Launches are scheduled for 0700, 1000, and 1300 hours, with additional launches as appropriate. Sounding data will be collected from 1 July through 31 August.

### 2. Lightning

The lightning data to be collected in Orlando consists of data from the French (ONERA) interferometer system and from a network of 20 corona point sensors to be installed on the masts of selected Mesonet stations. The French system should be operational in July, while the first corona point sensors should be installed in August. The schedule for corona point installations has slipped because of problems encountered with obtaining permits for the Mesonet sites. Every three days the lightning information from the corona data collection platforms is archived. Lightning data may be used to enhance the prediction and trend estimate of microbursts as well as to identify hazardous cells in the terminal area.

# 5. DATA ANALYSIS AND PROCESSING

## A. LEXINGTON COMPUTER SYSTEMS

Nearly 70 workstations, servers, and minicomputers support the experimental data reduction and algorithm development activities in Lexington, MA. An internal local area network permits electronic file transfer between machines of different architectures, allows peripherals to be shared among the systems, and provides file system support for the diskless nodes. Figure 5-1 presents a simplified view of this network, illustrating the backbone Ethernet and the five client subnets. The backbone connects two Concurrent minicomputers (VBU and AN2), three Symbolics LISP machines, a Sun compute server (Ceres), a Sun communications server (Guardian), and five Sun file servers (Juliet, Hamlet, Lear, Oberon, and Viola). Each client subnetwork links the individual Sun workstations to their parent file server and in turn to the rest of the network.

### 1. Concurrent Computers

In Lexington, the configuration of the Concurrent Computer Corporation (formerly Perkin-Elmer) minicomputer systems has been stable since late 1988. The resources available to Concurrent users are listed in Table 5-1. The three systems were used heavily during the spring, particularly for development of real-time software targeted for the Concurrent 3280 at FL-2C. With the exception of AN2, the systems were extremely reliable. Late in the spring, the cause of AN2's intermittent self-induced power failure recovery actions was finally identified and the problem corrected.

### 2. Sun Network

The Sun systems in Lexington are intended to provide uniform, high-speed, interactive computing resources to all group members. In creating a network of Suns to meet this goal, the following objectives were most important:

a. The structure of the network should be invisible to its users.

b. A user's environment should move with the user from workstation to workstation.

c. All file systems should be equally accessible across the network.

d. Addition of new workstations and/or servers should be possible without disrupting the rest of the system.

The keys to the success of the network architecture chosen are the organization of the servers on the backbone Ethernet and the structure of the client subnets. The file servers are Sun 3/280s, each with eight megabytes (MB) of memory and an internal 6250 bpi tape drive. The total on-line storage capacity provided by the file servers is approximately 11 gigabytes. The local disks on each file server hold the file systems for that server's clients (the users whose workstations are located on the client subnet). Using Sun's NFS, each server cross-mounts the file systems of non-local users so that all user files are visible at any workstation.

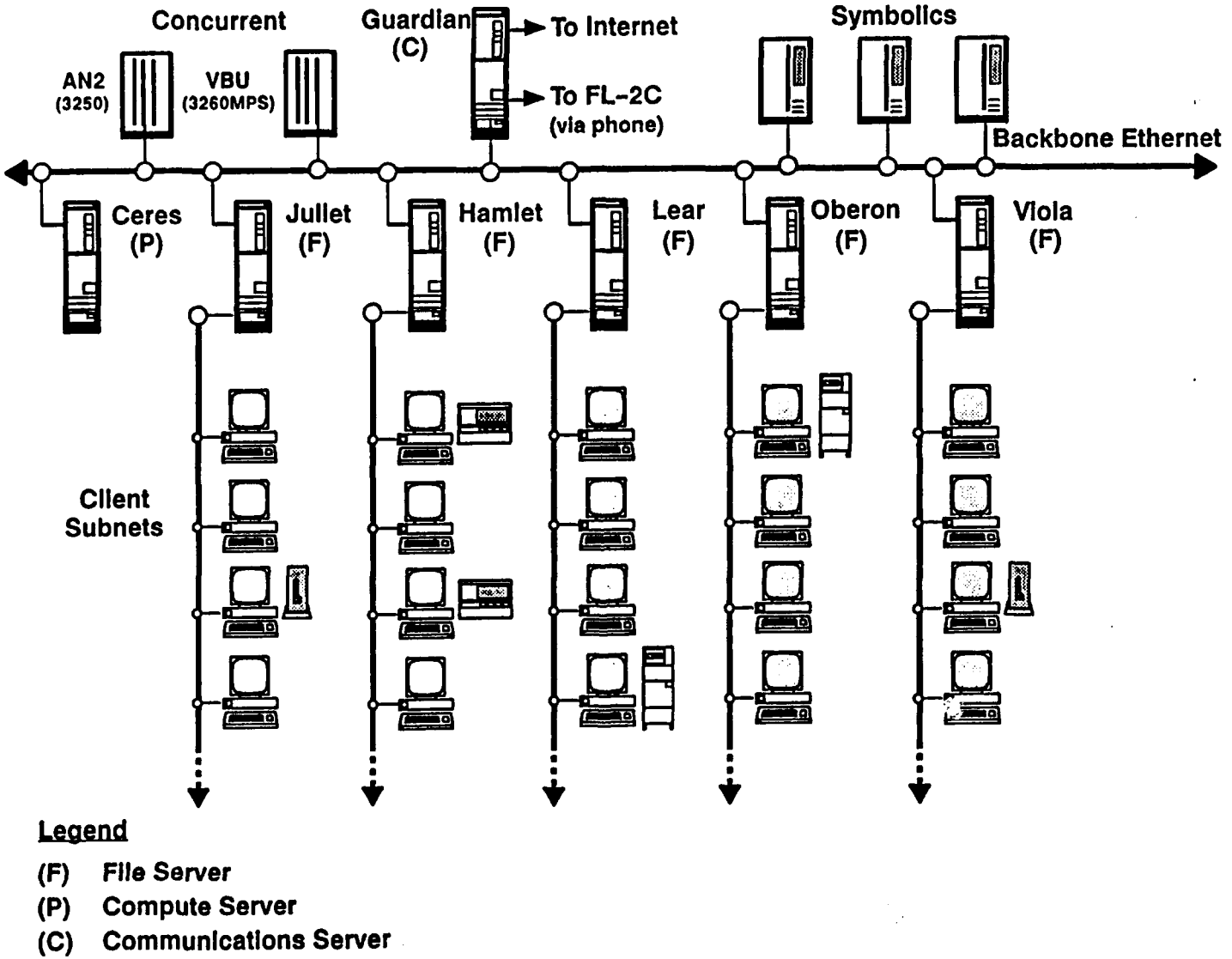


*Figure 5-1 Group 43 local area network.*

## Table 5-1.
## Concurrent Resources Available at Lexington.

| Machine | VBU | AN2 | BAT |
|---|---|---|---|
| Processors | CPU<br>APU | CPU | CPU |
| Memory (MB) | 16 | 16 | 8 |
| Fixed Disk Storage (MB)* | 1422 (1125) | 1422 (1125) | 948 (750) |
| Removable Disk Storage (MB)* | 300 (256) | 80 (67) | 80 (67) |
| Display | Genisco<br>(3 monitors) | Genisco<br>(1 monitor) | ---- |
| Hard Copy Graphics | Versatek printer/plotter<br>Tektronix ink-jet<br>color plotter | -- | -- |
| RS-232 Ports | 26 | 26 | 18 |
| Tape Drives<br>1600/800 bpi<br>6250/1600 bpi | <br>2<br>2 | <br>2<br>2 | <br>----<br>2 |
| Printers | 300 lpm | 300 lpm | |
| Ethernet Controllers | Local area network | Local area network<br>Base data Ethernet | (unallocated) |
| Special Interfaces | (none) | Primary DAA<br>Secondary DAA<br>New DAA (DR11) | Primary DAA<br>Secondary DAA<br>New DAA (DR11)<br>Signal Processor |

* Size of unformatted disks in megabytes is presented first. Disk space available after formatting is shown in parentheses.

Two servers are shared by all users:

a. A Sun 3/160, which is a communications gateway that provides access both to the Internet and to the remote field sites.

b. A Sun 4/300, which is both a computer server and a testing platform for the real-time Sun-based algorithms.

The resources associated with the servers are listed in Table 5-2. Although tape drives are local to a particular server, they can be accessed across the network using the Group's remote tape package.

To minimize the traffic throughout the network, the loads are balanced on both the client subnets and the backbone Ethernet. Certain contributors to network load cannot be anticipated; for example, local versus remote tape access by user programs is a function of resource availability, not design. However, examination of other components of the load has proven extremely useful. Since non-local disk access generates traffic on the backbone while local disk transfers between a server and its clients are confined to the appropriate subnet, the patterns of file sharing among individuals and projects are extremely important. Also critical to understanding network loading are the paging and swapping requests generated by individual users. File sharing contributes to both backbone and subnet traffic, while paging and swapping generate subnet traffic only. The analysis of network use is extremely subjective. Patterns of both file access and page/swap requirements change with assignment; therefore, the results must be re-evaluated on a regular basis.

The approach taken thus far, which allows individual users to be shifted between file servers as the needs change, has proven extremely successful. During the last reporting period, a fifth file server was added with virtually no disruption in network service. By the end of June, the client subnets hosted a total of 56 clients, most of them diskless. Network response time continues to be excellent.

A significant change to the network during this last reporting period was the addition of optical disk drives to the system. Seven rewritable, 300 megabytes/side optical disk drives have been strategically placed on selected client machines to provide storage for large volumes of data. These drives are shared by project groups needing access to the same data sets. Because disks contain formatted Unix file systems, no special mechanisms are required to access the files. Also during this period, the first Optimem Write Once Read Many (WORM) optical drive with a Ten-X interface was installed on the network. The Ten-X interface performs on-the-fly data compression, increasing the effective space available on the disk by 30 percent or more. The 1012 megabyte Optimem disks will be used to hold permanent data archives, such as the product output of the FL-2C real-time system. The resources available on client machines are presented in Table 5-3.

### 3. Peripherals

The Tektronix Inkjet printer/plotter, previously available only from the Concurrent, was upgraded and placed on the Sun network. The Inkjet is the preferred printer for draft color plots; the Tektronix thermal printer is reserved for production-quality output.

Table 5-2.
Sun Network Servers.

| Machine | | Hamlet | Juliet | Lear | Oberon | Viola | Ceres | Guardian |
|---|---|---|---|---|---|---|---|---|
| Machine Type | | 3/280S | 3/280S | 3/280S | 3/280S | 3/280S | 4/300 | 3/160 |
| Memory (MB) | | 8 | 8 | 8 | 8 | 8 | 32 | 8 |
| Disks | NEC (903 MB) | 1 | 1 | 1 | 1 | 2 | 0 | 0 |
| | Hitachi (851 MB) | 0 | 1 | 0 | 0 | 1 | 0 | 0 |
| | Aviv (687 MB) | 1 | 1 | 1 | 2 | 0 | 1 | 0 |
| | Pedestal (267 MB) | 0 | 0 | 0 | 0 | 0 | 0 | 1 |
| | Optical (1012 MB) | 0 | 0 | 0 | 0 | 0 | 1 | 0 |
| Magnetic Tape (6250 bpi) | | 1 | 1 | 1 | 1 | 1 | 1 | 0 |
| Modems | | 0 | 0 | 0 | 0 | 0 | 0 | 3 |

## B. GENERAL PURPOSE SOFTWARE

Most new software is developed on the Sun. The packages are designed to take advantage of the tools provided as part of the Sun Unix environment. Shared group software that was either newly developed or substantially enhanced during the reporting period is briefly described below.

### 1. Interprocess Communications Packages

With the preparation for the 1990 data-gathering season, the number of applications sharing data structures and software with real-time algorithms grew substantially. As a result, routines that had once been considered "real-time" were enhanced and incorporated into the Group's general purpose software structure. Two packages in particular, now used both for analysis and real-time support, are major examples of this transition:

a. Server-Client Communications Package (sc_pac).

b. Logical Record Reading/Writing Package (logrec and lrtemps).

Table 5-3.
Client Machines on the Sun Network.

| Type | | 3/60 | 3/75 | 3/80 | 3/110 | 3/160 | 4/280 | Total |
|---|---|---|---|---|---|---|---|---|
| Number | | 21 | 4 | 18 | 4 | 8 | 1 | 56 |
| Memory (MB) | 8 | 5 | 4 | 14 | 2 | 3 | 0 | 28 |
| | 12 | 13 | 0 | 3 | 2 | 5 | 0 | 23 |
| | 16 | 2 | 0 | 1 | 0 | 0 | 1 | 4 |
| | 20 | 1 | 0 | 0 | 0 | 0 | 0 | 1 |
| Monitors | Mono-chrome | 13 | 4 | 13 | 0 | 4 | 1 | 35 |
| | Color | 8 | 0 | 5 | 4 | 0 | 0 | 17 |
| | Dual | 0 | 0 | 0 | 0 | 4 | 0 | 4 |
| Disks | Shoebox * | 3 | 0 | 0 | 0 | 0 | 0 | 3 |
| | Pedestal (280 MB) | 0 | 0 | 0 | 0 | 1 | 0 | 1 |
| | Optical | 7 | 0 | 0 | 0 | 0 | 0 | 7 |
| | Internal (71 MB) | 0 | 0 | 0 | 0 | 4 | 0 | 4 |
| | Eagle (380 MB) | 0 | 0 | 0 | 0 | 0 | 1 | 1 |
| Tapes | 8 mm | 1 | 0 | 0 | 0 | 0 | 0 | 1 |
| | 6250 bpi | 0 | 0 | 0 | 0 | 2 | 0 | 2 |
| | 1/4 inch cartridge | 0 | 0 | 0 | 0 | 3 | 0 | 3 |
| Modems | | 1 | 1 | 2 | 0 | 1 | 0 | 5 |

* Shoebox SCSI units contain an internal 1/4 inch cartridge tape drive.

### a. Server-Client Package (sc_pac)

The server-client communications package was originally developed as part of the real-time microburst feature extractor. Two types of data were managed by the package: 1) packets carrying base data from the source (i.e., the Concurrent real-time system) to the Suns and 2) specially formatted archive records communicating intermediate and final results between algorithms. Support for several protocols was built into the package; among them, NIT and NIT FILE for ingesting base data (from the network or a file, respectively) and TCP and FILE for accessing archive streams (from the network or file, respectively). Switching between protocols

required no modifications to application developer's code; it was achieved by changing entries in a data file (called the algorithm services file).

Plans for the summer 1990 real-time demonstration called for an increase in the number of processes targeted for the FL-2C real-time testbed, each with a need to support multiple real-time data streams. These new algorithms were outside the microburst real-time software domain; moreover, the responsibility for the new off-line analysis tools required for algorithm development was spread across the group. Thus, in late December 1989 it was decided to move toward a coherent group-wide interprocess communications library that could be used both in real-time and off-line for development and analysis. Precedent for this approach existed. Early in the development of the advanced gust front algorithm, the essence of the server-client package was extracted from the microburst code and built into the advanced gust front feature extractor. Although the particulars of the libraries differed, the interfaces remained the same.

The new general purpose server-client library (sc_pac) was completed and widely adopted. As the summer approached, a flaw was discovered in the design of the TCP portion of the package that occasionally caused processes to lose a connection. With the order-of-magnitude increase in the number of connections required to support the FL-2C real-time system between 1989 and 1990, this flaw was likely to create problems during operations. System patches were applied to reduce the likelihood of a process disconnect; however, only a redesign and rewrite of this portion of the package can completely correct the problem. The rewrite of sc_pac is scheduled to begin in October 1990 and should be completed in time to guarantee a stable communications platform for operations in summer of 1991.

### b. Logical Record Package (logrec) and Logical Record Template Library (lrtemps)

A generic logical record stream is self-defining and is used to communicate data between processes. A stream contains template records that describe the format of each of the record types found within it. The basic logical record package (logrec) contains procedures that use these templates to facilitate the reading or writing of these data streams. Functions are provided to translate between the application-specific internal representation of data and the application-independent logical record external format.

The software was first developed in the fall of 1989, but it was not widely used. During this reporting period, the package was tested extensively. To correct flaws in the implementation and to make the package more flexible for both real-time and analysis use, modifications were made to both the low-level logrec primitives and the higher-level programmer interface routines. The original template definitions made it difficult to represent data that were most easily organized as sets of related data items (e.g., latitude, longitude, altitude, and transponder code for each of "n" beacon reports). Both the template definitions and *logrec* software were enhanced to incorporate the nested block structures that permit a natural representation of these sets.

Although an applications programmer is free to define his internal data structure in whatever manner he wishes, the logical record template library (*lrtemps*) provides a set of generally accepted record packing/unpacking routines for the standard logical records used group-wide. Use of these library routines provides "C" language data structures to represent these records in a way that matches the templates in order and data type. The *lrtemps* library is new this reporting period.

## 2. Data Access

### a. Common Format for Tapes (CFT) Library

The Common Format for Tapes (CFT) provides a flexible mechanism for describing radar data in polar coordinates. The data sets are divided into volume scans which are subdivided into tilts which are further subdivided into radials. The CFT library contains subroutines that allow users to read and write data in this format. The original version of the software presumed that

the primary input/output units were tapes; its data access mechanisms were optimized accordingly. Extensive use of disk files and the addition of large-capacity optical disks to the network motivated substantial enhancements to the CFT package. Key characteristics of the new version include support for multiple scans in disk files, rapid direct access to scans and tilts (rather than the current slower, sequential access), and better error-handling facilities. The new library has been tested extensively and a beta version is now available (in addition to the standard CFT library) for programming purposes.

### b. On-line Data Access

Software to provide on-line access to information about the Group's weather data has been completed for Sun-3 systems. Relevant data, such as PRF, tilt start and end times, tilt type, elevation angle, azimuth limits, have been extracted from the inventories of all CFT tapes and loaded into a CFT inventory database. The user interface to the software, *querytool*, assists the user in specifying values for these data items that will allow the system to identify the set of tilts (scans and tapes) of interest. The software translates the user's specifications into a set of search criteria and operates on the database using INGRES, a commercial database management package. For a given radar site and year, search criteria can be specified in terms of any of the data types in the database. The *querytool* support function (qual_tilts) allows programmers to incorporate this search function into applications programs. Because INGRES is licensed only for the Sun-3 systems in Lexington, the use of *querytool* is limited to those platforms.

### c. Radar Data Manipulation (cuisinart)

*Cuisinart* is a general purpose radar data manipulation package that makes it easy for users to read, write, and manipulate tilts of radar data. The original package was layered on top of the CFT library, making basic CFT access calls and placing the data into well-formed "C" language data structures. The CFT interface proved too slow for real-time data acquisition. Enhancements to the package allow direct transfer from raw data, as delivered by the base data Ethernet through the server-client interface, into *cuisinart* data structures. A variety of additional improvements were made to the support for comments, the treatment of range clipping, and the handling of I/O errors.

## 3. Translators

### a. Universal Tape Format translator

Deficiencies in our current capabilities for translating data tapes from Universal Tape Format (UTF) to CFT were identified as a result of the increasing number of requests by group members for data from a variety of sources. As a result, a new Universal-to-CFT translator was specified, the design completed, and implementation begun. The new translator will operate based on instructions for interpreting non-standard data that are associated with each radar site and year. These instructions will be maintained in simple, human-readable form in a data file that can be updated as needed. The new translator will function in either the Sun or the Concurrent environment.

### b. UND Translator

Modifications to the UND signal processor changed what was recorded on tape. As of 22 July 1989, signal-to-noise information was no longer provided. Since most of the applications for UND data use only reflectivity and velocity information, the omission went undetected through the fall. However, since signal-to-noise is required for clutter map generation and Lincoln microburst detection algorithms, the UND-to-CFT translator was modified so that it derives signal-to-noise from reflectivity. The new translator was installed at FL-2C and used to re-translate affected data tapes.

## 4. System Software

### a. Modemtool

A number of users access the Sun network remotely. *Modemtool* is an English language, command-driven, modem interface. It allows the user to set or query any of the modem's interface controls, turn CAPTURE on or off, or dial another machine. It has been completed but not released since the documentation is incomplete.

### b. Configuration Control

Reliable administration of the Group's general purpose software is extremely critical. The software must be operated on two Sun architectures (Sun-3 and Sun-4) and must be kept up to date at three sites (Lexington, FL-2C, and FL-3). Improvements to the general purpose software release and configuration control mechanisms were designed and partially implemented during this reporting period. Software to automatically generate the correct series of commands to regenerate all dependent utilities whenever a general purpose library is changed is part of this development. The syntax of the generic general purpose software makefiles is being improved to ensure that all include files are kept up to date and that all software has access to the most recent versions. Automatic flag setting has been improved as well. A study was made and some preliminary work done on improving general purpose Makefiles so that an automatic history is produced. The enhanced system should be completed during the next reporting period.

### c. Peripheral Control (printers, plotters, optical disks, etc.)

There were a number of enhancements to the suite of utilities that control the Group's printing and plotting resources. Among these were:

a. Utilities that provide access across the network to the rewritable optical disks,

b. Software that prints Sun files on the Inkjet plotter,

c. Enhanced utilities that print screen images using disk space on a remote machine as a print spooler, and

d. Spool queue managers that uncompress files automatically when plotting and compress them again when through.

### d. Applications Manager

The "messy desk" syndrome is as much a problem for an electronic desktop as a standard one. An new tool called the *Applications Manager* has been developed to allow users to locate processes and modify windows and icons on a desktop. The application manager has been coded and tested. It will be released as soon as documentation is complete.

## 5. Three-Dimensional Weather Analysis Workstation

The original time line slated for the three-dimensional weather analysis workstation called for a design document by the end of February. However, because of time spent on higher priority projects (server-client, scan mode selector, and the cockpit display), serious work on this document did not begin until the end of June. The document itself will contain the first serious attempt at software design and user interface design, based on third-party vendors and the group's needs. It also will contain our recommendations for a hardware platform.

## C. PROCESSING AND DISTRIBUTION

Raw radar data received from a variety of radar installations are translated into CFT, for further processing and distribution. Translations of data from the Lincoln Laboratory field sites are performed routinely for days of high activity or special interest. All remaining translations are done by request. Table 5-4 summarizes, by year, the number of raw tapes received from a particular source. Beginning in 1988, UND began translating their data internally and delivering only CFT tapes to Lincoln Laboratory. Table 5-5 lists the number of CFT tapes available by source and year.

**Table 5-4.**
**Raw Data Tapes Received from Various Sources.**

| Source | 1990 | 1989 | 1988 | 1987 | 1986 * | 1985 * |
|---|---|---|---|---|---|---|
| FL-2 | 415 | 817 | 815 | 511 | 249 | 963 |
| UND | 0 | 13 | 0 | 110 | 113 | 312 |
| LLWAS | 6 | 14 | 38 | 15 | 43 | 87 |
| Mesonet | 47 | 74 | 62 | 39 | 91 | 137 |
| MIT | 0 | 0 | 114 | 0 | 0 | 0 |
| ASR-9 | 1 | 0 | 31 | 0 | 0 | 0 |
| FL-3 | 21 | 105 | 124 | 0 | 0 | 0 |
| Kavouras | 0 | 0 | 44 | 6 | 0 | 0 |
| UND Aircraft | 35 | 31 | 0 | 50 | 58 | 50 |

* Beginning in 1987, raw tapes were recorded at 6250 bpi; before 1987, tapes were recorded at 1600 bpi.

**Table 5-5.**
**CFT Data Tapes Available by Radar.**

| Radar | 1990 | 1989 | 1988 |
|---|---|---|---|
| FL-2 | 373 | 476 | 856 |
| FL-3 | 31 | 118 | 27 |
| UND | 200 | 233 | 121 |
| MIT | 17 | --- | 122 |
| ASR-9 | --- | 43 | --- |

The Laboratory has gathered a wide variety of wind shear data, ranging from Mesonet weather station recordings to dual Doppler windfields. All data collected in support of wind shear studies are available to organizations, institutions, or individuals with a demonstrated need. Groups working in wind-shear related studies receive the highest priority. Other requests are honored but at a lower priority. In either case, an effort is made to distribute these data in a timely manner.

An ongoing cooperative effort between NSSL and MIT Lincoln Laboratory accounted for most of the data requests received during this period. Because the data were used to validate the gust front algorithm, additional processing was applied to the data before shipment. This processing, or Data Quality Editing, produces tapes in CFT format containing data that have been edited to remove the effects of residual ground clutter (clutter editing) and of distant weather (range obscuration editing). In addition, these tapes contain only the tilts of data (elevation angles of 0.5 and 1.0 degrees) used by the gust front algorithm. Table 5-6 indicates data requested by all outside organizations during this reporting period.

## Table 5-6.
## External Data Distribution: January through June 1990.

| Organization | Data Requested | | |
|---|---|---|---|
| | Radar | Format | Dates |
| CIRA | FL-2 | Universal | 13, 14, 19, 25, July 1986 |
| NCAR | FL-2 | Universal<br><br>Clutter and range obscuration edited; 0.5 and 1.0 degree tilts only | 01 September 1987<br>22, 25 June 1988<br>03, 04, 08 July 1988<br>10, 11, 16 July 1988<br>06 August 1988<br>27 March 1989<br>28 April 1989<br>18, 25 May 1989<br>18, 26 June 1989<br>27, 31 July 1989<br>15, 22 August 1989 |
| | FL-3 | CFT | 27 August 1989 |
| NOAA/ERL | FL-2 | Universal (base data) plus gust front algorithm output files | 11,17 July 1988 |
| NSSL | FL-2 | CFT | 11 July 1988 |
| | UND | CFT | 25 May 1989<br>28 August 1989 |
| | FL-2/UND | NCAR | Dual-Doppler Cartesian Files |
| | FL-2 | CFT<br><br>Clutter and range obscuration edited; 0.5 and 1.0 degree tilts only | 02 September 1987<br>22, 25 June 1988<br>03, 04, 08 July 1988<br>10, 11, 16 July 1988<br>06 August 1988<br>27 March 1989<br>28 April 1989<br>18, 25 May 1989<br>03, 18, 24, 26 June 1989<br>10, 12, 15 July 1989<br>27, 31 July 1989<br>15, 22 August 1989 |

## Table 5-6.
## (Continued)

| Organization | Data Requested | | |
|---|---|---|---|
| | Radar | Format | Dates |
| NSSL | FL-2 | RSM files | Resampled images for above days |
| | -- | Software | Shear and features routines<br>Man pages for WxShell |
| | FL-2 | CFT<br>Clutter and range obscuration edited; 0.5 and 1.0 degree tilts only | 02 July 1987<br>09, 10, 13 July 1988 |
| | UND | CFT | 28 August 1989 |

# 6. DATA QUALITY

## A. RANGE OBSCURATION

Range obscuration is the contamination of first-trip radar data by range-aliased signals from distant weather. The contamination may cause missed detections or false alarms either by obscuring or resembling wind shear events. The two techniques employed to minimize range obscuration effects on data quality in the TDWR system are adaptive PRF selection and range obscuration editing. The following sections discuss these techniques and associated data analyses.

### 1. PRF Selection Algorithm

The PRF selection algorithm serves as the primary means of obscuration mitigation. It selects a PRF that minimizes potential obscuration over the runways and in the microburst and gust front detection regions. During the reporting period, a new implementation of the algorithm was designed, coded, tested, and installed in the FL-2C testbed. Both the old and new implementations select PRFs in the general manner described in the TDWR specifications. [5] Several features were added, however, to conform to those specifications more fully, better emulate the Raytheon implementation, and improve algorithm flexibility. Those features are as follows:

a. Rectangular runway regions and circular regions centered on reference points other than the radar site. Figure 6-1 compares the regions used in Kansas City to those used in Orlando (the Orlando regions meet TDWR requirements).

b. Arbitrary list of available PRFs. Table 6-1 lists the Raytheon PRFs and their associated characteristics.

c. Raytheon velocity dealiasing dual scan PRF selection.

d. Run-time definition of adaptation parameters without source recompilation.

e. Archive records listing PRFs selected and other obscuration information.

Feature (c) above represents an extension to the original PRF algorithm specification, thus warranting further discussion. The Raytheon velocity dealiasing algorithm incorporates a feature wherein two successive 360° sweeps, made at complementary (primary and secondary) PRFs, are combined to resolve velocity ambiguities. Each primary PRF (selected by the algorithm for minimizing range obscuration) has an associated list of potential secondary PRFs, where the list is ordered by desirability of the primary-secondary PRF combinations for velocity dealiasing. The secondary PRF is chosen from the list according to criteria which attempt to minimize obscuration while maximizing desirability.

### 2. Kansas City Obscuration Analysis

Kansas City data were analyzed to assess the performance of the PRF algorithm and predict its effectiveness in the C-band TDWR system. The data set consisted of 250 long-range elevation scans from five days on which more microbursts than average occurred. Table 6-2 and Table 6-3 list results from this study and a previous study involving Denver data. [6] Table 6-2 lists the average S-band and C-band values of maximum, minimum, and "optimal" percent area obscured for each of the three detection regions. Table 6-3 lists the percent of time that each region was more than 10 percent obscured.

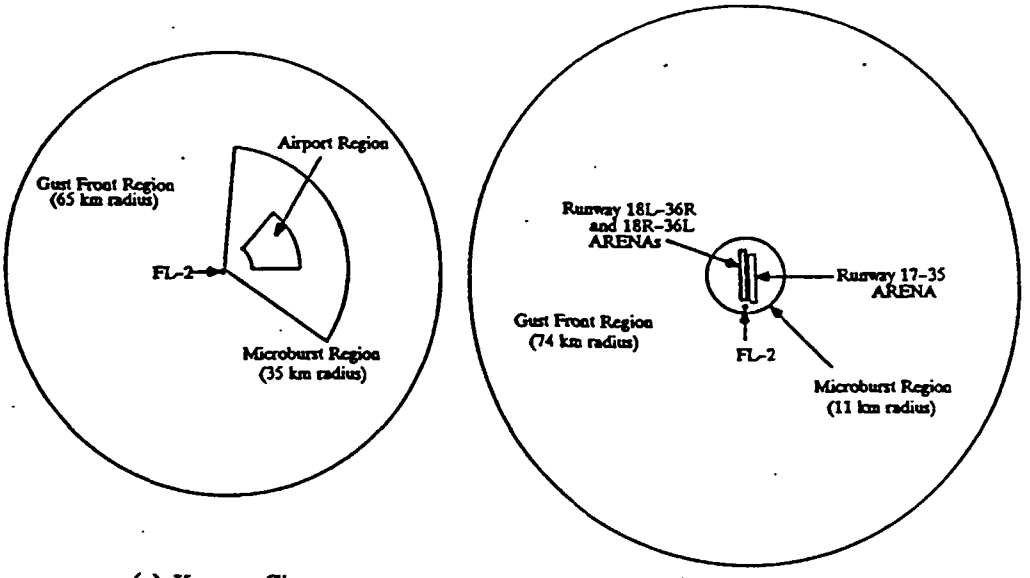


(a) Kansas City (b) Orlando

*Figure 6-1. (a) Former PRF selection regions, (b) new PRF selection regions.*

Kansas City obscuration levels were found to be generally higher than those in the Denver study for several reasons. The most significant factor in this difference was that the Kansas City storms were spatially much larger than those in Denver. Also, the Kansas City study focused on days with a great deal of precipitation, while the Denver data set was chosen to be representative of all weather conditions. Finally, in Denver the radar view of distant weather was partially blocked by the Rocky Mountains.

One of the conclusions of the Denver study was that for a given region, time spent with more than 10 percent of the region obscured "is expected to be on the order of between three and five times greater at C-band than at S-band." [6] The C-band to S-band ratio in Kansas City was, in general, lower than predicted. Table 6-3 shows that the ratio was about one for the airport region, one and a half for the microburst region, and two for the gust front region.

### 3. Effects of Radar Placement

To estimate the effects of radar placement on obscuration in Kansas City, the data were analyzed in three sectors. Sector 1 contained the actual airport and microburst regions. Sectors 2 and 3 were generated by rotating the airport and microburst regions about the radar by 120° and 240°, respectively. The region rotations simulate alternative sitings of the radar with respect to the airport and the weather.

## Table 6-1.
## Raytheon PRF Characteristics.

| PRF Number | Raytheon PRF (Hz) | FL-2 PRF (Hz) | PRI (μ sec) | Unambiguous Range (km) | (nml) | Nyquist velocity (M/s) | Available to PRF algorithm |
|---|---|---|---|---|---|---|---|
| 1 | 1930.5 | 1931 | 518 | 77.7 | 41.9 | 25.6 | |
| 2 | 1858.7 | 1859 | 538 | 80.7 | 43.6 | 24.7 | |
| 3 | 1792.1 | 1792 | 558 | 83.7 | 45.2 | 23.8 | |
| 4 | 1730.1 | 1730 | 578 | 86.7 | 46.8 | 23.0 | |
| 5 | 1672.2 | 1672 | 598 | 89.7 | 48.4 | 22.2 | √ |
| 6 | 1618.1 | 1618 | 618 | 92.7 | 50.0 | 21.5 | √ |
| 7 | 1567.4 | 1567 | 638 | 95.7 | 51.6 | 20.8 | √ |
| 8 | 1519.8 | 1520 | 658 | 98.7 | 53.3 | 20.2 | √ |
| 9 | 1474.9 | 1475 | 673 | 101.7 | 54.9 | 19.6 | √ |
| 10 | 1432.7 | 1433 | 698 | 104.7 | 56.5 | 19.0 | √ |
| 11 | 1392.8 | 1393 | 718 | 107.7 | 58.1 | 18.5 | √ |
| 12 | 1355.0 | 1355 | 738 | 110.7 | 59.7 | 18.0 | √ |
| 13 | 1319.3 | 1319 | 758 | 113.7 | 61.4 | 17.5 | √ |
| 14 | 1285.3 | 1285 | 778 | 116.7 | 63.0 | 17.1 | √ |
| 15 | 1253.1 | 1253 | 798 | 119.7 | 64.6 | 16.6 | √ |
| 16 | 1222.5 | 1222 | 818 | 122.7 | 66.2 | 16.2 | √ |
| 17 | 1193.3 | 1193 | 838 | 125.7 | 67.8 | 15.8 | √ |
| 18 | 1165.5 | 1166 | 858 | 128.7 | 69.5 | 15.5 | √ |
| 19 | 1139.0 | 1139 | 878 | 131.7 | 71.1 | 15.1 | √ |
| 20 | 1113.6 | 1114 | 898 | 134.7 | 72.7 | 14.8 | √ |
| 21 | 1089.3 | 1089 | 918 | 137.7 | 74.3 | 14.5 | √ |
| 22 | 1066.1 | 1066 | 938 | 140.7 | 75.9 | 14.2 | √ |
| 23 | 326.2 | 326 | 3066 | 459.9 | 248.2 | 4.3 | |

**Table 6-2.**
**Percent Area Obscured.**

| | Runway Region | | | Microburst Region | | | Gust Front Region | | |
|---|---|---|---|---|---|---|---|---|---|
| | Min | Max | Opt | Min | Max | Opt | Min | Max | Opt |
| **Kansas City** | | | | | | | | | |
| S-Band | 19 | 49 | 20 | 13 | 32 | 15 | 7 | 20 | 11 |
| C-Band | 21 | 52 | 22 | 21 | 35 | 23 | 15 | 23 | 18 |
| **Denver** | | | | | | | | | |
| S-Band | 0 | 14 | 1 | 1 | 11 | 1 | 1 | 6 | 1 |
| C-Band | 1 | 22 | 3 | 3 | 17 | 5 | 1 | 9 | 4 |

**Table 6-3.**
**Percent of Time With More Than Ten Percent Area Obscured.**

| | Runway Region | Microburst Region | Gust Front Region |
|---|---|---|---|
| **Kansas City** | | | |
| S-Band | 47 | 57 | 35 |
| C-Band | 51 | 74 | 75 |
| **Denver** | | | |
| S-Band | 2 | 4 | 2 |
| C-Band | 6 | 14 | 10 |

Table 6-4 lists the results of the three-sector analysis. Sector 1 was the most severely obscured, averaging 19 percent obscuration over the runway. Sector 3 was somewhat better, with an average of 12 percent. Sector 2, however, averaged only one percent obscuration over the runway. These results correlate well with the observed storm morphology in Kansas City. On days with heavy weather, the storms approached from the northwest and passed to the east or southeast, with few storms passing to the south of the radar. The gust front region geometry remained the same in all three analyses, but its obscuration level varied because gust front PRF choice is affected by runway obscuration.

At any given airport there are a number of important issues involved in choosing between prospective TDWR sites. The results of the three-sector study indicate that potential obscuration

might be used as one index of site desirability. The study shows that in some parts of the country, radar location and trends in storm evolution combine to be a first-order factor in the level of obscuration.

**Table 6-4.**
**Three-Sector Study: Percent Area Obscured at Optimal PRF.**

| Sector | Runway | Microburst | Gust Front |
|---|---|---|---|
| 1 (centered at $0^{o}$) | 20 | 15 | 11 |
| 2 (rotated $120^{o}$) | 1 | 2 | 8 |
| 3 (rotated $240^{o}$) | 12 | 12 | 10 |

### 4. Range Obscuration Editing

The secondary method of minimizing the effects of out-of-trip weather is range obscuration editing. In the technique used to date, a low PRF sweep is used to locate distant weather (the sweep is the same one used as the basis for PRF selection). During subsequent data collection, the out-of-trip contributions due to the distant weather, determined according to the current (PRF-dependent) unambiguous range, are estimated for each gate. If the measured signal in a gate does not exceed the total out-of-trip contribution for that gate by at least a site-adaptable obscuration threshold, the gate is flagged invalid.

Because storm structure varies with altitude, the distant weather information collected at a given elevation is not accurate for other elevations. Because storm structure also varies with time, distant weather information becomes less accurate with time. Due to scan strategy timing limitations, low PRF sweeps are made infrequently (approximately every five minutes), and at a limited number of elevations (typically one). Therefore, range obscuration editing of hazardous weather sweeps is almost always based on inaccurate distant weather information. To compensate for these effects, the editing test is weighted according to the age and relative elevation of the distant weather information.

Because the currently proposed Raytheon TDWR implementation does not include age and elevation weighting, these features were removed for the Orlando demonstration; in compensation, the obscuration threshold was raised from 1.5 to 3 dB.

### 5. Future Work

The combined results of PRF selection and range obscuration editing were favorable in Kansas City. Only five false wind shear detection alarms (three percent of all false alarms) were due to out-of-trip contamination during the Kansas City operational demonstration. However, the data indicate that even with adaptive PRF selection, there may be significant contamination. One area of concentration in the future will be to improve the effectiveness of range obscuration editing.

## B. VELOCITY DEALIASING

The TDWR requirements for unambiguous detection range (90 km) and velocity measurements (-40 to +40 m/s) cannot be simultaneously met using single PRT (pulse repetition time) radar signals and the standard pulse-pair velocity estimator. Hence, there is a need for

methods that either recover aliased velocities (post-estimation correction) or for signal designs and processing strategies that have an extended range of Doppler velocity observability.

Post-estimation correction represents one of the more successful approaches currently available. The velocity dealiasing algorithm proposed by Raytheon for TDWR is an example of this method. A similar technique, developed at NSSL, has long been used as part of the Group's data analysis and real-time efforts. However, post-estimation correction can be computationally intensive and, more importantly, prone to large systematic errors. Therefore, it is beneficial to continue investigations of improved estimation procedures which could incorporate constraints (e.g., continuity) or model structure.

### 1. Raytheon Velocity Dealiasing Algorithm

The Raytheon velocity dealiasing algorithm has three major features:

a. Two successive scans at a given elevation using complementary PRFs, allowing unambiguous velocity determination to several multiples of the Nyquist velocity. Due to scan strategy time constraints, this "dual-scan" method cannot be used at every elevation.

b. Radial and azimuthal velocity continuity constraints, including various quality checks.

c. A three-dimensional windfield model, initialized by the dual-scan process, and updated at every elevation. The windfield model velocities are used as dealiasing references when there are insufficient valid data points to determine radial or azimuthal continuity.

A real-time implementation of this algorithm for the *FL-2C testbed was designed*, coded, and tested. By the start of the 1990 demonstration in Orlando, this implementation had been accepted for operational use, pending results of continued observation of the dealiasing quality. Although the algorithm seemed to perform adequately, it was clear that there were concerns:

a. The error rate of the velocities produced by the dual scan portion of the algorithm seemed very sensitive to the PRFs chosen and to range-folded distant weather returns (range obscuration).

b. The windfield model was very sensitive to dual-scan errors.

Item a, and to a lesser extent b above, were addressed by more carefully constraining the choice of PRFs to be used during dual scans.

Toward the end of the reporting period, an effort was begun to independently verify the correctness of the real-time implementation and to analyze algorithm failures. This effort will continue into (and possibly through) the next reporting period.

### 2. Dual-PRT Velocity Estimators

Dual-PRT signal designs potentially can extend the range of unambiguous Doppler measurements well beyond the TDWR requirement. Two possibilities, alternating block and alternating PRT, are being investigated.

Handling of either signal design is straightforward when clutter filtering is not required; however, due to the added complexity of the radar signals, efficient and effective clutter removal is a significant obstacle to practical implementation. An alternating-PRT signal design has a statistical estimation performance advantage when clutter filtering is not required, but the

complexity of filter implementation and the effects of clutter removal on estimator performance may be practical factors which will outweigh the idealized performance advantage.

## C. CLUTTER FILTERS

Although clutter filters for uniformly spaced pulses are well understood theoretically, practical use in the FL-2C testbed has revealed certain anomalies in performance. There is an ongoing effort to characterize and reduce (or eliminate) these anomalies. Clutter filters for the more complex dual-PRT signals are not as well understood and were the subject of considerable study during the reporting period.

### 1. AGC/Normalizer Errors

FL-2C testbed experience in Denver and Kansas City suggested that AGC/normalizer step and impulse errors degrade the suppression performance of clutter filters. The effect of these errors on finite impulse response (FIR) and infinite impulse response (IIR) filter performance was studied, and it was determined that step and impulse errors should be no larger than 0.1 dB.

### 2. C-Band Filter Performance

The FL-2 testbed conversion to C-band necessitated a redesign of the testbed FIR filters. Deviations from anticipated filter performance in the areas of suppression depth and velocity estimator performance were observed. Studies were initiated to understand and alleviate these degradative effects. These studies initially focussed on performance of the testbed FIR filters but will probably be extended to determine possible consequences with IIR implementations.

### 3. Filters for Dual-PRT Signals

The analysis of candidate filtering methods for the dual-PRT signal formats has been considered a prerequisite to their testbed evaluation. Potential filtering methods have been identified for the alternating-block and alternating-PRT signals.

Although standard filtering schemes can be used with block-structured signals, undesirable signal transients are generated each time a block boundary is crossed. For FIR filters, the transients are finite in length but result in a loss of more than 50 percent of the collected data samples. This is significant when one considers that the TDWR scan requirements limit the block size to 20-40 pulses. Uninitialized IIR filters elicit transients which are much longer than their FIR counterparts; therefore, they are even less desirable. A new method for initializing IIR filters was developed at Lincoln Laboratory [7] which substantially reduces the initial IIR transients (well below the FIR bounds). This considerably improves the feasibility of using IIR filters for block-structured signals and will be the focus of efforts to implement alternating-block PRT schemes.

Alternating-PRT signals are more difficult to filter because their structure requires time-varying clutter filters, a research area with little or no precedent. Design methods for such filters were developed based on Chebyshev and mean-squared error criteria. Unfortunately, the time-varying structure of these filters results in a nonlinear phase response. Phase response is critical to the performance of the pulse-pair estimator. Piecewise linear phase and quasi-linear phase filters are being investigated as a means of dealing with this issue.

## D. CLUTTER RESIDUE MAPS

The attenuation resulting from clutter filtering is not sufficient to suppress all clutter returns to levels below those of all possible microburst and gust front outflow reflectivities, and returns from some clutter sources (such as vehicles moving along highways) are not affected at all by clutter filtering. Clutter breakthrough can significantly affect the accuracy of velocity measurements, with resulting velocity signatures possibly containing weather-like patterns.

Clutter residue map-based data flagging (editing) is called for in the TDWR specification to improve overall clutter rejection, reducing algorithm false-alarm rates at the expense of slightly degraded detection performance.

The clutter residue map editing system uses a polar map of residual clutter powers as thresholds to which weather measurement signal powers are compared. Measured signal powers not exceeding the residual clutter power at a given range/azimuth location are flagged invalid. For each map range/azimuth cell, the entry is the sample median of clutter residue power measurements plus a map threshold. A valid sample median for each map resolution cell must exceed a predetermined clear air reflectivity.

### 1. Clutter Residue Maps Generated

Two 1988 Denver clutter residue maps were re-generated with a different clear air reflectivity and map threshold than used with the maps in place during the 1988 OT&E. Arcs of clutter patches induced by sidelobe returns from downtown Denver were inserted using the polygon editing facility. These maps were used to support development and testing of the advanced gust front algorithm.

The procedure for creating clutter residue maps from non-indexed beam data was implemented and tested. Three sets of non-indexed beam clutter residue maps (1986 and 1987 FL-2 maps, and 1989 UND maps) were generated. The 1989 UND maps were used to support dual Doppler data analysis of Kansas City data.

### 2. Clutter Residue in Orlando

Initial Orlando FL-2C clutter measurements were made on 22 May 1990. The clutter environment in Orlando appears to be much more benign than in Kansas City, but further studies are needed to determine the relative influence of the smaller beamwidth (now 0.5 degrees), the Raytheon point target editor, and the flat terrain.

Range-folded distant weather and anomalous propagation (AP) are much more of a problem in Orlando than at previous sites. Routine AP in the mornings and severe weather in the afternoons interfered with clutter residue measurements prior to the summer demonstration. Clutter residue measurements will be attempted again when the AP and weather patterns permit.

### 3. Clear Air Reflectivity Issues

Summer clear air reflectivities are highly nonhomogeneous and range from 0 to 10 dBZ. Because these reflectivities can contaminate clutter residue maps, it is necessary to determine a representative clear air reflectivity to be used as a quality check when generating maps. Clutter residue whose estimated median reflectivity is smaller than the estimated clear air reflectivity is discarded. The effect of clutter residue breakthrough will be more serious at the microburst outflow region, because of the weaker weather signal than at the microburst core. Appendix A compiles summer microburst outflow reflectivity distributions at Denver and Kansas City based on FL-2 data.

The choice of clear air reflectivity value is critical to the quality of a clutter residue map. If it is set too high, significant clutter residue may be left out of the map (allowing clutter breakthrough during the editing process); if set too low, the map may contain significant clear air returns that will be treated as clutter. In almost all cases the optimal clear air reflectivity will cause some clutter residue to be discarded and some clear air to be treated as clutter. While human experts can select appropriate clear reflectivity values from analysis of clear air and clutter residue data, it is desirable (particularly for an automated system such as TDWR) to be able to perform this function without the benefit of expert analysis.

A representative clear air reflectivity can be determined systematically by comparing a clear air reflectivity distribution, created from data collected during special scans, with a spatial distribution of clutter residue reflectivity. Comparison criteria must be established which will appropriately balance the amount of clutter residue to be discarded with the amount of clear air reflectivity to be treated as clutter. One basic criterion is to attempt to discard no more than 10 percent of the clutter residue. On cases examined to date, this corresponds to the elimination of approximately 90 percent of the clear air returns in a clutter residue map and is comparable to results achieved by expert analysis.

The current ability to compensate for clear air reflectivity contamination is considered a fundamental limitation in the quality of most of the clutter residue maps generated to date. However, since virtually no clear air returns were found in Denver and Kansas City during the winter season (see Appendix A), it is possible that clutter residue measurements taken during that time of the year might be free of clear air reflectivity effects. If it is possible to reconcile (or ignore) seasonal changes in the clutter environment at a given site, winter measurements might be the best basis for high-quality clutter residue maps year-round. Work in this area will continue.

## 4. Clutter and Clutter Residue Statistics

Temporal S-band clutter residue reflectivity fluctuations in Denver (over the Rocky Mountains and downtown Denver) and Kansas City (in the Missouri River area) were studied. Two-dimensional non-central Gamma distributions fit well with the clutter residue reflectivity fluctuations about the means. It was found that 95 percent of S-band clutter residue reflectivity fluctuations are less than 5 dB above the mean. This implies that the clutter residue map threshold should be set about 5 dB. A similar study will be conducted for Orlando when sufficient C-band clutter residue samples are available.

Spatial clutter and clutter residue reflectivities collected in the Missouri River area can be fitted by K-distributions. Further study is needed to assess the potential of using K-distributions during the determination of a representative clear-air reflectivity value in Orlando.

Clutter and clutter residue time series data collected in the Missouri River area can be fitted by autoregressive processes. If the fitted parametric models can be shown to be reliable, then they can be used to improve weather signal processing in the general clutter environment.

The joint probability density function of reflectivity and pulse-pair Doppler mean velocity estimates can be approximated by the product of exponential, modified Bessel and confluent hypergeometric functions. The derived joint probability density function is the basis for evaluating the effectiveness of a clutter residue map in terms of its ability to improve shear detection in a clutter environment. The shape of the function reveals its high sensitivity to the ratio of weather signal to clutter residue. This suggests that simple data flagging may not be the optimal strategy for using clutter residue information in conjunction with shear-finding algorithms. Future work will address this issue.

# 7. ALGORITHM DEVELOPMENT

## A. MICROBURST ALGORITHM DEVELOPMENT

### 1. Divergence Region Detection

A number of minor changes were made to Lincoln Divergence Regions implementation to conform to the formal algorithm specification (AEL). The segment cropping and shear trimming tests required minor changes. Some additional information was added to the divergence segment archives, for contractor support. Altitude processing limits also were added, as specified in the AEL.

### 2. Convergence Region Detection

Work was completed on improving the convergence detection algorithm. The purpose of the algorithm is to identify regions of converging winds aloft. Identified convergence regions are then used in the microburst system to create microburst precursors and to make microburst predictions. An initial investigation by staff meteorologists indicated that the convergence detection algorithm did not have acceptable performance. This prompted an effort to improve the algorithm.

The convergence detection algorithm looks for radial segments of decreasing velocity and groups the segments into two-dimensional regions. The performance of the original algorithm is shown in Table 7-1. The original algorithm has a low Probability of Detection (POD) and a high Probability of False Alarm (PFA).

Several techniques to improve performance were tried. The first involved modifying some of the algorithm's parameters to improve performance. Several parameters were modified, improving the POD by 25 percent while lowering the PFA by five percent. An experiment using the radar's spectrum width product was able to further reduce the PFA, at a slight cost in POD. Convergence regions which were in areas of low spectrum width (less than 2.75 m/s) were eliminated.

**Table 7-1.**
**Convergence Detection Performance.**

| Algorithm | Truths | Hits | Alarms | False | POD | PFA |
|---|---|---|---|---|---|---|
| Original | 645 | 340 | 1805 | 817 | 52% | 45% |
| Optimized Parameter | 645 | 495 | 2604 | 1058 | 77% | 40% |
| Spectrum Width | 645 | 432 | 1619 | 520 | 66% | 32% |
| Discriminant Analysis | 645 | 505 | 1759 | 464 | 78% | 26% |

One other experiment involving validation of convergence regions based on Quadratic Discriminant Analysis also was very successful. A large set of known convergence regions were used to create models for valid and false convergence regions. The models were then used to classify new convergence regions by determining whether the new region was closer to the valid convergence region prototype or the false convergence region prototype. This technique reduced the PFA of the optimized parameter algorithm by 14 percent while increasing the POD by one percent.

Several memos and a project memorandum were written describing the convergence algorithm improvements. The optimized parameter algorithm will be used during the operational demonstration in Orlando.

### 3. Rotation Region Detection

The Rotation Region Detection Algorithm detects regions of cyclonic and anti-cyclonic rotation first by searching radar image data for runs of azimuthal shear. These runs are then associated spatially by range and azimuth into two-dimensional regions. The output of the algorithm is used by the microburst algorithm by interpreting the rotation region as a precursor to the detection or prediction of subsequent surface outflow.

The rotation algorithm suffered from an unacceptable PFA. Two changes were made to the algorithm to improve the PFA: 1) the addition of a threshold which would allow a shear segment to continue to grow only if adding to its length would not significantly decrease its overall shear and 2) changing site-adaptable parameters such as feature area, minimum segment length, velocity differential, and range and azimuth association criteria. The addition of the threshold made a significant improvement in algorithm performance.

The algorithm was tested on radar data collected at Huntsville, Denver, and Kansas City. The total number of detections declared by the algorithm decreased, as seen by the Alarms-to-Truth Ratio (ATR), which translated to an overall decrease in false alarms. Taken as a whole, the impact of these changes on the algorithm appeared to be small. However, when the results were analyzed on a site-by-site basis, a pattern emerged. Table 7-2 shows that the PFA in the wet Kansas City and Huntsville environments decreased 17 percent (from 54 to 37 percent) whereas the PFA for the dry Denver environment increased 4 percent (from 60 to 64 percent). The POD decreased for both environments. These results indicated that parameter tuning must be done on a regional basis.

**Table 7-2.**
**Probability of Detection (POD), Probability of False Alarm (PFA), and Alarms-to-Truth Ratio (ATR) for Wet and Dry Microbursts.**

| | POD | PFA | ATR |
|---|---|---|---|
| wet | 89 | 54 | 2.9 |
| dry | 59 | 60 | 1.9 |

old

| | POD | PFA | ATR |
|---|---|---|---|
| wet | 84 | 37 | 2.1 |
| dry | 40 | 64 | 1.5 |

new

wet = Kansas City and Huntsville

dry = Denver

This analysis showed that segments must be allowed to be shorter and more numerous, while at the same time the azimuthal association criteria should be relaxed. In this way, spurious segments will be grouped together into regions that ultimately will be invalidated because of insufficient area, while legitimate rotation will be detectable. Therefore, the texture of the data will be modelled by the regions representing its first derivative.

A preliminary discriminant analysis was performed to assess its impact on algorithm performance. Discriminant analysis involves the problem of determining if an algorithm declaration is a good or false detection, based on a set of measured features such as deltaV, segment length, etc. A distribution model is specified through estimation of the mean feature vector and covariance matrix for each class. The covariance matrix shows the relationships and dependencies between the various features of a rotation region and their relative importance in classifying the alarm. If this discriminant function were to be implemented in the rotation algorithm, then when an alarm had passed all its current validation thresholds, the probability that the alarm is valid would be calculated from the discrimination function metric. This, as a final test for the alarm, would invalidate those regions judged to be ultimately false alarms and keep only those considered hits.

The preliminary discriminant analysis indicated that if the discriminant function were included in the algorithm's implementation, 27 percent of the false alarms would be eliminated while the decrease in POD would be seven percent. The number of segments in a region is its most distinguishing characteristic, although other features such as shear area and velocity differential should be included in the covariance matrix calculation.

A project report describing the parameter tuning and discriminant study is presently being prepared.

Even with all of the improvements described above, the algorithm detects azimuthal shear which are not necessarily associated with a microburst. Thus, without benefit of reflectivity or storm cell information, there is a limit to the decrease in the PFA.

### 4. Reflectivity Region Detection

The reflectivity region detection algorithm detects regions of significant reflectivity on a tilt-by-tilt basis. This is achieved by associating reflectivity segments–runs of data on a radial which have a reflectivity above a threshold. An area, centroid, bounding-box, and other parameters are calculated for each region. Regions are detected at three different thresholds: 15, 30, and 45 dBZ. These regions are passed on to the three-dimensional reflectivity structures alogorithms and are eventually used as features aloft.

The reflectivity region detection algorithm was modified to support the verification of contractors' implementations. Unique feature identifiers were added and a run-length parameter was added. These modifications were subsequently tested and verified. The resulting segments agreed with at least 90 percent of Prototype Regional Observing and Forecasting Service's (PROFS) segments.

### 5. Storm Mass and Volume

Storm mass and volume were added to the real-time system to reduce the data processing requirements for studies being run at the Lincoln. The products presently are not used by the algorithm in the prediction or detection of microbursts.

The capability to estimate the liquid water content and mass of reflectivity structures was added to the real-time system. This capability is divided between the Sun and the Symbolics systems. Two-dimensional features are extracted on the Sun systems and then combined into

three-dimensional structures on the Symbolics. A simulation was performed to check the performance of the algorithm, and the result was a 12 percent worst-case error in the normal operating range of the storm.

A case from 30 July 1989 in Claycomo, MO was studied in detail. In this case, the liquid-water-based measurements of vertically integrated liquid water (VIL) and the center of gravity altitude (CGZ) were able to detect significant reflectivity events in the storm which were associated with pulses in the microburst differential outflow. This case was described in a paper [8] to be presented at the AMS 16th Conference on Severe Local Storms .

Studies are underway to correlate the outflow strength of microbursts with the various liquid-water-based measures.

### 6. Microburst Prediction

The Microburst Prediction (MBP) product is a simple extension of the microburst precursor recognition already performed by the TDWR. Microburst precursors are recognized when a reflectivity core occurs in conjunction with velocity structures (rotation aloft, convergence aloft, etc.) and when certain criteria are met. For example, in the Kansas City testing, each reflectivity core was required to have a maximum reflectivity of at least 54 dBZ and a height of at least 4.5 km. In addition, one of two additional criteria needed to be satisfied: either the reflectivity core was descending or the velocity structure (convergence or rotation aloft) extended below 3.5 km altitude.

Once a microburst precursor is initially declared, the MBP product issues the prediction that the outflow will begin five minutes later. The prediction is then counted down by one minute for each subsequent surface scan until a microburst outflow occurs or until seven minutes elapse. Both the prediction time and the cut-off time are site-adaptable parameters.

The prototype MBP product was tested off line during TDWR testbed operations at Kansas City in 1989. The MBP product was able to predict 61 percent (22 of 36) of events reaching at least 15 m/s outflow intensity. The mean warning time from initial prediction to onset of surface outflow was five minutes. For all predictions, 89 percent (40 of 45) resulted in a microburst outflow of at least 10 m/s (i.e., 11 percent of the predictions were false). Analysis showed that further tuning of the site-adaptable parameters could raise the probability of microburst prediction (PMP) to 67 percent and reduce the probability of false prediction (PFP) to seven percent.

An interesting observation concerning the Kansas City results is that five percent of the microbursts correctly predicted by the MBP product did not reach 10 m/s outflow as observed by the TDWR testbed radar (FL-2) but did reach 10 m/s from the UND radar's perspective. This suggests that asymmetry was present in these cases. Moreover, since features aloft were detected, indicating the presence of a significant downdraft, features aloft may be useful in compensating for asymmetry. For example, the presence of features aloft might be used to increase the reported outflow intensity to compensate for asymmetric outflow.

Preliminary testing of the MBP product also was done at the TDWR testbed at Orlando, FL during the summer of 1990. Initial results for five days in June indicate a 56 percent PMP and a seven percent PFP. The mean prediction time was 6.4 minutes. Some adjustments were made to the site-adaptable parameters for the Orlando environment, such as increasing the reflectivity core maximum reflectivity and height criteria to 57 dBZ and 5.2 km, respectively. An additional threshold also was added requiring the reflectivity core bottom to be below 3.5 km.

Given that the initial performance results for the MBP product are encouraging, the issue of operational use of the product arises. One potential operational use is in aiding ATC tactical planning and evaluation of potential weather hazard. Advance notice that a microburst outflow

will impact an approach path would allow TRACON controllers to reroute or hold traffic instead of incurring missed approaches. It would also provide early warning of an impending weather hazard situation. A second operational use is in Mode S Data Link to aircraft to aid pilots in planning and situation awareness. Awareness of an impending microburst several minutes in advance potentially would allow pilots to modify their landing strategy (e.g., by increasing approach speed or planning a longer landing).

### 7. Microburst Shape Algorithm

Because of the need for Lincoln Laboratory to recode the GSD to emulate the Raytheon Display Function Unit (DFU), it also was necessary to re-implement the Microburst Shape algorithm. The recoding was done from the Algorithm Enunciation Language (AEL) description, and the new software was installed in the TDWR testbed.

Some microburst over-warning problems occurred during the operational demonstration which were traced to three causes: 1) shape algorithm coding errors, 2) incorrect use of the 1988 shape algorithm parameter settings, and 3) long shear segments generated by the divergence regions algorithm. Coding errors and parameter settings were corrected for the shape algorithm, and the parameter settings also were adjusted in the divergence regions algorithm to reduce the incidence of long shear segments.

Although these changes reduced the incidence of over-warning, this issue requires further study and evaluation of potential changes. One change would be to add a segment validation test in the divergence regions algorithm, requiring a minimum shear over the entire segment (no such test is currently performed). Another change would be to relax the requirement that microburst shapes must enclose all segments composing them and instead use a weighted least-squares fit of shapes to segments. Such an approach was considered prior to the 1988 operational demonstration, but it was not implemented due to a concern to provide conservative warnings. A third change would be to narrow the 1-nmi-wide buffer zone around the flight path for runway warnings. This buffer zone appears to be larger than needed for the Orlando area, where microbursts and storms tend to be slow moving (unlike Kansas City, where they move rapidly).

These issues need to be addressed because of the substantial negative effect of over-warning on an airport such as Orlando. Unlike Denver or Kansas City, the Orlando runways are all oriented in the same direction. The lateral separation between the two runways is about 2.5 km (a little over 1 nmi), so the buffer zones nearly touch. The microburst shapes need to be very localized to prevent simultaneous warning on both runways. The complaint was frequently heard from ATC personnel that runway warnings were issued for both runways when clearly only one runway was actually impacted. Because pilots have been trained not to land when given a microburst warning, this over-warning situation effectively shut down the airport, resulting in a substantial impact on ATC operations. Thus, addressing this issue is important to prevent a negative ATC perception of the TDWR system and needless loss of airport capacity.

### 8. Trend Prediction

Work began on developing a new product for the microburst system (the microburst trend prediction product). The goal of the work is to create an algorithm to predict, for each microburst alarm, whether the strength of the microburst will increase or decrease over the next few minutes. The current focus of the research is to develop an algorithm which will detect times when a microburst is going to increase in strength by at least 4 m/s in the next three minutes.

The approach to the problem is one of classification. The system has to classify each microburst alarm either as being about to increase in strength or not. It does this based on a number of alarm attributes which are measured at the surface and aloft. These include the height of the core above the alarm, the current strength of the alarm, the volume of the storm cell above the alarm, the height of the convergence above the alarm, the shear of the rotation above the

alarm, etc. There are about 1200 such attributes available for each observation of each microburst alarm. It also has the time history, the last 10 observations of each of the base features. One of the biggest challenges with the trend prediction project is to choose the most discriminating set of measurements from the possible 1200 to use for decision making.

The data being used for the algorithm development consist of all the 1989 Kansas City data collected, which were truthed by a meteorologist. The data set contains approximately 40 hours of microburst observations. The large set of data is necessary because the algorithm development consists largely of sophisticated statistical procedures processing the data in search of discriminating features. The discriminating features are then used to build linear discriminant functions and exceptional case rules.

A number of tools, which also are useful to other projects, were written to support the creation, analysis, and display of the large set of data used. Tools also were written to automatically score the trend predictions produced by the algorithm.

There are two versions of the algorithm under development: a surface-only algorithm and an algorithm which uses features aloft. The advantage of the surface-only algorithm is that since it uses only those features which can be computed from the history of the surface outflow, it runs faster, and possibly its parameters will be less sensitive to regional meteorological characteristics. The advantage of the algorithm which uses features aloft is that it is able to incorporate features dealing with the aloft velocity and reflectivity behavior. Those features seem to be very important for accurately making trend predictions.

## B. MICROBURST ALGORITHM REAL-TIME IMPLEMENTATION

### 1. Feature Extraction

Several new versions of the microburst feature extractor were created. The feature extractor is the software, residing on the Sun, which processes the base radar data and produces two-dimensional divergence, convergence, rotation, and reflectivity regions. The changes made to the feature extractor fall into several categories:

#### a. New Capabilities

The most important addition to the feature extractor is the ability to produce segment archive records of all varieties (divergence, convergence, rotation, and reflectivity). The segment output is necessary for contractor support and verification and also for the new scan-mode selection function.

#### b. Formal Documentation (AEL) Compliance

Many of the algorithms used by the feature extractor required modifications to comply with the algorithms as described in the formal algorithm specifications written several years ago. The latest feature extractor matches the formal documentation more closely than it did before.

#### c. Bug Fixes

Several bugs in the feature extractor were tracked down and resolved. The bugs varied from memory allocation problems leading to system crashes to errors in the altitude calculations in regions.

Several memos were written which describe the changes made to the feature extractor in detail.

### 2. Symbolics

The software on the Symbolics system was parameterized to allow for site adaptation. Hard-coded constants were moved from the code into a separate parameter file which can be changed and loaded without recompiling the whole system. During this process, several discrepancies between the Lincoln Laboratory implementation and the AEL were located.

## C. MICROBURST ALGORITHM ANALYSIS

### 1. Sensitivity to Clutter Map XCR Value

The TDWR microburst algorithm allows for a number of site-adaptable parameters which might be adjusted according to the location. During the 1988 Operational Test and Evaluation in Denver, the clutter breakthrough adjustment value (XCR) was 10, while the SNR was 6 dB. The microburst scoring cases from Denver were replayed with an XCR of 5 and an SNR of 4 dB to determine the effects on the algorithm's performance. Lowering the XCR increased the POD by 1.2 percent, with little change in the PFA. A SNR of 6 dB increased the POD and the PFA by 3.3 and 1.2 percent, respectively. These changes improved the detection of the drier outflows typical of Denver and keep the PFA near six percent.

### 2. Sensitivity to Signal-to-Noise Threshold

During 1989 in Kansas City, the SNR threshold of the microburst algorithm was 6 dB, just as it was in Denver. However, there were excessive clear-air false alarms noted in real time in regions with noisy velocities. The performance with an SNR threshold of 8 dB was evaluated with data from seven days in Kansas City. Raising the SNR threshold eliminated 24 false alarms and reduced the overall PFA to less than six percent. This change resulted in five fewer detections, reducing the POD by less than 0.5 percent. This would have a positive impact on the performance of the system since many of the microburst false alarms were not associated with a reflectivity signature and were considered a nuisance by air traffic control.

## D. MICROBURST ALGORITHM CONTRACTOR SUPPORT

A Technical Interchange Meeting (TIM) was held on 10 April 1990 to discuss algorithm changes to Build 4. The most important change was to add a Running Mean test which was inadvertently omitted from the Divergence Regions algorithm AEL. Analysis had shown that the Divergence Regions algorithm would not produce acceptable results without this test. This change, plus a number of other small changes, was agreed upon to comprise a modified version of Build 4, designated Build 4a. It was agreed that STX corporation would generate a revised AEL reflecting the Build 4a changes.

Exchange Format data were provided to PROFS for the purpose of AEL verification, and a number of discrepancies between the Lincoln Laboratory implementation and the AEL were resolved. PROFS also was able to begin supplying Exchange Format data to Lincoln Laboratory for comparison. An automated tool for comparing two Exchange Format files was written to aid in the comparison process.

Exchange Format data also were supplied to Raytheon for testing purposes. These data were used by Raytheon primarily to test the higher-level functions of their algorithm (i.e., microburst outflow detection, features aloft, etc.). Although some minor discrepancies were found, agreement was found to be generally very good between the two data sets. The approach of exchanging algorithm results and close interaction between organizations appears to be working very well and is expected to continue over the next one to two years.

## E. GUST FRONT ALGORITHM DEVELOPMENT

There are currently two gust front algorithms: the operational algorithm and the advanced algorithm. The operational algorithm was developed at the NSSL. This algorithm is used during operational demonstrations to provide wind shear hazard and wind shift information to air traffic controllers and supervisors. The algorithm relies on the detection of radial convergence to identify gust fronts, and it will be delivered with the first TDWR systems.

A number of deficiencies were identified in the operational algorithm. Using the operational algorithm as a base, the advanced algorithm employs techniques such as the detection of azimuth-to-azimuth shear and thin lines to counter these deficiencies. Much of the work on the advanced algorithm is performed at Lincoln Laboratory.

### 1. Operational Algorithm

The operational gust front algorithm (GFA) is maintained primarily by NSSL. The role of Lincoln Laboratory with respect to the GFA is to run the algorithm in the real-time system, evaluate the performance of the algorithm, provide feedback to NSSL concerning problems with the algorithm, and maintain the algorithm on the Mile High Radar (MHR) at Denver, CO. In addition, Lincoln Laboratory is responsible for distributing output from the algorithm to Raytheon and PROFS for algorithm validation.

By January 1990, a number of special-use versions of the GFA existed. For example, there were versions corresponding to Build 4, Build 4a, Build 5, and a version which generated human-readable output format (known as exchange output format) for validation purposes. To halt this proliferation of versions, parameters and flags were implemented such that a single source code could be used to serve all functions, depending upon the parameter settings.

The GFA was ported to a Sun workstation for use in the MHR system. Modifications to the code were required to complete the porting.

During the Denver and Kansas City operational demonstrations, gust front forecasts were computed in the GSD. The GSD used for the Orlando demonstration was intended to mirror the Raytheon DFU, which does not compute forecasts. Therefore, the forecast computation was moved into the gust front algorithm. Forecast records to be used by the Orlando GSD were specified, and the code to generate these records was put into the algorithm.

In preparation for enhancing the GFA, the algorithm was coded on the Sun using the Build 4a Program Definition Language (PDL) written by NSSL. During this process, a number of issues emerged concerning inaccuracies in the PDL. These issues were discussed with NSSL, resulting in a number of improvements and clarifications to the PDL.

### 2. Advanced Algorithm

#### a. Front End

A LISP version of the AGFA thin line detection algorithm was ported from the Symbolics LISP environment to the Sun C environment. The porting involved developing and modifying general software packages to facilitate the resampling of polar data to a Cartesian grid as well as developing and modifying a data manipulation package. The porting from LISP to C went smoothly, and a number of enhancements were added to the algorithm. The first enhancement dealt with how the base reflectivity data were smoothed. The original LISP implementation used a two-dimensional averaging filter on the Cartesian image before any thin line extraction processing was begun. The C implementation uses a two-dimensional median filter on the original polar image. In addition to the preprocessing changes to the algorithm, the polygonal analysis routines were modified to take advantage of the processing speed of the Sun

workstations. A memo describing issues in porting a LISP-based algorithm to C was written and distributed in February.

Bulk runs of two versions of the Sun-based thin line algorithm were compared. The two versions differed in their methods of determining anti-parallel line segments. Results showed the newer version had an improved percent of length detection of the thin line over the old version.

The AGFA velocity feature extraction algorithms produce features that comprise the boundary of the region at a user-specified shear threshold. There are problems with this boundary representation in that the exact location of the peak values are not accurately depicted. Another effect of this boundary representation is that shear boundaries often contain forks. These forks make it difficult for back-end association logic to represent the exact nature of the gust front. A method for representing these features by connecting locations of closest peak shear was tried and will form the basis for future development in this area.

A prototype algorithm was developed which generates spined representations of shear regions. The prototype uses a "tree-building" approach. Work also was done on looking at more advanced methods of feature analysis (i.e., pruning, joining). Work began on a more advanced technique which will be able to support complex feature junctions (feature forks consisting of more than two branches).

Work was completed on an improved version of the skewing combined shear estimator. The improvement consisted of modifying the method used to generate the algorithm's pseudo-radials.

A prototype least-squares linear fit estimation routine was developed and tested in convergence-only and skewing combined shear modes.

A set of tools was built and debugged to analyze low-level shear feature extractor output. The tools ingested truth data and determined POD for shear features. The POD was estimated from the percent of length of the truthed gust front shear event that was seen by the estimator. The tools also allowed POD analysis with respect to orientation (measured from the radar radial) and strength of the event. A number of scripts were assembled to generate features and display outputs with respect to various orientation and strength criteria. Using these tools, an in-depth analysis was initiated on the current shear feature extractor combinations/options available for convergent shear extraction. Three feature extractor options were analyzed, and performance for various parameterizations is being investigated.

**b. Back End**

Evaluation began on an experimental software configuration control mechanism for use on the gust front project Sun system code. Work on feature extractor evaluation and the configuration control software continued through May. A version of the Sun portion of the gust front algorithm, to be run at site in Orlando, was finalized and installed in May. This configuration of the feature extractor generated reflectivity thin lines, radial convergence features, and combined shear features. A flexible window-based parameterization tool also was developed to allow site personnel to easily monitor and change the behavior of the feature extractor.

A stand-alone version of the NSSL wind shift algorithm was ported to the AGFA platform. The wind shift algorithm will work either as an off-line analysis tool or as a real-time module that can be used by the Lincoln Laboratory gust front algorithm back end. A large portion of the time spent in porting the algorithm was developing an environment that produced the exact inputs as seen by the NSSL wind shift estimator. This task was necessary to prove that the new AGFA wind shift estimator produced the same results as the NSSL wind shift estimator.

In porting the the NSSL wind shift algorithm, two errors were found. The first error was in the uniform wind analysis (UWA) velocity preprocessor. The gust front algorithm improperly

edited the UWA velocity values. The effect was that in some cases, wind shift estimates could not be made because the UWA velocity editor marked an excessive amount of UWA velocity values as "BAD." Another effect of improper editing was that in some cases, UWA velocity values which should have been marked as "BAD" were used by the wind shift algorithm as valid velocity values, causing invalid wind estimates to be produced.

The second error was found in the wind shift code and also was reflected in the wind shift PDL. The wind shift algorithm computed wind shifts over a sector at the midpoints ahead and behind a gust front. To compute this sector, the algorithm first computed the azimuth indices that made up a gust front. However, when an azimuth index of one was computed, the algorithm retrieved velocity values from the tilt at radial zero. In the operational gust front code, the zero$^{th}$ radial was undefined, and therefore the velocity values being retrieved for this radial were indeterminate. The wind shift PDL was unclear as to what action should occur when processing the first radial of a velocity tilt.

Two NSSL enhancements to the GFA were partially implemented in the AGFA. These enhancements consisted of two major techniques: one for forecasting and another for tracking fronts over the radar. The improved forecasts generated by the new forecasting technique provided the capability to make more aggressive use of forecasts internal to the AGFA. Additionally, this implementation allowed the AGFA to generate external forecasts, an important part of the operational product. A start was made in implementing the Build 5 Overhead Tracking on the Symbolics. The majority of the code was implemented, but it has not yet been tested. No major problems are forseen.

An important bug in the low-level association logic was found and fixed. After the fix, improvements were noticed both in POD and percent of length detected.

The Symbolics-based AGFA back end was ported to Sun Common LISP. This allowed the system to be distributed to organizations, such as NSSL, that do not have Symbolics hardware. In addition, it allowed the pursuit of long-range goals, such as more tightly integrating the front end and back end of the AGFA.

The AGFA was augmented to produce all the information needed to be operational. The added products were a wind shear hazard number and a propagation speed. In addition, a curve-fitting routine was added so that the final output would be smooth curves. With these additions, AGFA output was used to generate output for the Orlando training cases.

## F. GUST FRONT ALGORITHM CONTRACTOR SUPPORT

Unisys requested and received clarification of the validation criteria for the gust front algorithm. The human-readable gust front algorithm exchange format was revised to include intermediate output from the wind shift detection algorithm.

The validation criteria and exchange format documents were sent to Unisys, PROFS, and Raytheon. Algorithm results were forwarded to Unisys and PROFS.

A multi-page block diagram showing the structure of the operational algorithm was drawn up after consultation with NSSL. A copy of this diagram was given to Ian Harris of STX for modularization of the PDL. A meeting with STX was held in June on the subject of PDL modularization. The Lincoln Laboratory-generated block diagrams of the algorithm were reviewed, and the correspondence between the existing PDL and the block diagrams was discussed.

Further contact was made with Raytheon regarding the gust front PDL. Jim Wheeler provided internal Raytheon diagrams of their current understanding of the operational algorithm. In addition, questions from Carlton Andrews concerning the PDL were answered. The Raytheon technique for determining when a gust front was 20 minutes from an airport was reviewed.

## G. GUST FRONT ALGORITHM TOOLS

The real-time truthing utility, rtt2tru, was upgraded to handle two new entries: thin line truth and total velocity.

Several modifications were made to the pre-existing gust front scoring utility called autoscore. The first major implementation was the addition of gust front forecast scoring. Since the automation of forecast scoring could not exactly equal the method used in manually scoring forecasts, new scoring rules were written, and two methods were developed to score forecasts. Thin line feature scoring and a dump of orientation data on each truth box bin also were added to the autoscore utility.

## H. GUST FRONT ALGORITHM ANALYSIS

### 1. Added Value Study

The operational version of the gust front algorithm uses only convergence to detect gust fronts. The algorithm's performance may be improved by using reflectivity thin lines and/or azimuthal shears. Conventional wisdom supports the opinion that the radial convergence-finding technique used in the algorithm is optimized and that algorithm performance can be improved only by taking advantage of other radar signatures; namely, reflectivity thin lines and azimuthal shears. Given that there are limited resources for investigating these approaches, the purpose of the study was to determine which other signature would provide the greater benefit in terms of improvement in algorithm performance.

Single Doppler gust front cases from Denver and Kansas City were used to determine the effects of additional features on the algorithm's performance. The length of the gust front containing azimuthal shear or a reflectivity thin line was calculated for the missed events to determine which feature would best improve the POD. For detected fronts, the potential increase in percent of length detected using thin lines or azimuthal shear was determined.

For missed events, the data indicated that thin line detection would improve performance more in Denver, whereas azimuthal shear detection would result in an equal improvement in both locales. For detected events, the ability to detect thin lines would improve the performance of the algorithm over azimuthal shear detection both in Denver and in Kansas City. These results were documented.[9]

### 2. Comparison of Operational and Advanced Algorithms

A study was conducted to evaluate the performance of one of the candidate combined shear estimators. Data and tools were assembled for the job, and several cases (25 case dates) were evaluated.

A performance evaluation of the AGFA and the Build 5 version of the operational algorithm was completed for Denver and Kansas City fronts. Detections from both algorithms and features from the AGFA were compared to determine which algorithm performed better. Among the reasons for differences in performance were Build 5 coasting, gust front azimuthal orientation, feature only on one tilt, no advanced features, or advanced features but no detection.

In terms of the advanced gust front algorithm, reflectivity and/or velocity features were generally present, which could have improved performance even further. Hopefully this analysis will lead to refinements in the AGFA rules for declaring an event.

## I. SUPPORT TO OTHER GUST FRONT RESEARCHERS

A database of gust front cases was defined. This database consisted of 10 days from 1989 (Kansas City) and 12 days from Denver (10 from 1988 and two from 1987). The 1989 and 1988 data were passed through the data quality editing program (cftdqe). Common Format Tape were copied and sent to NSSL, and Universal tapes were sent to NCAR.

NSSL requested and received output from the combined shear and thin line feature extractors.

New versions of rtt2tru, trutharc, and WxShell were distributed to NSSL. This software was changed to allow the truthing and plotting of thin line truth. The real-time truthing software was changed to provide the ability to enter total velocity truth and total gust front truth. These changes were not distributed to NSSL since they felt that adding another outline would adversely impact their ability to generate ground truth in a timely manner.

The Sun version of the operational gust front algorithm was distributed to NSSL. NSSL is using some of the gust front code to port the tornado vortex (TVS) algorithm from the Concurrent to the Sun.

## J. SCAN STRATEGY

### 1. Automatic Scan-Mode Selection

The TDWR is specified to automatically change from Monitor to Hazardous scan modes when hazardous weather moves or develops in proximity to the airport. In past years, the TDWR testbed did not have this capability, so it was decided to implement automated scan mode selection for the 1990 Orlando demonstration. The scan selector is an intelligent filter that examines incoming data streams for possible hazardous weather conditions, then passes the information to the Concurrent's scan editor program as feedback for radar control.

The automated scan mode selection software was implemented and installed at the TDWR testbed for off-line testing. Because of the need to modify the GSD software to allow different time-outs for the Monitor and Hazardous scan modes, the scan mode selection could not be used in real time during the first part of the operational demonstration, but was planned for use at a later time.

An improved queue manager system was designed for handling input and output buffers. This input/output handler was later used in the design of the cockpit display server.

### 2. Scan Strategy Issues

A simulation was developed to test the reflectivity core detection performance of the TDWR algorithm for different scan strategies. An idealized descending core was simulated and sampled into Common Format Tape (CFT). These data were then presented to the TDWR algorithms. It was found that for our operations in Orlando, Florida, a new scanning strategy, which goes to 60 degrees in elevation, performed better than the original 40-degree scan. It detected descending cores up to 1.5 minutes earlier and 2 km closer to the radar.

## K. STORM MOTION ALGORITHM

This algorithm is designed to provide storm motion information in the form of a vector overlay for concurrent display with the TDWR Precipitation product. Motion information is determined solely from the analysis of sequential Precipitation maps.

Considerable effort was devoted to improving the real-time interface of the algorithm and to the development of a Sun-compatible version of the algorithm. Some algorithm refinements also were made, and these changes are discussed in the next section.

The Sun conversion proved very useful because it enabled algorithm installment at MHR in Denver, CO. Hence, the algorithm received exposure in the Denver as well as Orlando air traffic environments during the summer months.

Tower observers for the demonstration period reported that air traffic controllers and supervisors responded favorably to the Storm Motion product (refer to Section 8 regarding the Operational Demonstration). No major algorithm malfunctions were reported. However, a number of minor problems were identified and will be the focus of work in future months.

### 1. Algorithm Refinement

#### a. Algorithm Modifications

Small modifications were made to the rules for determining vector display locations, and an addition was made to allow optional modification of motion-vector update timing. Some restructuring of the source code also was engineered to create an automated release mechanism for the algorithm, including options for omitting Lincoln Laboratory-specific test/research modules.

#### b. Real-Time Implementation

Real-time Sun-3 and Sun-4 versions of the algorithm were created. Although the Sun-4 version was verified to operate in the Lincoln Laboratory environment, it was not running properly at the NCAR Mile High Radar site by the end of the reporting period.* A difference in operating system version numbers was noted, but to date we have been unable to verify the exact cause of the problem. There are no reported differences in Sun-3 operation between the Lincoln Laboratory or NCAR sites. The real-time output interface was restructured to use the Lincoln Laboratory-developed LOGREC software facility. This change was necessary to unify the structure of Sun-3 and Sun-4 algorithm versions. It is not yet known if this change will make the algorithm less sensitive to Sun-4 operating system differences

#### c. Real-Time Extensions

The algorithm also was included in an ASR-9 operational demonstration at Orlando, FL. Operating with a different input map, the algorithm's performance was reported to be more erratic than in TDWR operations. The selection of optimal operating parameters for ASR-9 operation has not been studied. The problems noted during the ASR-9 operation did, however, center on known deficiencies with the motion algorithm, particularly the algorithm's sensitivity to motion near the edge of a map and large and quick alterations in the map content (growth and decay effects).

---

* Run-time errors prevented successful execution. on the Sun-4. However, the storm motion algorithm ran successfully on the Sun-3 at MHR. The problem with the Sun-4 was traced to the Fortran library software.

### d. Algorithm Deficiencies

As stated above, storms moving into the field of view across the map edge and large convective changes (relative to the map update rate of five minutes) can result in poor measurements and output vectors illustrating gross error. These instances were few and were usually corrected after the processing of an additional map in sequence. In addition, the occurrence of significant second-trip weather in Orlando and the presence of significant clutter breakthrough from mountains in Denver highlighted the algorithm's sensitivity to reflectivity measurements from non-meteorological objects. The short-term solution was to readjust algorithm operating parameters. However, it is felt that attention should be placed on improving the algorithm design to reduce these potential perturbations.

### e. Planned Improvements

Two areas were identified for improvement and are proposed as areas of focus for future work. First, an improvement to the binary correlation feature of the algorithm is proposed to include coding of multiple threshold levels. This improvement could decrease the algorithm's sensitivity to stationary, low-reflectivity objects. No increase in computational requirements are envisioned, as the correlation process itself will remain binary. Second, an improvement to use model-constrained estimation of motion is planned as a means for decreasing the algorithm's sensitivity to outlier measurements, which are usually the direct cause of the grossly errant output vectors. The current methods of sequential spatial and temporal filtering have not proven completely effective in this regard.

## L. AIRCRAFT STUDIES

### 1. Cockpit Display System

A new effort was initiated under funding from NASA Langley Research Center to investigate the integration of ground-based and airborne wind shear information. As part of this effort, a system was developed for real-time cockpit display of wind shear warnings generated by the TDWR testbed radar. This system was installed in the University of North Dakota (UND) Cessna Citation II aircraft used for wind shear penetration flights during the summer of 1990 in Orlando, FL.

A block diagram of the cockpit display system is shown in Figure 7-1. The TDWR testbed radar applies wind shear recognition algorithms to the base radar data and generates graphical and alphanumeric displays. These results, plus aircraft beacon transponder data, are sent to a Cockpit Server module for conversion to cockpit display data. The serial (RS-232) output generated by this process is transferred to the Citation aircraft via a Dataradio packet radio system. The data received at the aircraft is sent to the cockpit display, which is a modified Argus 5000 Moving Map Display from Eventide Avionics.

The Argus 5000 is a small, monochrome cathode ray tube (CRT) unit with an on-board 68000 microprocessor and serial ports. Figure 7-2 shows the cockpit display format. Wind shear hazards are shown graphically as microburst shapes and gust front lines, in a manner similar to the graphics of the TDWR GSD. Microburst predictions are shown as dashed circles, with the expected time to onset of surface outflow given in minutes. Alphanumeric RDT messages are also provided at the bottom of the screen. The display is fixed to magnetic north up and centered on the airport.

The cockpit display system has several display modes, selectable by the four buttons to the right of the screen. When departure ("DEP") mode is selected, the screen display scale is for an area is 10 nmi by 10 nmi, and departure RDT messages are shown at the bottom of the screen. The arrival ("ARR") mode is similar, except that approach RDT messages are shown. In en route ("ENR") mode the RDT messages are not shown, and the screen scale is for an area 12 nmi wide by 15 nmi high. Pressing the "AUX" button causes three levels of reflectivity structures to

be shown. Low reflectivity (15 dBZ threshold) and moderate reflectivity (30 dBZ) structures are shown as rectangular stippled regions. High reflectivity structures are shown as a letter "C," indicating a reflectivity core.

The cockpit display system provides the first demonstration of real-time transmission of TDWR-generated wind shear hazards to an airborne display. This work has important implications for the eventual use of Mode S Data Link for providing wind shear hazard information. The graphical display of microburst hazards was found to be useful by the Citation pilots in conducting penetration flights. Such a capability is likely to be of use to air-carrier and general aviation pilots (although it would probably be a moving map-type display). Although present Mode S Data Link formats envision only alphanumeric messages, the human factors studies indicate that graphical presentation of microburst hazards are preferred by pilots over textual messages.

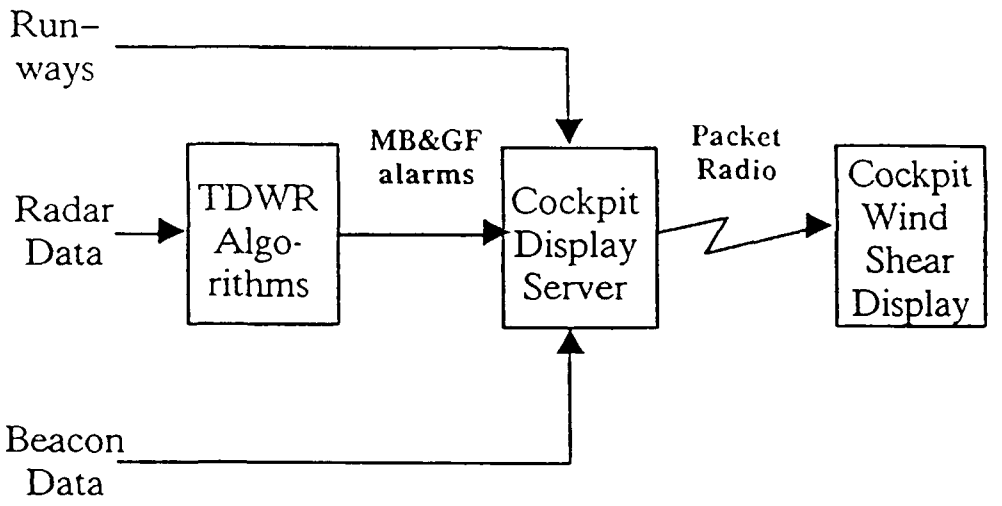


*Figure 7-1. Cockpit display system organization.*

## 2. Hazard Characterization

Work continued on the issue of aircraft hazard characterization. Craig Wanke of the MIT Aeronautics and Astronautics department continued his investigation, under Professor John Hansman, of microburst impact on aircraft performance. Using simulated aircraft approaches through three-dimensional microburst model data, Wanke studied the effect on aircraft of penetrating microbursts at various altitudes and offset distances.

The performance impact was measured by determining the F factor resulting from these penetrations. The F factor is a dimensionless quantity which shows the degradation in potential climb rate due to a microburst encounter. An F factor of 0.1 or more will negate the maximal climb performance of a typical air-carrier aircraft.

The F factor can be viewed as comprising two elements: $F_x$ and $F_z$. $F_x$ is the component due to headwind-tailwind shear, and $F_z$ is the component due to downdraft. $F_x$ is directly related to the shear (delta V / delta R), computed by the TDWR, and is maximized near the surface. The $F_z$ is directly proportional to the downdraft velocity (not directly measurable by TDWR) and is maximized in the downdraft itself. Although the relative values of the two components change with the altitude of the microburst encounter, Wanke showed that the **total** F factor remains relatively constant. This encouraging result suggests that the F factor can be estimated from surface outflow measurements, even though the aircraft is at higher altitudes (e.g., 1000 ft at 3 nmi final).

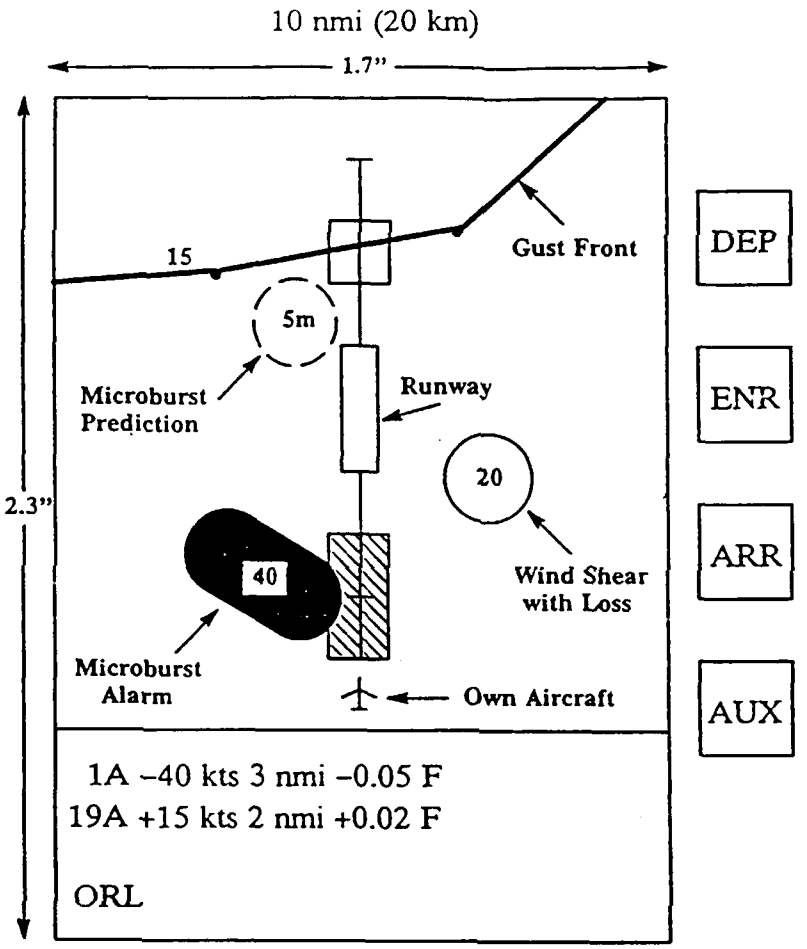


*Figure 7-2. Cockpit wind shear display layout (Arrival mode).*

Wanke also examined the F factor experienced as a function of offset distance from microburst center. Previous studies by Lloyd Stevenson suggest that pilots tend to confirm the TDWR alarm when the aircraft penetrates the microburst center. However, when they penetrate to the microburst edge, the TDWR alarm tends not to be confirmed. Wanke's study showed a rapid decline of the experienced shear as a function of offset distance. These results help explain the observed result that off-center penetrations result in alarms that are perceived by pilots as false and suggest that the current runway alarming procedure needs modification.

It should also be noted that studies by Roland Bowles of NASA Langley Research Center and others indicate that velocity difference (delta V) is not a good representation of microburst hazard. Since the shear value (delta V/delta R) is directly related to F, it would appear that the hazard warning should be based on microburst shear, not on microburst velocity difference. To maintain compatibility with current practices, shear could be converted to a velocity value by integrating over the expected flight path.

Finally, it should be noted that another discrepancy between the TDWR reported loss value and that actually experienced by pilots involves the definition of loss. The TDWR reports the peak-to-peak loss value, which is actually a velocity gain followed by a loss. Pilots tend to report only the loss from the reference speed instead of the total change. This simple fact helps account for the large difference reported by Stevenson between TDWR and pilot report (PIREP) loss values for penetrations through microburst centers.

# 8. ORIENTATION AND TRAINING FOR RADAR PRODUCTS DEMONSTRATION

## A. A BRIEFING TO THE AIRLINES

A briefing was presented to representatives of the airlines to inform them of the operational demonstration of the TDWR system to take place at MCO during the summer of 1990. Topics covered during the briefing included an overview of the TDWR system, the objectives of the demonstration, the schedule, past performance of the TDWR system in Denver and Kansas City, construction and delivery of wind shear and microburst alert messages, and suggested pilot responses to alert messages. This briefing was performed jointly by the FAA, FAA Technical Center, NCAR, and Lincoln Laboratory.

## B. TRAINING

Based on the 1989 operational demonstration in Kansas City, it was concluded that the air traffic controllers and supervisors did not receive adequate training on the GSD and RDT prior to that demonstration. Since the Orlando demonstration was scheduled to coincide with an operational demonstration in Denver, it was decided that Lincoln Laboratory would train the MCO personnel. To provide more training for air traffic controllers, a training system was developed consisting of a stand-alone GSD and RDT with data cases that could be replayed to generate runway alerts. At the beginning of the training period, these alerts were generated by overlaying Kansas City radar data on Orlando runways. The Kansas City data were replaced as Orlando data became available.

Training of the controllers and supervisors was performed over a two-week period. The first part of training included of a 45-minute briefing during the first week to provide the following:

a. An overview of the TDWR,

b. The objectives of the Orlando demonstration,

c. Locations of sensors,

d. System performance based upon past demonstrations (Denver, 1988 and Kansas City, 1989),

e. The technique for generating wind shear messages (intersection of alarms and runway boxes),

f. Pilot response to wind shear messages and potential operational impact (avoidance under microburst alert conditions),

g. Overview of GSD products and functions, and

h. The function of TRACON and tower observers.

During the second week of the training period, the supervisors and controllers were given the opportunity for hands-on experience with the GSD and RDT. Air traffic control supervisors and controllers were encouraged to become familiar with the functionality of the GSD and to read wind shear and microburst messages aloud to simulate the delivery of the messages to pilots. The training machine was made available to air traffic controllers throughout the demonstration to allow personnel the opportunity to use the GSD off line or to demonstrate new products before their introduction into the operational ATC environment.

## C. GSD ISSUES

Prior to the demonstration, representatives from the control tower were provided with photos of the GSD overlays, runway configurations, and RDT formats, etc., for comments. All of these were provided in the form in which they would appear on the GSD console. Control tower personnel identified errors and expressed preferences in the overlays and formats, which were then implemented, where possible.

## D. OBSERVERS

Lincoln Laboratory personnel were the "observers" during the Orlando demonstration and were scheduled for eight-day shifts. Prior to their stay in Orlando, the observers received the same overview briefing as the air traffic control personnel as well as in-depth training on the functions and use of the GSD, the interpretation of the products, and the kinds of observations being sought. There were two kinds of observer positions: tower and TRACON. The tower observers' duties included the following:

a. Answering questions from the controllers or supervisors concerning the GSD and RDT,

b. Logging any comments, complaints, or suggestions from personnel,

c. Noting how the system was used by personnel,

d. Identifying the "begin" and "end of alert" periods for future analysis

e. Noting times of and reasons for runway changes,

f. Noting the impact of weather on ATC operations, and

g. Observing the correlation between the weather as seen from the tower and as shown on the GSD.

These data were recorded on log forms designed for this demonstration. In addition to these duties, TRACON observers were responsible for logging information pertaining to the locations of storms and their impact on air traffic operations.

# 9. METEOROLOGICAL ANALYSIS

## A. MESONET–LLWAS–RADAR COMPARISONS

Surface meteorological data were collected continuously by the Lincoln Laboratory Mesonet and the FAA LLWAS system over specific periods during 1988 in Denver, CO and 1989 in Kansas City, MO. The Mesonet anemometer wind data were compared to Doppler radar data that had been collected during convectively active weather periods. The results of the comparison study are used to:

a. Confirm low altitude wind shear and other possible hazardous weather events observed by the radar,

b. Determine wind shear events not observable in Doppler radar data due to:

   1. low signal-to-noise ratio,

   2. very shallow outflows missed by the lowest radar beam,

   3. blockage of the radar beam, and

   4. asymmetry in the surface outflow.

c. Provide support to the microburst and gust front detection algorithm development efforts.

The additional meteorological data collected by the Mesonet (temperature, relative humidity, rainfall rates, etc.) will be used to diagnose the relationship between these variables and wind speeds for gust fronts and microbursts to gain a better understanding of low-altitude wind shear. An abstract describing work based on this dataset was submitted in February to the IEEE 29th Conference on Decision and Control, and it was accepted in June.[10] Results of that work will be reported in the next semiannual summary.

### 1. 1988 Data

A project report was published in May 1990. [11] A total of 184 microbursts impacting the surface Mesonet were identified. Of those microbursts for which both radar and surface data were available, 97 percent were observable by single-Doppler radar. Two strong microbursts (>20 m/s differential velocity) were unobservable by radar throughout their lifetime: one due to low SNR and the other initially due to an asymmetric outflow, with low SNR also a contributing factor. Two other microbursts with differential velocities from 10-19 m/s were unobservable by radar: one due to a shallow outflow with a depth limited to a height below that of the radar beam and one due to asymmetric outflow oriented unfavorably with respect to the radar viewing angle.

### 2. 1989 Data

Analysis of Mesonet and LLWAS wind data during the 1989 TDWR demonstration showed that approximately 17 gust fronts and 12 microbursts impacted the anemometer network around the airport. Comparison with Doppler velocity data showed that in most cases, the radar and anemometer winds compared favorably. In one striking case, however, the Doppler velocity signature of a microburst was recorded by the radar, but the anemometer data showed this was a false alarm. The uniform winds blowing from north to south are shown by the Mesonet wind arrows in Figure 9-1. An RHI cross section through the storm (Figure 9-2) shows that the measurement of winds flowing away from the radar in the very low reflectivity region at the surface (15-29 km range) was caused by sidelobe contamination from the overhanging echo

aloft. There was no real low-altitude wind shear in this case. This is one example of why integration of the TDWR and LLWAS systems is important.

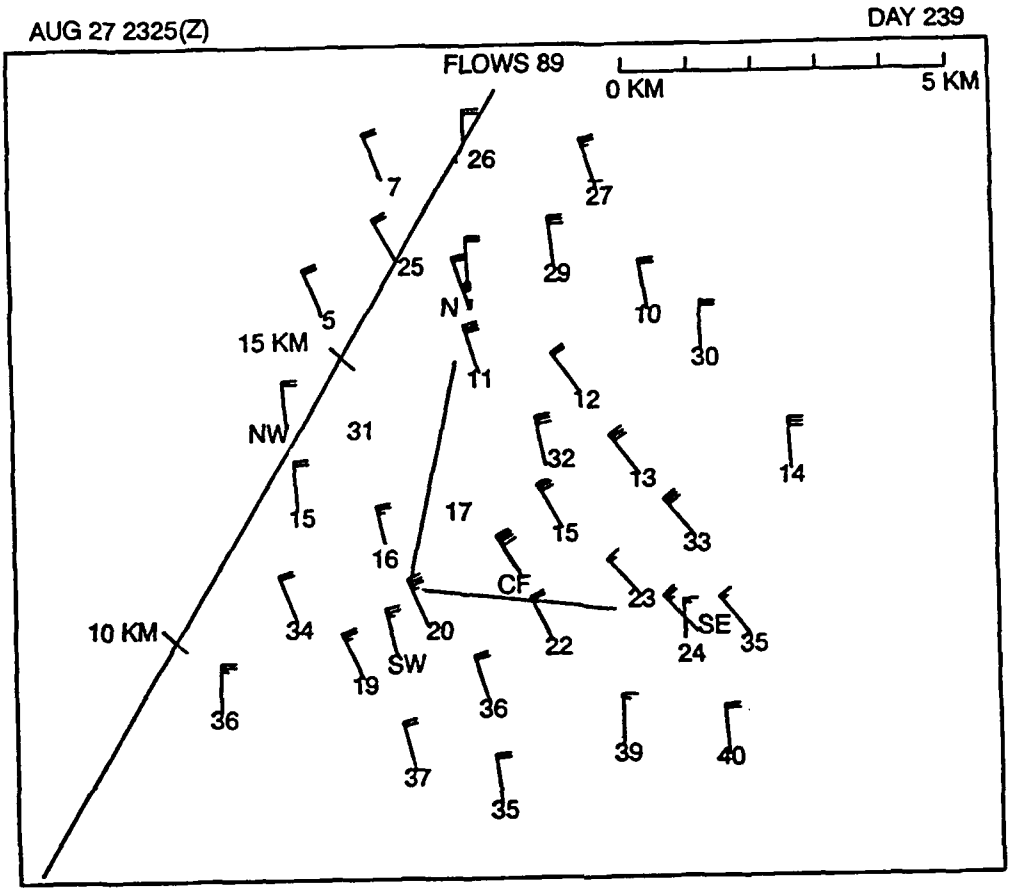


*Figure 9-1. Anemometer winds recorded with Lincoln Mesonet (numbered stations) and FAA LLWAS (identified with letters, e.g., SE = southeast, etc.) around MCO airport on 27 August 1989 at 2325 GMT. A long wind arrow barb represents 5 m/s wind speed, and a short barb, 2.5 m/s. The station identifier represents the head of the arrow and points in the direction toward which the wind is blowing. Notice the prevailing winds are from the north toward the south, and there is little variation in wind direction. The diagonal line at the left indicates the radar cross section shown in the following figure. The 19 km and 15 km range intervals are shown.*

## B. TDWR–LLWAS INTEGRATION

A quantitative comparison of surface anemometer and Doppler radar winds during wind shear events was conducted to gain a clearer understanding of the basic relationship between the wind information provided by the two very different sensing systems and to determine the impact this relationship may have on integration of the two operational systems. A proposed mathematical technique for "correcting" LLWAS winds where needed to match radar winds better was evaluated for cases of microburst (divergent) and gust front (convergent) wind shear. The results were presented in a conference paper [12] for the American Meteorological Society (AMS) 16th Conference on Severe Local Storms. A summary of the results is presented below.

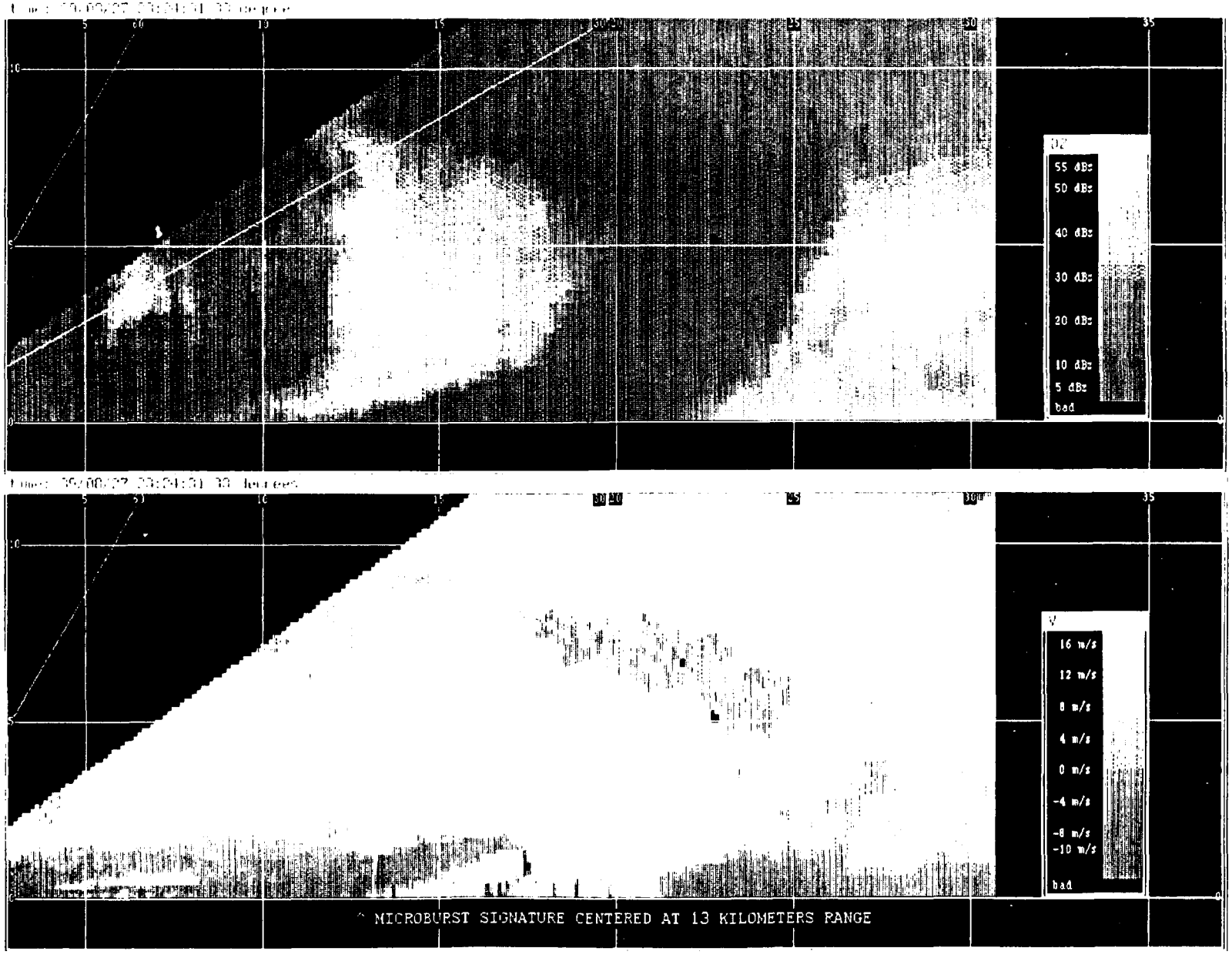


*Figure 9-2. RHI vertical cross-section through storm on 27 August 1989 that caused false microburst surface wind signature. Reflectivity (top, DZ) shows overhanging echo with high reflectivity around 15-20 km range, but with low surface reflectivity. The surface Doppler velocity signature (bottom, V) in this weak echo region was caused by side-lobe contamination from above.*

Twelve cases collected during 1988 in Denver, CO were chosen for the study. These included a variety of meteorological events and a wide range of radar reflectivity values. Doppler wind measurements were taken from the lowest elevation scan (either 0.3° or 0.4°) of FL-2, which typically updated once per minute. Surface anemometer wind measurements were collected from 12 LLWAS sensors situated in the vicinity of Denver's Stapleton International Airport. These stations had an update rate of six to seven seconds.

For the study, we chose to use a boundary layer power law profile, which accounts for differences in wind sampling height, to represent the winds measured by the anemometer and radar. The power law profile is stated:

$$U / U_1 = ( Z / Z_1 )^p$$

where U and $U_1$ represent the wind speeds at heights Z and $Z_1$, respectively, and $0 \leq p \leq 1$. The exponent $p$ is empirically derived by comparing a large number of radar and anemometer wind values measured during a variety of wind shear events. In our case, $p$ is dependent not only on the lapse rate and ground roughness, but also on the inherent differences in the two sensors.

Values of $p$ were calculated for each station, and the probability density versus the value of $p$ was plotted. The plots yielded an approximately normal distribution for each station. We found a wide range of mean values $\bar{p}$ and standard deviations ($\sigma$) for the distribution. Wind speeds recorded at station CF were found to be most representative of the radar wind speeds, with $\bar{p}$ nearly zero, while station SSE displayed the most difference, with $\bar{p} = 0.4$ (Figure 9-3). There appears to be little correlation between the variability of $\bar{p}$ with either the height of the LLWAS station or its distance from the radar. Large $\bar{p}$ values such as displayed by SSE indicate a probable sheltering problem or a mechanical difficulty with the LLWAS anemometer.

The representation of the difference in measured wind speed between the radar and LLWAS with a power law profile provides a method for "adjusting" the LLWAS speed to some radar height equivalent. This application was studied in the case of gust front and microburst events. The results showed the adjustment makes the LLWAS winds more comparable to Doppler radar winds during gust front events. However, during microburst events, the adjustment seems to overestimate the LLWAS wind speeds.

In general, wind speed measurements by surface anemometers and by Doppler radar were found to be quite comparable over the Denver 1988 LLWAS network. Stations with high values of $\bar{p}$ are most likely poorly sited or have mechanical sensor problems. The best solution would be to relocate or raise the anemometer, and maintain it well. Account should be taken of the individual LLWAS sensor measurement capabilities in any TDWR-LLWAS integration scheme.

## C. MICROBURST FREQUENCY AT U.S. AIRPORTS

Using microburst data as measured by the Lincoln Laboratory Mesonet and FAA LLWAS systems and thunderstorm day data from the National Weather Service for five summers at three different sites (Memphis, 1984 and 1985; Huntsville, 1986; Denver, 1987 and 1988), a method was developed for determining the level of summer microburst hazard at any site in the U.S. for which thunderstorm day data is available. The details of this study were reported in a paper [13] for the AMS 16th Conference on Severe Local Storms. A summary of the results is presented below.

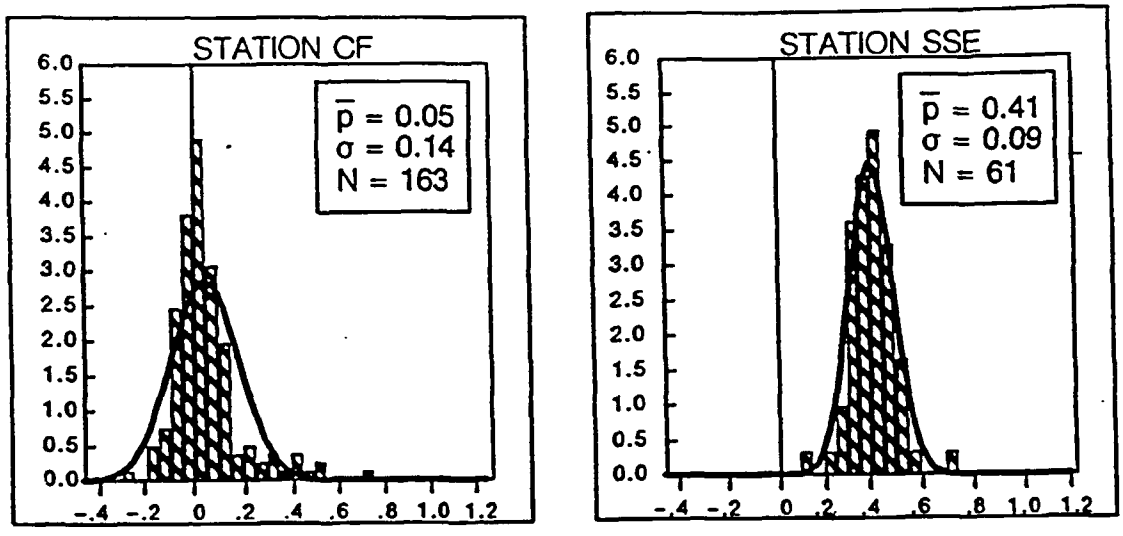


*Figure 9-3. Histogram plots of the probability density of p for each station where $\bar{p}$ is the value of the power law profile exponent, σ is the standard deviation, and N is the total number of data points used to determine the distribution.*

The number of microbursts observed during the summer months from 1984-1988 were scaled, according to the coverage area of their respective networks, to represent the total microbursts occurring in a Thunderstorm Day Observation Region (TDOR), a circular area of radius 15 km (centered on the airport) in which thunder should be audible at the airport. A statistical regression technique was used to mathematically relate the number of wet summer microbursts (those associated with significant surface rainfall) to the number of thunderstorm days. A linear relationship was found, but the *rms* error was large. In the southeastern U.S., most microbursts are wet, so direct use of this relationship is appropriate. Since dry microbursts (those with little or no surface rainfall), which occur in significant numbers only over the Western Plateau, were consistently found to comprise about 70 percent of the microbursts totals in Denver, the expression relating wet microbursts to thunderstorm days was increased by 70 percent to represent the total number of summer microbursts in the Western Plateau region.

To convert the predicted number of summer microbursts to a true aviation microburst hazard, two additional factors were incorporated. During the 1988 TDWR Operational Demonstration, the wind shear threshold for pilot warnings was increased from 10 m/s (used as the definition of a microburst) to 15 m/s. This threshold increase necessitated a 35 percent decrease in the microburst frequency predicted by our original equation. Also, the area in which microbursts pose a threat to aviation is much smaller than the TDOR. Therefore, the equations were multiplied by a factor **R**, the ratio between the area of the wind shear alarm region of an airport and the TDOR.

The final microburst hazard equations are given below. T represents the mean number of summer thunderstorm days, and R is defined above.

| EQUATION A: To be used for all parts of the country except the Western Plateau | EQUATION B: To be used for the Western Plateau region only |
|---|---|
| $(2.4 \pm 0.3)\,T\,R$ | $(8.0 \pm 1.1)\,T\,R$ |

The range of thunderstorm days used in our derivation was limited to 21-30 days during June, July, and August because of the climate in Memphis, Huntsville, and Denver. Since we currently lack data in regions where summer thunderstorm day totals are significantly lower or higher than this, we suggest the equations be used only for those locations where mean summer thunderstorm day totals fall within this range. Furthermore, significant interannual variability was evident in the two years of Denver data. For these reasons, the relationship we have presented could contain substantial error and can be refined only by incorporating additional data. It is hoped that data obtained in Kansas City and Orlando will support our assumptions and stabilize the results of this study.

## D. MICROBURST ASYMMETRY STUDIES

Asymmetry, or aspect angle dependence, in microbursts refers to divergent surface outflows in which the outflow strength or extent varies depending on the aspect (or viewing) angle of the radar. The TDWR detection algorithms utilize input from a single Doppler radar, so an asymmetric microburst may be underestimated or go undetected if the outflow is weak from the radar viewing angle. Additionally, the size and location of the event may be distorted when the outflow extent is significantly asymmetric. Most of the present outflow modeling and detection methods are based on the assumption of axial symmetry, both in the strength and extent of outflows. Asymmetry in microbursts is thus a major concern for TDWR microburst detection performance. A study was undertaken to examine the asymmetry of microburst events in Denver, CO, and the results have been reported in a paper [14] for the AMS 16th Conference on Severe Local Storms. A summary is presented below.

### 1. Data

Doppler radar measurements were collected in Denver during 1987 using the FL-2 and UND radars. The radar scanning was coordinated to cover microbursts that occurred in favorable dual-Doppler regions. Surface dual-Doppler windfields at 250 m resolution were synthesized from the radar radial velocity fields. The paired radar scans were all surface tilts (0.3° - 0.5°) and had time differences of less than one minute. In addition, the beam intersection angle of the radars had to be greater than 30° and less than 150°. These windfields were then smoothed using a simple three-by-three median filter. The 10-percent trimmed mean wind was then removed; all analyses were performed on this final perturbation windfield.

A wide variety of cases were chosen for this analysis to obtain a representative sample of the microbursts found in the Denver environment. Some 96 observations from 27 separate microburst events were examined.

## 2. Analysis Methodology

To analyze regions of divergent microburst outflow, the perturbation windfield was examined visually, and a bounding polygon was subjectively drawn around each microburst region. Once an event was drawn, the velocity difference across every unique grid point pair within the polygon was calculated, taking into account the relative aspect angle of the segment. The strength calculations were performed only on points whose connecting lines were completely contained within the defined polygon.

Differential velocity and shape measurements were obtained from all possible aspect angles and then grouped into one of 18 aspect angle categories. The categories ranged from $0^o \pm 5^o$ to $170^o \pm 5^o$, in $10^o$ steps. Aspect angles over $18^o$ were not considered because they generally reflect measurements made from $0^o$ -$180^o$.

## 3. Types of Asymmetry

There are primarily two types of asymmetry that may occur in microbursts: strength and shape. An example of a shape and strength asymmetric microburst is shown in Figure 9-4.

The strength asymmetry of an event is measured by estimating the largest differential velocity within the microburst outflow at multiple aspect angles. Differential velocity is the magnitude of the wind change between any two points within the event. The severity of the aspect angle dependence for strength in an observation may be measured by dividing the maximum strength by the minimum strength over all aspect angles. A single-Doppler radar will, in general, underestimate the maximum strength of a microburst that is strongly asymmetric in strength. The strength asymmetry of the microburst shown in Figure 9-4 is 2.3:1.

The shape asymmetry of an event is measured by estimating the largest spatial extent of the microburst outflow at multiple aspect angles. The shape of an event (outflow extent) is measured by estimating the cross-distance from one end of the outflow polygon to the other at a variety of aspect angles. The level of aspect angle dependence for outflow extent is calculated by dividing the largest cross-distance by the smallest cross-distance over all aspect angles. A highly aspect-angle-dependent outflow shape makes it difficult to capture the shape, and sometimes central location, of the microburst using a single-Doppler radar. Shape asymmetry could result in over- or under-warning on a specific runway, depending on the microburst-radar-runway geometry. The shape asymmetry of the microburst shown in Figure 9-4 is 1.7:1.

## 4. General Characteristics of Asymmetry in Denver

The maximum strengths of all Denver microbursts studied ranged from 5 to 26 m/s. The aspect angle dependence of strength for all events is between 1.3:1 and 3.8:1, with a median value of 1.9:1. As shown in Figure 9-5, this cumulative probability does not change significantly between weak (thin solid line) and moderate-strong (dotted line) events.

The maximum outflow extents ranged from 2.4 to 9.5 km. Shape asymmetry ratios for all Denver events range from 1.1:1 to 2.4:1, with a median value of 1.6:1. Just as for strength asymmetry, the cumulative frequency of shape asymmetry ratios does not vary significantly between weak and moderate-strong events.

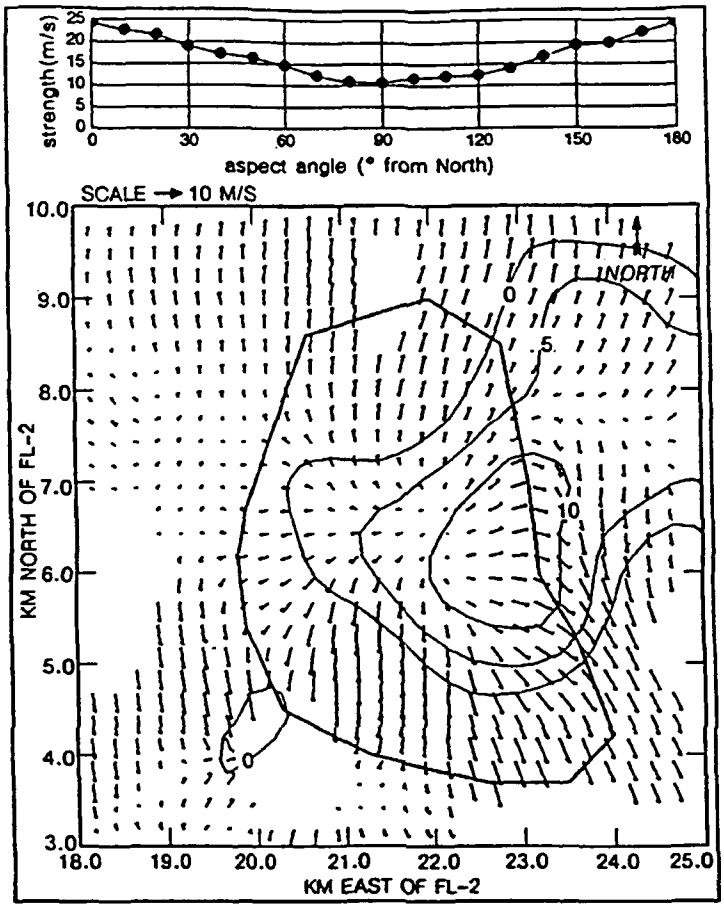


*Figure 9-4. Graph (top) indicating variation of measured strength with aspect angle. Dual-Doppler windfield (bottom) for a shape- and strength-asymmetric Denver microburst on July 16, 1987 at 23:07:41 UT. Polygon for event shown in center; contoured lines are of reflectivity at 0, 5, and 10 dBZ.*

Figure 9-5, and further statistical analyses not discussed here, indicate that the maximum strength of a Denver event has little or no correlation with the degree of the strength or shape asymmetry. Additionally, the two forms of asymmetry are statistically unrelated. None of the microbursts parameters (mean wind speed, peak reflectivity, strength, etc.) analyzed during this study showed significant correlation to the strength or shape asymmetry of individual observations.

## 5. Conclusions

Over 27 events encompassing 96 total observations of microbursts were examined for asymmetry. Two types of asymmetry were studied: strength and shape. The median strength and shape asymmetry ratios for the cases presented here were 1.9:1 and 1.6:1, respectively. The representation of microbursts as symmetric flows is clearly inaccurate.

The magnitude of the shape and strength asymmetry ratios were found to be independent of the magnitudes of the maximum cross-distance (shape) and strength measurements. No preferred orientation angles were found for maximum strength or shape, although the orientation angles did remain relatively stable throughout the lifetime of the events.

Based on these findings, a single-Doppler radar has an equal change of viewing a microburst of all sizes and strengths from any random aspect angle. Therefore, the radar will underestimate the overall maximum strength of the event, on average, by approximately 30 percent (based on median strength asymmetry ratio of 1.9:1). The primary cause of asymmetry (or at least fluctuations in its magnitude) in microbursts appears to be the proximity of other wind shear events (gust fronts, microbursts, or weak divergences). There appear to be no reliable, single-Doppler-radar-based measurements (reflectivity, peak radial strength, mean wind, etc.) which indicate the severity or orientation of asymmetry in microbursts.

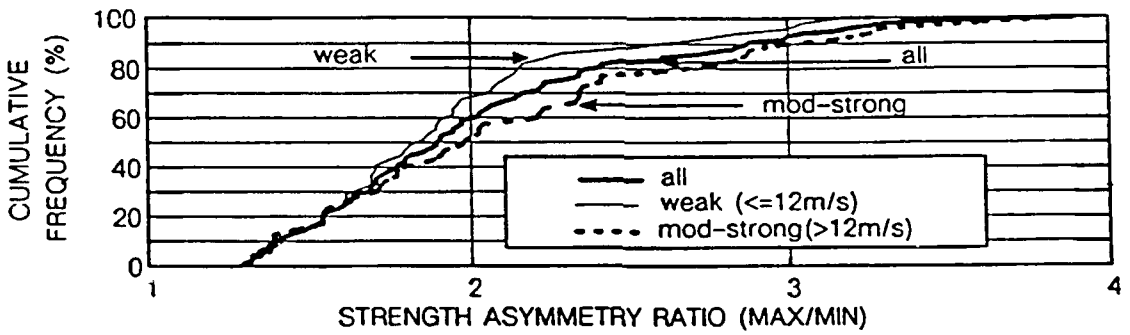


*Figure 9-5. Cumulative frequency of strength asymmetry ratios for various maximum strength classes.*

## E. GUST FRONT CHARACTERISTICS

A study was conducted comparing the characteristics of Denver and Kansas City gust fronts and how these differences might affect the performance of the gust front algorithm, and the results were presented in a paper [15], for the AMS 16th Conference on Severe Local Storms. Gust front characteristics such as length, duration, strength, and propagation speed and direction were recorded, and some simple statistics were computed for Denver (1988) and Kansas City (1989). A comparison of the gust fronts that occurred at each location showed significant differences in gust front characteristics. Although Kansas City gust fronts were fewer in number, they tended to be stronger, longer, faster-moving, and shorter-lived than Denver gust fronts.

In general, there was no significant difference (between Kansas City and Denver) in the ability of the algorithm to detect gust fronts within 60 km of the radar. However, the capability of the operational algorithm (which uses only radial convergence) to generate wind shear hazard warnings at MCI was poorer than at Denver. There appears to be a preferred gust front orientation (northeast to southwest) in both Denver and Kansas City. Stapleton airport was located northwest of FL-2, and gust fronts moving over the airport were perpendicular to the beam. Kansas City International Airport was located northeast of FL-2, and gust fronts over MCI were aligned along the radar beam. The incorporation of reflectivity thin line and/or azimuthal shear detection into the gust front algorithm would improve detection capability in cases of unfavorable viewing angle.

## F. MULTIPLE-DOPPLER WIND SYNTHESIS

A software facility is being developed for the synthesis of three-dimensional windfields from multiple Doppler radar data. Two Doppler radars, one owned by MIT and the other by UND, in addition to the TDWR testbed radar (FL-2C), are to be deployed in Orlando in late August 1990 to form a roughly equilateral triangle with FL-2C (Figure 9-6). The radars will be scanned so that accurate estimates of the air velocity and precipitation particle motions within storms near the Orlando airport can be derived.

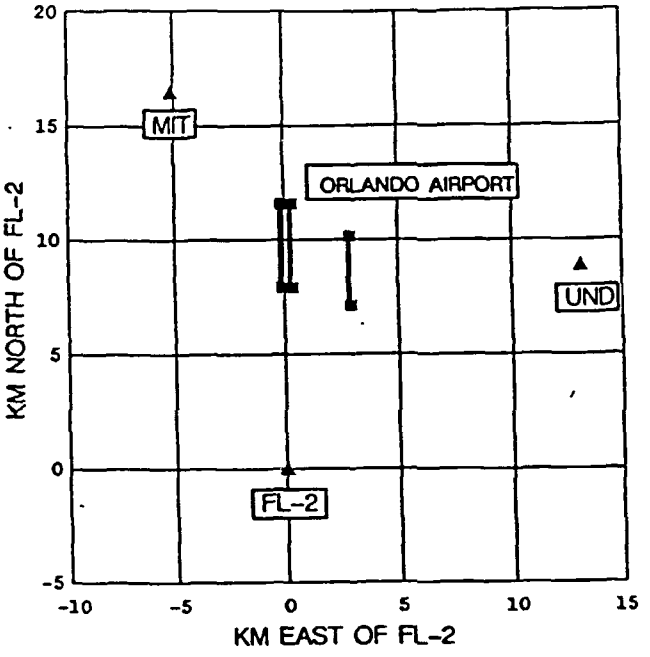


*Figure 9-6. Map showing radar locations around Orlando airport. The MIT, UND, and FL-2C radars will be scanned so that accurate estimates of the air velocity within storms near the Orlando airport can be derived.*

Two triple-Doppler wind synthesis techniques are commonly used: Direct (DIR) and Overdetermined Dual (ODD). DIR resolves the radial velocity wind vectors directly into the Cartesian windfield components $u$, $v$, and $W$ ($\equiv w + V_t$, where $V_t$ = particle terminal velocity). $V_t$ is estimated from reflectivity data, and the vertical velocity $w$ is then recovered. ODD resolves the radial velocity vectors into the horizontal windfield components $u$ and $v$, and then integrates the mass continuity equation to find the vertical velocity $w$. These techniques amplify the radial velocity and terminal velocity error variances differently (Figure 9-7), and the differences can be used to choose the best windfield synthesis technique for a given radar network geometry and Cartesian analysis grid.

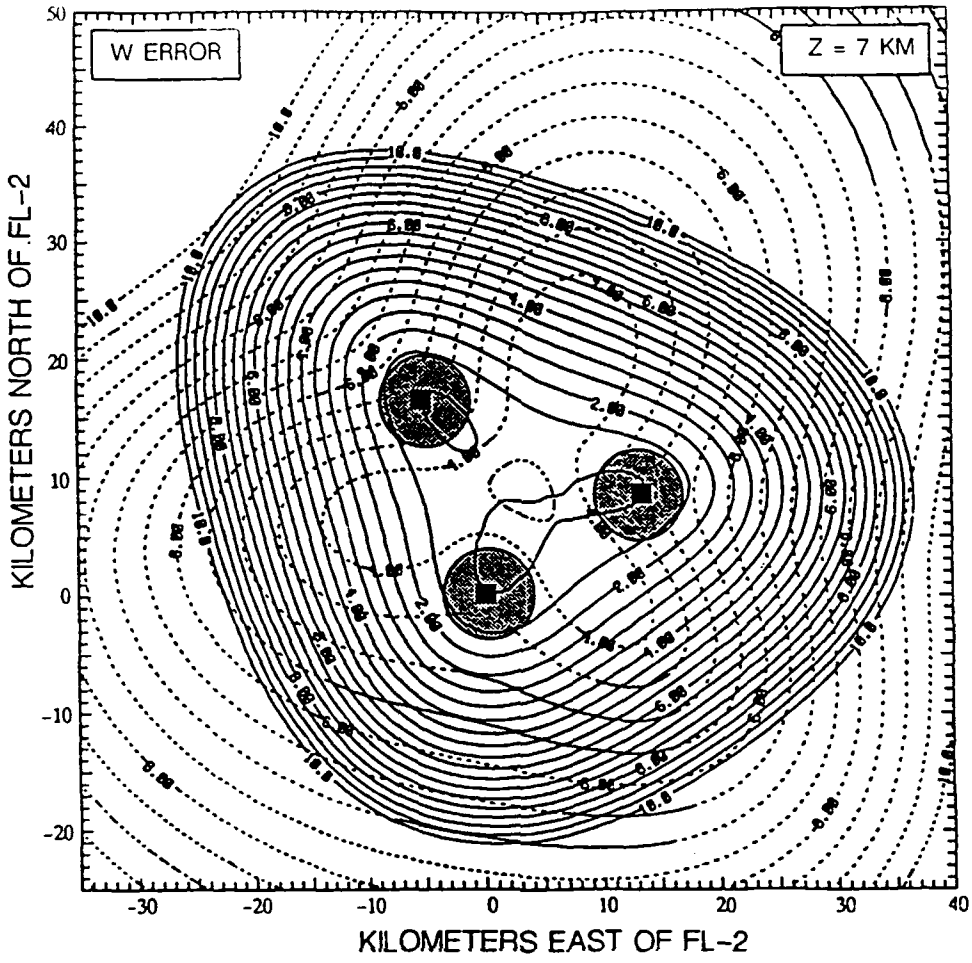


*Figure 9-7. Vertical velocity (w) errors in m/s are shown for the overdetermined dual-Doppler (ODD) technique with upward integration (dashed lines) and for the triple Doppler direct technique (DIR; solid lines) at 7 km AGL, for the three-radar network planned for Orlando. The ODD error decreases downward toward the surface, and the DIR error decreases in the opposite direction. The radar locations are shown as black squares surrounded by grey circles, which represent the unscanned area above each radar for an upper elevation angle of 58°.*

We are developing a hybrid windfield synthesis technique (HYB) that applies the better synthesis technique at each altitude in the grid. We calculate windfields and variances at the highest altitude of the grid, typically 12-15 km AGL, via the DIR technique. At each successive lower altitude of the grid, variances from both DIR and ODD are calculated. One of several criteria may be used to determine which technique is better: the technique whose vertical velocity variance is smaller at the larger number of points, the technique with the lower average vertical velocity variance, etc. The comparison process continues until ODD is judged better; windfields at the remaining altitudes in the grid are then synthesized via ODD, integrating the continuity equation downward.

HYB offers several improvements over both DIR and ODD and other previously published combined techniques. DIR yields rather consistently good results for $u$ and $v$ throughout the grid, but estimates of $w$ at lower altitudes are poor ($\sigma_w^2$ is proportional to $1/z^2$). ODD, with upward integration of the continuity equation, yields good results at low altitudes, but errors in $w$ accumulate quite rapidly due to the integration. Downward integration of the continuity equation lessens the magnitude of accumulated error but requires an accurate estimate of $w$ at the top boundary of the grid, which may be impossible to obtain. HYB overcomes these problems by applying DIR and ODD only where they are most accurate. The use of DIR at high altitudes

supplies an accurate upper boundary condition on $w$, with known variance for the synthesis of windfields at lower altitudes via ODD with downward integration.

## G. PREDICTING THUNDERSTORM DOWNDRAFT AND OUTFLOW STRENGTH

A great deal of research over the last few years has attempted to quantify the factors influencing the development of the strongest thunderstorm downdrafts and outflows (microbursts). One of the apparent mysteries is that thunderstorms with quite different downdraft and outflow strengths can occur simultaneously, in the same environment. Even when the reflectivity or water content of these cells is taken into account, differences remain that are related to cell forcing, geometry, or the proximity and strength of neighboring convection. Another apparent mystery is that storms with similar reflectivity levels on different days produce very different strength outflows. Because of the proportionality between reflectivity and the downward acceleration due to water loading, some argue there should be a monotonic relationship between downdraft/outflow strength and reflectivity. Yet evidence is to the contrary. This is, in part, because environmental factors that promote the thermodynamic generation of negative buoyancy are of crucial importance in determining the ultimate downward acceleration and observed downdraft strength. Subtle differences in the vertical temperature structure of the environment, such as the existence and height of any elevated stable layers or inversions, also play an important role in determining the ultimate downdraft strength.

Although a number of observational studies on determining reliable precursors for microbursts have been performed, none has gone beyond basic statistical correlation of these precursors with resultant outflow strength. Our approach is to quantitatively predict thunderstorm downdraft and outflow strength with a simple model based on the vertical momentum and continuity equations. This model was described in a conference paper [16] for the AMS 16$^{th}$ Conference on Severe Local Storms. The vertical momentum equation is used to indicate the expected dependence of the vertical velocity on the various forcing mechanisms at work in the thunderstorm downdraft. The rationale behind the model development is to relate each term in the vertical momentum equation to the observable environmental or storm characteristics that are physically responsible for its ultimate magnitude.

Testing and development of a model of this kind requires that environmental sounding data be taken at regular intervals during collection of Doppler weather radar data. The NSSL sounding system was used in Kansas City and is planned for use in Orlando, FL beginning in July. We have developed software for examining these and other soundings that also will compute the statistics needed for the prediction of thunderstorm downdraft and outflow strength. An example of a sounding is shown in Figure 9-8.

The ability of the model to correctly rank, and fairly closely estimate, the eventual downdraft and outflow velocities in several different cases adds confidence to the assertion that it approximately captures the essential physics of accelerating downdrafts and outflows. By developing a physically-based predictive system, there is hope that the system can remain reliable as the storms it has to detect change from the very dry virga shafts typical of the Denver area to the very wet thunderstorms in the humid southeastern part of the country. This model shows that the radar reflectivity of a storm alone cannot be used as a hazard index; information about the static stability of the lower atmosphere also is essential.

## H. DETAILED CASE STUDIES

A microburst that occurred on 30 July 1989 near Claycomo, MO was examined in a conference paper [8] for the AMS 16$^{th}$ Conference on Severe Local Storms. The microburst winds in excess of 55 mph damaged trailers and uprooted trees in the area and were accompanied by 3.5 in of heavy rain. This was the strongest microburst observed during the 1989 data collection season in Kansas City. Various features of the storm, such as the outflow velocity, the

altitude of the center of mass, the height of the reflectivity core, etc., are tracked throughout its lifetime. It was found that each pulse in the outflow velocity was preceded by a descent in the center of mass of the storm core.

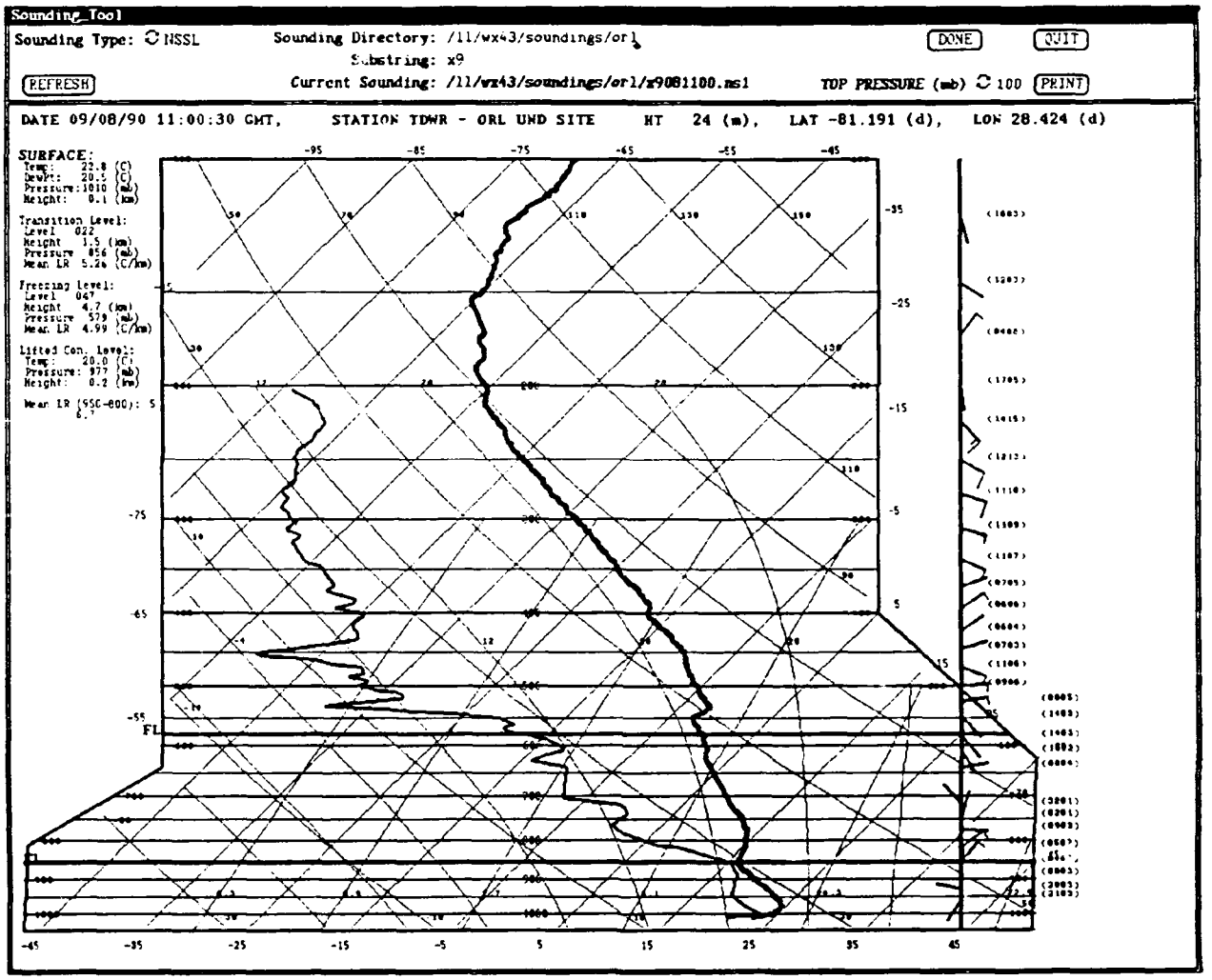


*Figure 9-8. Lincoln Laboratory plot of sounding in standard meteorological skew-T format. The thick black line is the temperature trace and the thinner line is the dew point temperature trace. Calculated parameters such as the transition level, freezing level, and lifted condensation level are shown to the left of the graph, and the wind speed and direction are shown to the right.*

# I. UNIVERSITY RESEARCH

## 1. University of Chicago

### a. Meteorological Analysis

Dr. Ramesh Srivastava of the University of Chicago has been investigating the microphysics of microburst downdraft development using a one-dimensional, time-dependent model. Comparisons between calculated and observed microburst intensities have been made using rawinsonde and radar data from Huntsville, Denver and Kansas City. A microburst severity index has been developed which is calculated based on sounding information and precipitation content (or radar reflectivity) at cloud base. It is hoped that the severity index will be useful in estimating the likelihood and strength of microburst occurrence.

Recent simulation results have indicated that a burst of peak winds occurs at the initial onset of the outflow. This burst phenomenon is related to large-diameter raindrops which precede the cool air of the downdraft. It is planned to further investigate this burst phenomenon in the coming fiscal year and to extend these results to the Florida environment.

The current results assume steady-state forcing by precipitation at cloud base. Based on Lincoln Laboratory results indicating that reflectivity core height is important in microburst prediction, the model will be extended to provide for transient forcing at cloud base.

Finally, it is planned to compare the one-dimensional model results with multi-dimensional models. Initially, the one-dimensional model will be compared to an axisymmetric model developed at the University of Chicago. Later, the results will be compared to three-dimensional results generated by Dr. John Anderson and his colleagues at the University of Wisconsin.

During this reporting period, Dr. Srivastava visited Lincoln Laboratory and provided his research results as described. The microburst severity index results were received for the Kansas City soundings from last summer. The software for computing these results will be provided in the next reporting period.

**2. University of Wisconsin**

**b. Numerical Thunderstorm-Microburst Forecasts**

John Anderson and Jerry Straka have been conducting research into the physics of microburst development. Their approach employs a three-dimensional microphysical model of cloud development. As with Srivastava's work, the initial conditions for the model are set from an atmospheric sounding; however, the storm cell is initiated by a temperature pulse at the surface rather than by precipitation aloft. The virtue of this approach is that a storm is grown from surface heating rather than assuming a reflectivity distribution aloft. On the other hand, the three-dimensional model is also more difficult to interpret than the one-dimensional model because of the complex interactions within the simulated storm.

Jerry Straka performed a series of simulations on a series of Huntsville microbursts suggested by Lincoln Laboratory, and he found a reasonable correlation between the simulated and observed outflows, provided the sounding was within roughly two hours of the radar observations. Straka has prepared a journal article describing these results.

Another area of interest is to perform three-dimensional simulations on past soundings from the Orlando area and to convert these simulation results to single-Doppler radar (CFT) data reflecting the TDWR scan strategy. (The capability to correctly write CFT format tapes has recently been verified.) This simulated CFT data could be fed into the TDWR algorithms to get an early idea of algorithm behavior in the Orlando area. These results could be used to perform preliminary tuning of site-adaptable parameters. This concept could have additional relevance in addressing the problems of tuning the site-adaptable parameters for the 45 operational TDWR sites. It would be preferable to provide the best set of parameters for each site when initially installed rather than having to wait until a large amount of data is collected. Also, there is a danger that the parameters might be adapted to one particular year which might not be very representative.

A graduate student has been selected to perform a systematic parameter study using the subcloud model. This study will vary parameters such as the depth, width, and strength of the water content core used to initiate the down draft and the subcloud lapse rate and measure the resulting maximum downdraft and outflow speeds. The results will be combined into a simple prediction model to be verified with Lincoln observations. Anderson also is interested in performing a three-dimensional simulation of M. Wolfson's hypothesized scenario of the Dallas-Fort Worth (DFW) crash in which two thunderstorm outflows were present.

## J. CAPE EXPERIMENT

The Convective and Precipitation/Electrification experiment (CAPE) is planned for the summer of 1991 around Cape Canaveral, about 40 miles from Orlando. The FAA will be partially supporting this experiment. M. Wolfson is a member of the scientific steering committee. One goal of CAPE is the prediction of convection initiated at the leading edge of old thunderstorm outflows (gust fronts) where the convergence is strong. In an effort to prepare for the "nowcasting" experiment, scientists at NCAR (J. Wilson, C. Mueller, and C. Kessinger) have requested FL-2C data from Orlando. We will select a two-week period and send them all of the 360° gust front tilts collected during that time.

# APPENDIX A
# MICROBURST OUTFLOW REFLECTIVITY DISTRIBUTION

The TDWR reduces ground clutter residue during adverse weather by comparing measured data with a stored map based on clutter residue measured during fair weather. If the measured signal level is less than the stored map, the measured data for that range gate is flagged.

During the process of making a TDWR clutter residue map, clear air reflectivity is determined first from clear air samples. Summer clear air reflectivities at Denver, Kansas City, and Orlando can be as high as 20 dBZ. Clutter residue whose reflectivity is less than the determined clear air value cannot be ascertained during the map-generating process. The effect of clutter-residue breakthrough will be more serious at the microburst outflow region because of weaker weather signal strength than at the microburst core. Two microburst outflow reflectivity distributions are complied in this appendix; they may be germane as well for those who are designing radar-based detection systems, tweaking STC settings, SNR, and point target editor thresholds, etc.

Figures A-1 and A-2 show estimated microburst outflow reflectivity distribution functions based on samples collected during the summer at Denver and Kansas City. Reflectivity measurements were taken at the locations of peak approaching and receding velocities and at the time of maximum delta V and maximum shear. The sample sizes are about the same (500), implying that the 95 percent confidence bound at the $10^{th}$ percentile is about 5 and 10 dBZ, respectively, at Denver and Kansas City. The estimated microburst outflow reflectivity distributions suggest that clutter residue breakthrough will affect low-altitude microburst reflectivity, mean velocity, and spectrum width estimation, especially at the Denver site, unless we can measure low-level clutter residue. Figures A-3 and A-4 show examples of estimated winter and summer clear air reflectivity distributions at Denver and Kansas City. The 95 percent confidence bounds of the clear air reflectivity probability distributions are about 2 dBZ at the $90^{th}$ percentile. The TDWR sensitivity is -5.5 dBZ at 50 km, varying as $1/R^2$. Virtually no winter clear air returns were measured at Denver, and very little was measured at Kansas City.

Figures A-3 and A-4 suggest that winter clutter residue maps are more useful because of less clear air contamination. If seasonal clutter residue reflectivity variations are within a few dB, then winter clutter residue maps can serve as back-ups for other seasons when clear air contaminations are more severe. Even if seasonal clutter reflectivity variations are large, low-level reflectivity portions of winter clutter residue maps may be merged with clutter residue maps made during other seasons. Ideas proposed above will be investigated further in the future.

Much of the past understanding on microburst reflectivity has been based on the site weekly summaries which show core reflectivity. Figures A-5 and A-6 compare microburst reflectivity distributions for the core and the outflow edges at the time of maximum shear. We see that the Denver core reflectivity is typically 10 - 20 dBZ higher than the peak velocity reflectivity, while Kansas City and Orlando core reflectivities can be as much as 25 dB above the outflow reflectivity.

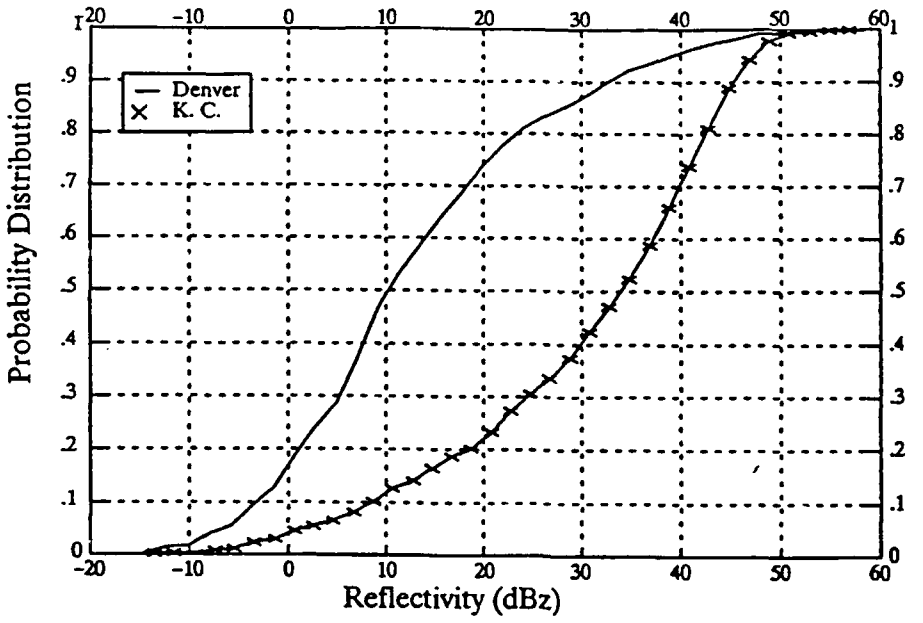


*Figure A-1. Summer microburst outflow reflectivity at the time of maximum shear.*

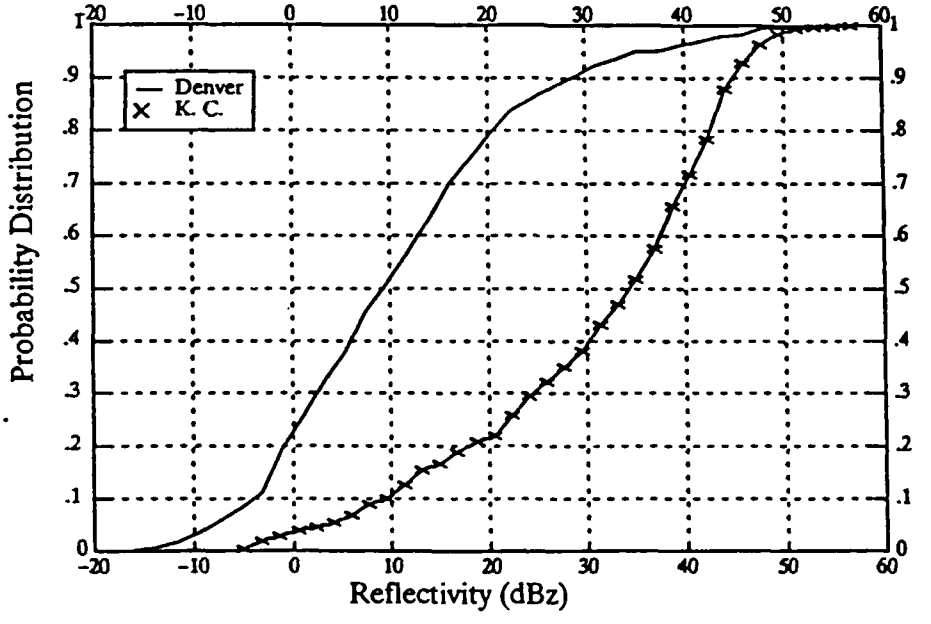


*Figure A-2. Summer microburst outflow reflectivity at the time of maximum Delta V.*

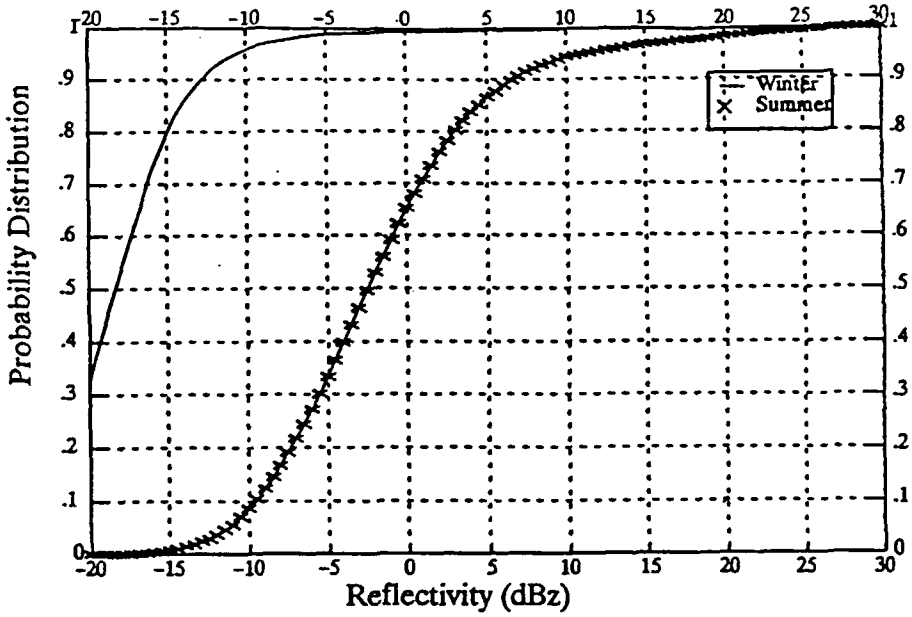


*Figure A-3. Example of Denver clear air levels.*

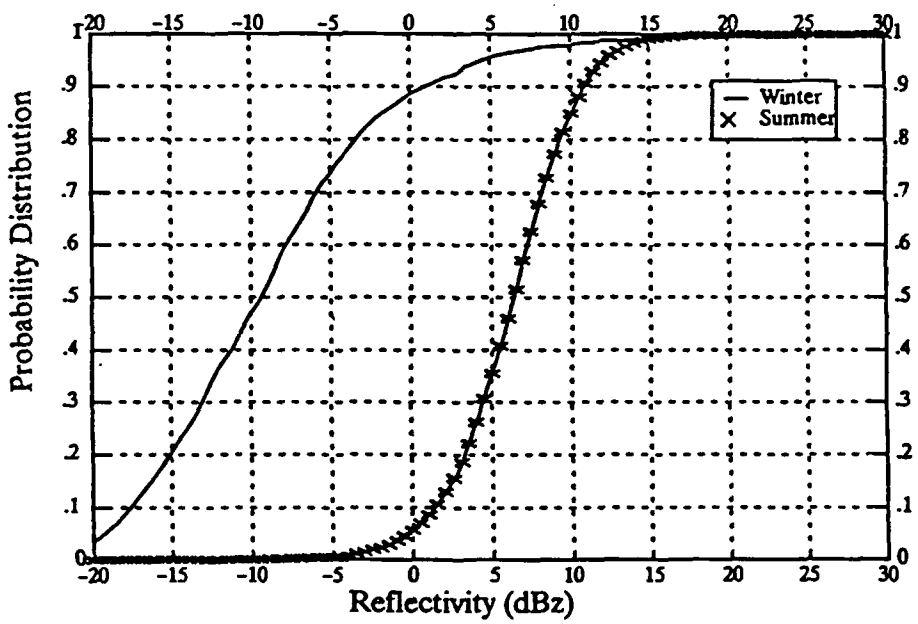


*Figure A-4. Example of Kansas City clear air levels.*

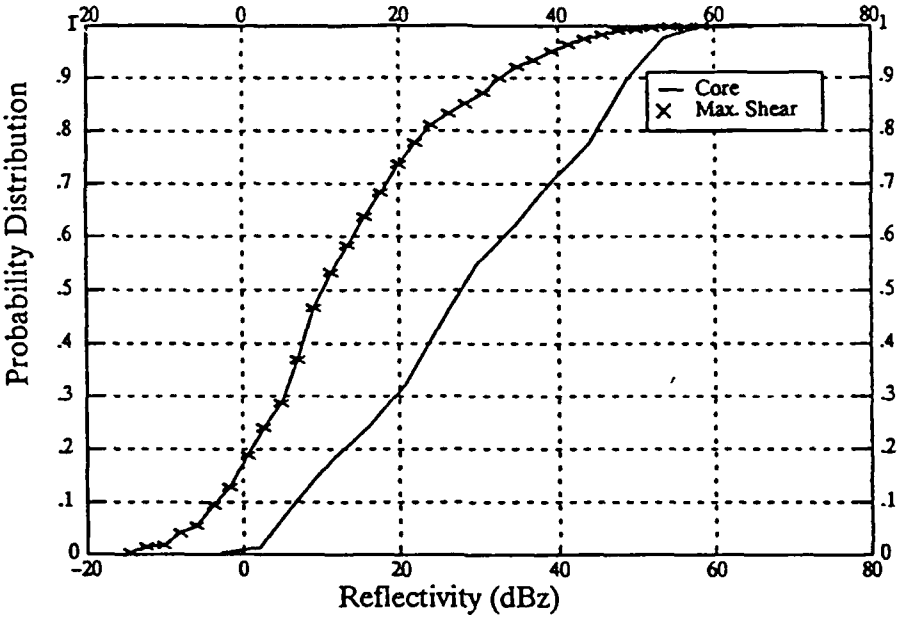


*Figure A-5. Summer microburst reflectivity at Denver.*

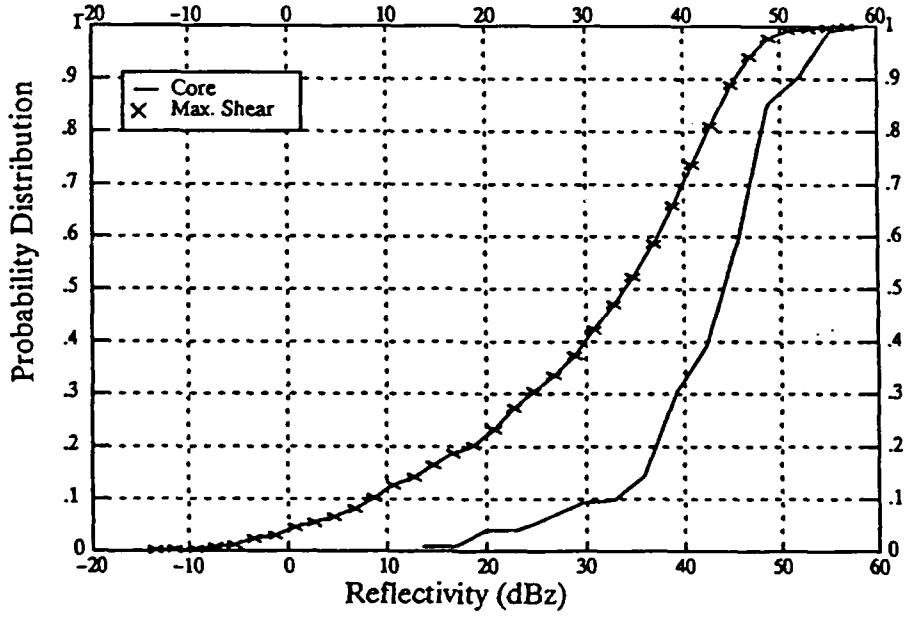


*Figure A-6. Summer microburst reflectivity at Kansas City.*

## LIST OF ABBREVIATIONS

| | |
|---|---|
| A/D | Analog-to-digital |
| AEL | Algorithm enunciation language |
| AGC | Automatic gain control |
| AGFA | Advanced gust front algorithm |
| AGL | Above ground level |
| AMS | American Meteorological Society |
| AP | Anomalous propagation |
| ASR | Airport surveillance radar |
| ATC | Air traffic control |
| ATR | Algorithm-to-truth ratio |
| bpi | bits per inch |
| CAPE | Convective and precipitation/electrification experiment |
| CCC | Concurrent Control Computer |
| CFT | Common format tape |
| CGZ | Center of gravity altitude |
| CLASS | Cross-Loran atmospheric sounding system |
| CLAWS | Classify, Locate, and Avoid Wind Shear |
| COHMEX | Cooperative Huntsville Experiment |
| COHO | Coherent local oscillator |
| CPU | Central processing unit |
| CRT | Cathode ray tube |
| DAA | Data acquisition and analysis |
| DDAA | Dual Data acquisition and analysis |
| dB | Decibel |
| dBZ | Decibel (referenced to reflectivity factor Z) |
| DFU | Display function unit |
| DFW | Dallas-Fort Worth |
| DIR | Direct wind field synthesis technique |
| DMA | Direct memory access |
| FAA | Federal Aviation Administration |
| FIR | Finite impulse response |
| FLOWS | FAA-Lincoln Laboratory operational weather studies |
| GF | Gust front |
| GFA | Gust front algorithm |
| GSD | Geographic situation display |
| HYB | Hybrid windfield synthesis technique |
| I and Q | In-phase and quadrature |
| I/O | Input/output |
| IIR | Infinite impulse response |
| ips | inches per second |
| JAWS | Joint Airport Weather Studies |
| km | kilometer |
| kW | kilowatt |
| LISP | List Processing language |
| LLWAS | Low-level wind shear alerting system |
| lpm | lines per minute |
| μ sec | microsecond |
| m | meter |
| m/s | meters per second |
| mb | millibars |
| MB | Megabyte; microburst |
| MBP | Microburst prediction |

| | |
|---|---|
| MCI | Kansas City International Airport |
| MCO | Orlando International Airport |
| MHR | Mile High Radar (Denver, CO) |
| MIST | Microburst and Severe Thunderstorm program |
| MIT | Massachusetts Institute of Technology |
| NASA | National Aeronautics and Space Administration |
| NBS | National Bureau of Standards |
| NCAR | National Center for Atmospheric Research |
| NEXRAD | Next Generation Weather Radar |
| NFS | Network file system |
| NRC | New radar control (interface) |
| nmi | nautical mile |
| NSSL | National Severe Storms Laboratory |
| NWS | National Weather Service |
| ODD | Overdetermined dual wind field synthesis technique |
| ONERA | French interferometer system |
| PDL | Program definition language |
| PE | Perkin-Elmer (now Concurrent Computer) |
| PFA | Probability of false alarm |
| PFP | Probability of false prediction |
| PIREP | Pilot reports |
| PMP | Probability of microburst prediction |
| POD | Probability of detection |
| POINT | Fixed azimuth and elevation indicator |
| PPI | Plan position indicator |
| pps | pulses per second |
| PRF | Pulse repetition frequency |
| PROFS | Prototype Regional Observing and Forecasting Service |
| PRT | Pulse repetition time |
| PSP | Programmable signal processor |
| RC | Radar controller |
| RDT | Ribbon display terminal (an alphanumeric display terminal) |
| RF | Radio frequency |
| RHI | Range height indicator |
| RTS | Real-time system |
| rms | root mean square |
| SCSI | Small computer systems interface |
| SDC | Synchro-to-digital converter |
| SP | Signal processor |
| STC | Sensitivity time control |
| STX | ST Systems, Inc. |
| T/R | Transmitter/receiver |
| TCP | Transmission control protocol |
| TDOR | Thunderstorm day observation region |
| TDWR | Terminal Doppler weather radar |
| TIM | Technical interchange meeting |
| TRACON | Terminal radar approach control facility |
| TSB | Time series buffer |
| TVS | Tornado vortex signature |
| TWT | Travelling wave tube |
| ULI | Universal logic interface |
| UND | University of North Dakota |
| UTF | Universal tape format |
| UWA | Uniform wind analysis |
| VIL | Vertically integrated liquid water |
| WORM | Write once read many |
| XCR | Clutter breakthrough adjustment value |

## REFERENCES


1. J. McCarthy, J.W. Wilson, and T.T. Fujita, "The joint airport weather studies project."*Bull. Amer. Meteor. Soc.*, vol. 63, pp.15-22, 1982

2. J. McCarthy, J.W. Wilson, "The classify, locate, and avoid wind shear (CLAWS) project at Denver's Stapleton International Airport: operational testing of terminal weather hazard warnings with an emphasis on microburst wind shear," in Preprint Volume, *Second Int. Conf. on the Aviation Weather Systems*, Montreal, Amer. Meteor. Soc., Boston, MA, pp. 247-256, 1985.

3. D. Turnbull, J. McCarthy, J. Evans, and D. Zrnic', "The FAA terminal doppler weather radar (TDWR) program," Preprint Volume, *Third Int. Conf. on the Aviation Weather System*, Anaheim, CA, Amer. Meteor. Soc., Boston, MA, 1989.

4. J.E. Evans, ed., "Results of the Kansas City 1989 terminal Doppler weather radar (TDWR) operational evaluation testing," MIT Lincoln Laboratory, Lexington, MA, ATC-171, 17 August 1990.

5. S.C. Crocker, "TDWR PRF selection criteria, MIT Lincoln Laboratory, Lexington, MA, Project Report ATC-147, 15 March 1988.

6. S.C. Crocker, "The effectiveness of adaptive PRF selection in minimizing range obscuration in the TDWR system," MIT Lincoln Laboratory, Lexington, MA, Project Report ATC-164, 27 July 1989.

7. E.S. Chornoboy, "Initialization for improved IIR filter performance," MIT Lincoln Laboratory, Lexington, MA, Technical Report 828, 31 December 1990.

8. P. Biron, M. Isaminger, K. Flemming, and A. Borho , "A case study of the Claycomo, Missouri microburst on July 30, 1989," American Meteorological Society *16th Conference on Severe Local Storms: Conference on Atmospheric Electricity*, Kananaskis Provincial Park, Alberta, Canada, 22-26 October 1990, pp. 388-392.

9. D.L. Klingle-Wilson, (internal memorandum, 1990).

10. M. Wolfson, D. Klingle-Wilson, M. Donovan, J. Cullen, D. Neilley, M. Liepins, R. Hallowell, J. DiStefano, D. Clark, M. Isaminger, P. Biron, B. Forman, "Characteristics of thunderstorm-generated low altitude wind shear: a survey based on nationwide terminal Doppler radar testbed measurements," IEEE 29th Conference on Decision and Control, Honolulu, HI, December 1990.

11. J. DiStefano and D. Clark, "Microburst observability and frequency during 1988 in Denver, CO," MIT Lincoln Laboratory, Lexington, MA, Project Report ATC-170, May, 1990.

12. M. Liepins, M. Wolfson, D. Clark, B. Forman, "a comparison of anemometer and Doppler radar winds during wind shear events," American Meteorological Society *16th Conference on Severe Local Storms: Conference on Atmospheric Electricity*, Kananaskis Provincial Park, Alberta, Canada, 22-26 October 1990, pp. 356-361.

13. J. Cullen and M. Wolfson, "Predicting summer microburst hazard from thunderstorm day statistics," American Meteorological Society *16th Conference on Severe Local Storms: Conference on Atmospheric Electricity,* Kananaskis Provincial Park, Alberta, Canada, 22-26 October 1990, pp. 383-387.

14. R. Hallowell, "Aspect angle dependence of outflow strength in Denver microbursts: spatial and temporal variations," American Meteorological Society *16th Conference on Severe Local Storms: Conference on Atmospheric Electricity,* Kananaskis Provincial Park, Alberta, Canada, 22-26 October 1990, pp. 397402.

15. D. Klingle-Wilson and M. Donovan, "Observed differences between denver and Kansas City gust fronts and their impact upon the performance of the gust front detection algorithm," American Meteorological Society *16th Conference on Severe Local Storms: Conference on Atmospheric Electricity,* Kananaskis Provincial Park, Alberta, Canada, 22-26 October 1990, pp. 236-239.

16. M. Wolfson, "Understanding and predicting microbursts," *16th Conference on Severe Local Storms: Conference on Atmospheric Electricity,* Kananaskis Provincial Park, Alberta, Canada, 22-26 October 1990, pp. 340-351.